THE APPLICATION OF POLE MOUNTED AMORPHOUS CORE TRANSFORMERS TO THE ELECTRICAL DISTRIBUTION NETWORK

Jasoda Naidoo

In fulfilment of the Masters of Science, College of Agriculture, Engineering and Science, University of KwaZulu-Natal

22 February 2017

Supervisor: Andrew Swanson

COLLEGE OF AGRICULTURE, ENGINEERING AND SCIENCE

DECLARATION 1 - PLAGIARISM

I …Jasoda Naidoo…., declare that

1. The research reported in this dissertation, except where otherwise indicated, is my original research.

2. This dissertation has not been submitted for any degree or examination at any other university.

3. This dissertation does not contain other persons' data, pictures, graphs or other information, unless specifically acknowledged as being sourced from other persons.

4. This dissertation does not contain other persons' writing, unless specifically acknowledged as being sourced from other researchers. Where other written sources have been quoted, then:
   a. Their words have been re-written but the general information attributed to them has been referenced
   b. Where their exact words have been used, then their writing has been placed in italics and inside quotation marks, and referenced.

5. This dissertation does not contain text, graphics or tables copied and pasted from the Internet, unless specifically acknowledged, and the source being detailed in the dissertation and in the References sections.

Signed

……

As the candidate's Supervisor I agree to the submission of this dissertation.

Signed

……

COLLEGE OF AGRICULTURE, ENGINEERING AND SCIENCE

DECLARATION 2 - PUBLICATIONS

DETAILS OF CONTRIBUTION TO PUBLICATIONS that form part and/or include research presented in this dissertation (include publications in preparation, submitted, *in press* and published and give details of the contributions of each author to the experimental work and writing of each publication)

Publication 1:

J. Naidoo and A. Swanson, "A simulation study of the inrush current performance of amorphous core and c.r.g.o transformers," South African Universities Power Engineering Conference, Vaal University of Technology, 2016, ISBN 978-1-77012-386

Publication 2:

J. Naidoo and A. Swanson, "Mechanical forces during short-circuit and inrush current conditions in amorphous core transformers," South African Universities Power Engineering Conference, Stellenbosch University, 2017, ISBN 978-0-620- 74503-1.

Signed:

……

ACKNOWLEDGEMENTS

The author, whom is an Eskom employee, is grateful to God and the following people for helping her complete her dissertation:

1. Tertiary Education Support Programme (TESP)
2. Eskom
3. Andrew Swanson: UKZN supervisor
4. Eskom employees
5. Revive Transformers
6. Family and friends
7. Daphne Morwalle
8. Shabnum Behari
9. Bilha Kaguima

ABSTRACT

With the drive to save money when supplying electricity to customers, utilities are looking for solutions to decrease losses on distribution lines while maintaining good quality of supply. Amorphous core transformers are known for having the lower no-load losses compared to cold rolled grain orientated transformers and hence may be an important technology to decrease losses on the distribution network. The amorphous material is easily magnetised, however this comes at the expense of a lower saturation point and the transformer may need to be designed at a lower peak flux density.

Inrush currents are a phenomenon that occurs when a transformer is switched on. The combination of the voltage switching angle and the remnant flux lead to an overflux and subsequent saturation of the core material, this leads to a high current.

The purpose of this dissertation is to investigate the performance of amorphous core transformers installed on distribution lines, where they are switched onto the network from the high voltage side, and conclude if they are a suitable replacement for cold rolled grain oriented steel core.

Inrush currents have been investigated through a circuit model developed in Alternative Transients Program/Electromagnetic Transients Program (ATP/EMTP) to determine the currents for various designs of transformers. The model consists of the non-linear component related to the core used as well as the air core of the high voltage winding. The circuit model has been validated through an experiment.

A study was undertaken to understand the difference in the forces between amorphous core transformers and cold rolled grain orientated, this was investigated in Finite Element Method Magnetics (FEMM) by determining the distribution of magnetic flux. Additionally, as the inrush current is only seen on the high voltage winding and not the low voltage winding, the models were compared to the forces due to short-circuit currents, where there is current on both high voltage and low voltage windings and a different magnetic flux distribution. The position of the tap winding was of interest as it results in an unsymmetrical force distribution.

CONTENTS

LIST OF FIGURES

LIST OF TABLES

Acronyms

AMDT:	Amorphous Metal Distribution Transformer
ATP:	Alternative Transients Program
CAD:	Computer Aided Design
CFF-RTA:	Continuous Fast-Forward Rapid Thermal Annealing
CRGO:	Cold Rolled Grain Oriented steel core transformer
CTC:	Continuously Transposed Conductor
DETC:	De-energised tap changer
EMTP:	Electromagnetic Transients Program
FEM:	Finite Element Model
FEMM:	Finite Element Method Magnetics
HV:	High voltage
IEC	International Electrotechnical Commission
IR:	Inrush
LV:	Low voltage
Matlab:	Matrix Laboratory software using vectors and matrices from MathWorks®
MV:	Medium voltage, or high voltage of a MV/LV transformer
NERSA:	National Energy Regulator of South Africa
NLTC:	No-load tap changer
OLTC:	On-load tap changer
rms:	Root mean square
SC:	Short-circuit
TESP	Tertiary Education Support Programme
%V:	Percentage voltage
%Vmax:	Percentage maximum voltage
%Vmin:	Percentage minimum voltage

1 INTRODUCTION

Distribution networks in the South African national utility, Eskom, are generally 33 kilovolt (kV) and below. The quality of electricity that Eskom supplies to customers is regulated by the National Energy Regulator of South Africa (NERSA) [1].

Transformers are electrical devices that use a magnetic field to transform or regulate voltage at the same frequency. They are built in different sizes, have different ratings, different cooling methods, different insulation, can be used to increase or decrease the primary voltage which enters the transformer or regulate the voltage [2], [3].

This study is focused on pole mounted transformers rated at 16 kilovolt-ampere (kVA) installed on 22 kV distribution networks and are required to decrease the primary voltage from 22 kV to a lower voltage to supply customers. Figure 1 - 1 displays a 16 kVA pole mounted transformer installed on a distribution network at Eskom. This was part of a pilot project done in 2014. A utility generates electricity at a certain voltage and transports it to substations, which use transformers to distribute electricity at a specified voltage to other substations and customers. Revenue is received by the utility from customers for supplying electricity.

Figure 1 - 1: 16 kVA Transformer installation (courtesy of Eskom)

Eskom generates about 95% of electricity that South Africa uses and about 45% of electricity Africa uses. Eskom also supplies electricity to diverse customers via transmission and distribution networks [4].

Pole mounted transformers are transformers connected on a utility pole. They provide final voltage conversion in a distribution system. They consist of a core material, windings, solid insulation (e.g.: paper insulation), liquid insulation (e.g.: transformer oil), metal casing and materials used for connections and protection [5].

Pole mounted transformers should be durable as they are subjected to adverse weather conditions, multiple switching operations, overloading and short-circuit forces [6].

Transformer type test and routine test includes short-circuit test (load loss), measurement of short-circuit impedance on the principal tap and open-circuit test (no-load loss) [7], [8].

According to International Electrotechnical Commission (IEC) 60076-5:2000 Power transformers – Part 5: Ability to withstand short-circuit in reference [8], for transformers rated up to 630 kVA, the recommended minimum short-circuit impedance at rated current is 4%.

These aspects are discussed further in Chapter 2, Chapter 3 and Chapter 4.

A transformer failure results in loss of supply to customers and loss of revenue. It could be a safety and environmental issue if there is an oil leak or the transformer is burning.

Amorphous core transformers (AMDTs) have the same network application as the cold rolled grain orientated (CRGO) transformers but are designed to have low no-load losses [9].

1.1 Research question

The aim of this dissertation is to investigate the effects of inrush (IR) currents and short-circuit (SC) currents on AMDTs and determine if there are any problems installing them in the distribution network.

AMDTs are known to be energy efficient; however, their application on the network may have other implications which need to be considered. There is a significant amount of switching on the distribution network which means that transformers may be subjected to many inrush current events. AMDTs have lower flux density; hence they have higher inrush currents compared to the CRGO steel core transformers [10], [11].

AMDTs have been tested and comply with the national and international standards [12].

Inrush currents are dependent on the properties of the core whereas short-circuit currents depends on leakage reactance [13], [14].

These currents lead to forces, which when exerted may have an impact on the mechanical integrity of the transformer [15].

1.2 Hypothesis

The hypothesis is that AMDT has a higher inrush current due to its lower saturation level and the forces it experiences are similar to that of CRGO with the same design flux density.

1.3 Importance of study and contribution

This study is to determine if AMDTs are adequate for installation as pole mounted transformers and a suitable replacement for CRGO transformers. The main focus is how inrush currents affect the performance of AMDTs compared to CRGO transformers.

The study will contribute to the specification and design of AMDTs to account for inrush currents.

1.4 Dissertation structure

The chapters in this dissertation are structured in the following manner:

Chapter 1 is the introduction: This chapter explains the proposition of this research. The importance of this study and its contribution to a utility are also discussed here.

Chapter 2 is on transformers and magnetic circuits: This chapter is a literature review and introduces transformers and magnetics. It then focuses on the differences between AMDTs and CRGOs.

Chapter 3 is on inrush currents: This chapter presents how source switching angle, winding resistance, residual flux in the transformer core, air core inductance and voltage drop on the network affects inrush currents in AMDT and CRGO transformers.

Chapter 4 is on electromagnetic forces: This chapter presents how forces affect the different core type transformers. These forces result from inrush currents and short-circuit currents. The effects of the electromagnetic forces due to the arrangement of the tap changer winding are also discussed here.

Chapter 5 is the conclusion: This chapter presents the conclusions derived from Chapter 3 and Chapter 4. It concludes in what way the different currents and forces impacts on AMDTs and CRGO transformers as well as the most suitable tap changer winding arrangement. Finally, it discusses if AMDTs are a suitable replacement for CRGO.

Appendix A contains the MathWorks® (Matlab) codes used to determine the graphs in Chapter 4.
Appendix B contains the email with regard to pictures courtesy of Eskom.

2 TRANSFORMERS AND MAGNETIC CIRCUITS

From Figure 2 - 1, transformers are used to transmit electrical power from generation stations to the customer. Electricity is transmitted from generation stations at high voltages over long distances to decrease losses on the power lines to transmission substations. Transformers in this case are used to step-up the voltage. Transformers at transmission substations step-down the voltage transmitted to distribution substations. Transformers at these substations further decrease the voltage. Transformers connected on distribution networks are used to step-up, step-down or regulate the voltage been transmitted to the customer. Some customers are supplied directly from generation stations or transmission stations. Basically, customers are supplied from the power grid depending on their requirements [16], [17].

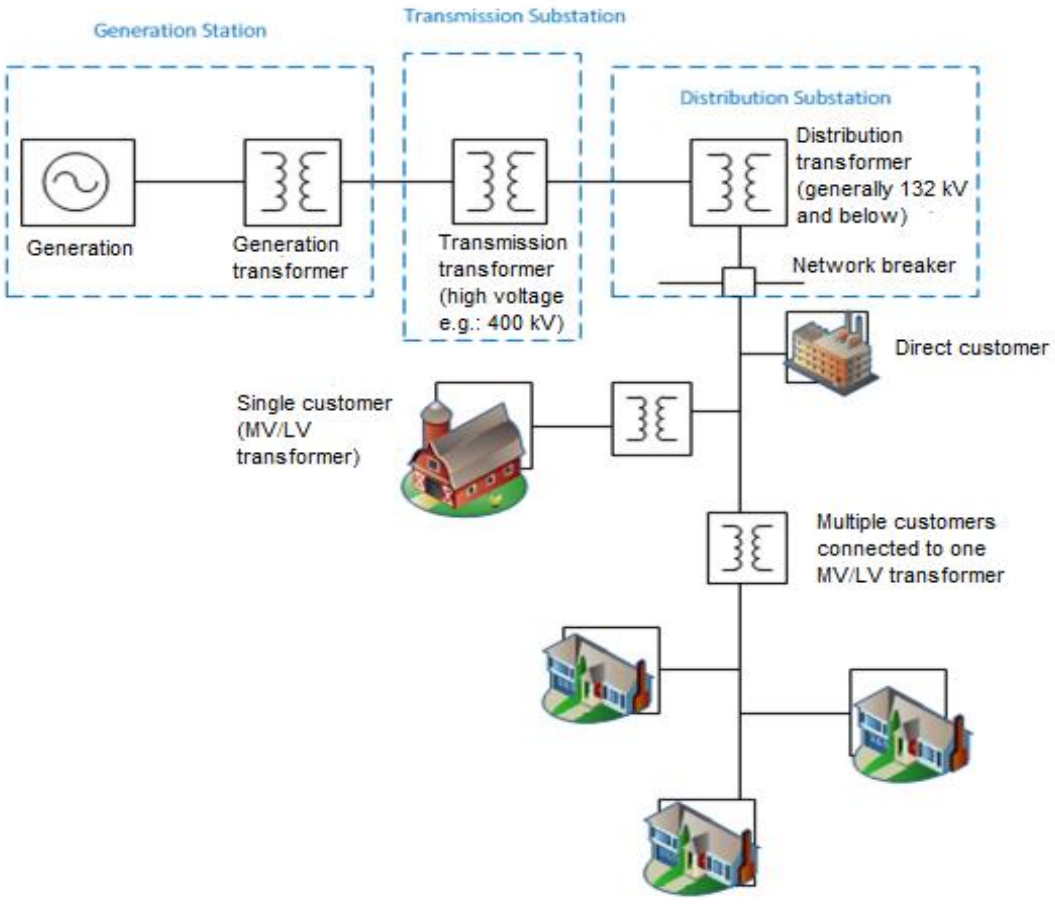

Figure 2 - 1: Diagram of electricity from the generation station to the customer

There are three different types of customers that can be supplied by a distribution substation viz: single customer e.g.: farmer; direct customer e.g.: factory and multiple customers been supplied from one medium voltage/low voltage (MV/LV) transformer e.g.: in a street with nine customers connected to a three phase MV/LV transformer, three customers will be sharing a single phase supply from this transformer. This method balances supply to the customers [5], [16].

In Eskom 60% to 75% of the total losses occur in the distribution networks. Losses from distribution transformers account for about one third of total losses on the electricity network [12], [18].

These losses are broken down into technical and non-technical losses. Technical losses are due to equipment that create unnecessary emissions that prevent the electricity generated to equal the electricity the customers are supplied. Basically, generation businesses need to supply more electricity than the customer requires to cater for losses on the networks. Non-technical losses are generated by situations where it is beyond the capabilities of the utility to resolve such as theft of electricity [19].

AMDTs, developed in Asia, are intended to decrease the technical losses in distribution transformers. The advantages of using this technology include reduced carbon dioxide and other greenhouse gas emissions, lower no-load losses and magnetising current as well as a lower temperature rise compared to CRGO core transformers [20], [21], [22].

2.1 Magnetics of a transformer

To understand the transformer and the behaviour of the transformer under abnormal conditions, the basic magnetic concepts are introduced.

Transformers are static electromagnetic devices that couple two electrical circuits through a magnetic circuit. In Figure 2 - 2, the primary winding is wrapped around a ferromagnetic core. The applied voltage drives a magnetic flux through the core and a voltage is then induced on the secondary winding according to Faraday’s law.

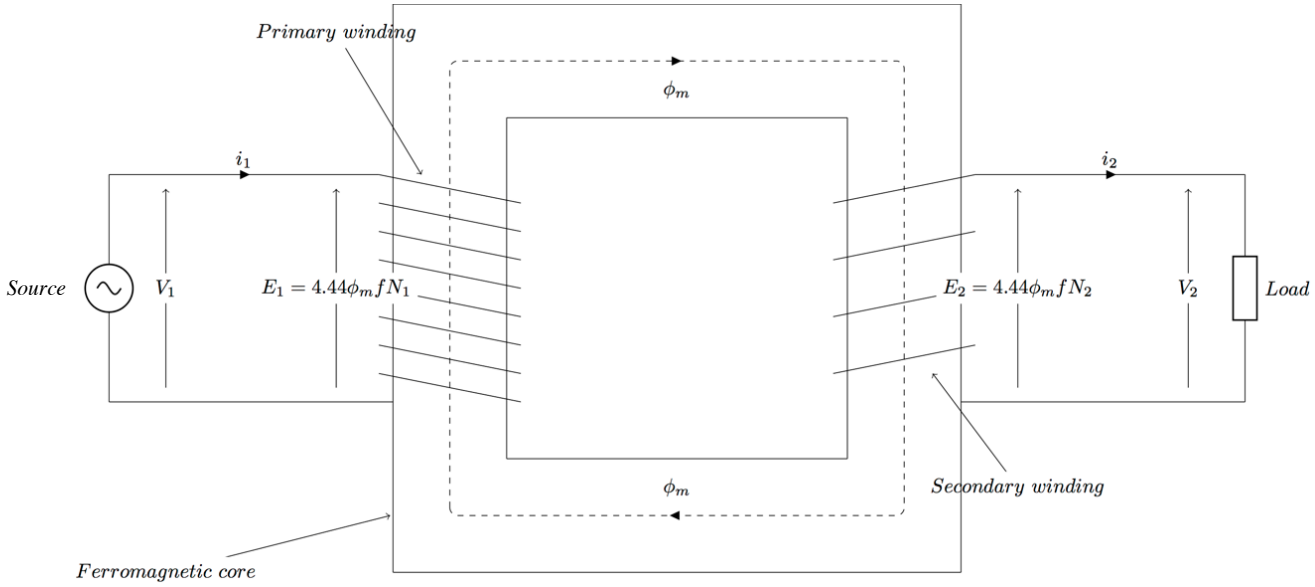

Figure 2 - 2: Representation of a transformer

Transformers have both electrical and magnetic parameters. The main parameter calculations are displayed in Table 2 - 1.

Table 2 - 1: Electrical and magnetic equations [23]

Electrical	**Magnetic**
$\sum_i I_i = 0$	$\sum_i \phi_i = 0$
$\sum_i V_i = \oint E.dl = emf$	$\sum_i (NI)_i = \oint H.dl = mmf$
$I = \int J.dA$	$\phi = \int B.dA$
$J = \sigma E$	$B = \mu H$
For uniform J and A: $I = JA$	For uniform B and A: $\phi = BA$
For uniform E: $V = EL$	For uniform H: $NI = HL$
$\frac{I}{A} = \sigma\frac{V}{L} => V = \left(\frac{L}{\sigma A}\right)I$	$\frac{\phi}{A} = \mu\frac{NI}{L} => NI = \left(\frac{L}{\mu A}\right)\phi$
$R = \frac{\rho L}{A}$	$\mathcal{R} = \frac{\sigma L}{A}$

Description of symbols in Table 2 - 1 is [23]:

A = mean area enclosed by a winding turn or net core area measured in square metre (m^2)

B = flux density measured in tesla (T)

E = root mean square (rms) voltage induced in the winding measured in volt (V)

emf = electromotive force (V)

H = field intensity measured in ampere per metre (A/m)

I = rated current measured in ampere (A)

J = current density measured in ampere per square metre (A/m^2)

$l = L$ = length of wire or core measured in metre (m)

mmf = magnetomotive force measured in ampere turn (AT)

N = number of turns

R = resistance measured in ohm (Ω)

V = voltage drop (V)

$\mathcal{R}$ = reluctance measured in ampere turn per weber (AT/Wb)

σ = conductivity measured in siemens per metre (S/m)

ϕ = flux measured in weber (Wb)

μ = permeability of material measured in henry per metre (H/m)

ρ = resistivity of material measured in ohm metre (Ωm)

2.1.1 Equivalent circuit parameters of a transformer

Figure 2 - 3 and Figure 2 - 4 displays a simplified transformer model with parameters.

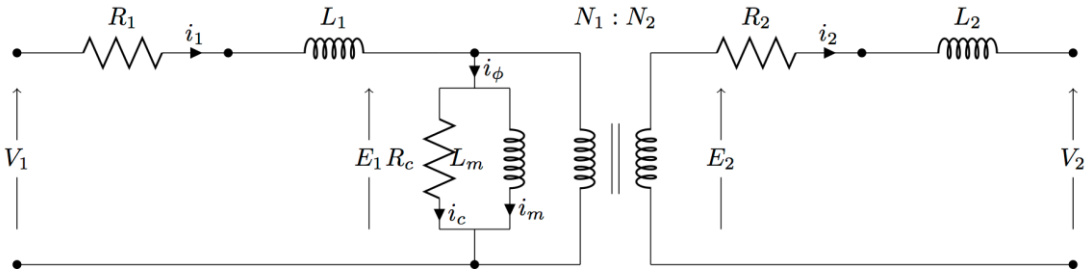

Figure 2 - 3: Transformer model parameters

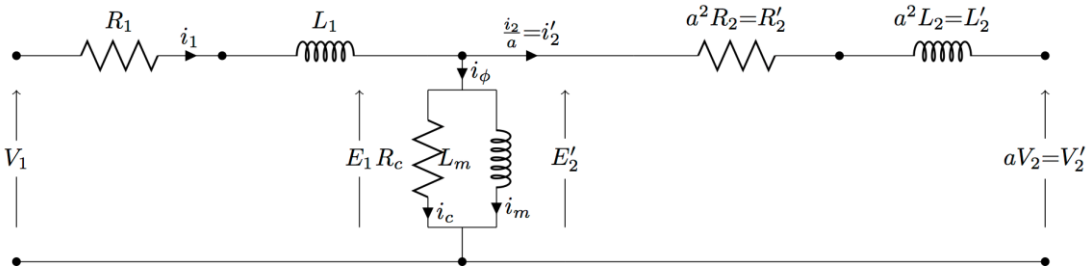

Figure 2 - 4: Transformer simplified model parameters

Description of symbols in Figure 2 - 2 to Figure 2 - 4 are [24]:

a = ratio of primary and secondary number of turns

E_1 = primary induced emf (V)

E_2 = secondary induced emf (V)

f = frequency measured in hertz (Hz)

i_c = equivalent core loss current (A)

i_m = magnetising current (A)

i_1 = primary current (A)

i_2 = secondary current (A)

i'_2 = transformer current (secondary side referred to primary side) (A)

i_ϕ = shunt current (A)

L_m = magnetising inductance measured in henry (H)

L_1 = primary leakage inductance (H)

L_2 = secondary leakage inductance (H)

L'_2 = equivalent value of secondary terminal inductance when referred to primary winding (H)

N_1 = number of turns in primary winding

N_2 = number of turns in secondary winding

R_c = core loss equivalent resistance (Ω)

R_1 = primary winding resistance (Ω)

R_2 = secondary winding resistance (Ω)

R'_2 = equivalent value of secondary winding resistance referred to primary winding (Ω)

V_1 = primary terminal voltage (V)

V_2 = secondary terminal voltage (V)

Φ_m = instantaneous value of flux at any time t (Wb)

The parameters for the equivalent transformer models in Figure 2 - 3 and Figure 2 - 4 are calculated as follows [24], [25]:

$$R'_2 = R_2 \left(\frac{N_1}{N_2}\right)^2 \quad (1)$$

$$X'_2 = X_2 \left(\frac{N_1}{N_2}\right)^2 \quad (2)$$

$$a = \frac{N_1}{N_2} \quad (3)$$

$$E'_2 = E_1 \quad (4)$$

$$V'_2 = V_2 \quad (5)$$

$$R_L = R_1' + R_2' \tag{6}$$

$$X_L = X_1' + X_2' \tag{7}$$

Short-circuit impedance percentage is calculated as [25]:

$$V_z = Z_{\%} = \frac{IZ}{E} \times 100 \tag{8}$$

Short-circuit impedance per unit is calculated as [25]:

$$V_z = Z_{pu} = \frac{IZ}{E} \tag{9}$$

Impedance is calculated as [24]:

$$Z = \sqrt{(R_L^2 + X_L^2)} \tag{10}$$

Where [24], [25]:

E_2' = equivalent value of secondary induced emf when referred to primary winding (V)

I = rated current (A)

R_L = resistance (Ω)

R_1' = equivalent value of primary winding resistance referred to secondary winding (Ω)

V_z = transformer voltage drop (%)

V_2' = equivalent value of secondary terminal voltage when referred to primary winding (V)

X_2 = secondary winding leakage reactance (Ω)

X_2' = equivalent value of secondary leakage reactance referred to primary winding (Ω)

X_L = leakage reactance (Ω)

X_1' = equivalent value of primary leakage reactance referred to secondary winding (Ω)

Z = impedance (Ω)

$Z_{\%}$ = impedance (%)

Supply voltage is calculated as follows [24]:

$$E = K\Phi_{mp}\, fN \tag{11}$$

When supply voltage is sinusoidal, Equation (11) becomes [24]:

$$E = 4.44\Phi_{mp}\, fN \tag{12}$$

Since [24]:

$$\Phi_{mp} = B_{mp}A_{core} \tag{13}$$

Equation (12) can be [24]:

$$E = 4.44B_{mp}A_{core}fN \tag{14}$$

Where [24]:
A_{core} = area of the core (m^2)
B_{mp} = instantaneous peak flux density value (T)
K = constant
Φ_{mp} = instantaneous peak value of flux (Wb)

2.1.2 Relationship between the primary and secondary windings

There is no physical connection between the primary and secondary windings. The only connection is through magnetisation. The relationship between the main parameters is as follows [24]:

$$\frac{E_1}{N_1} = K\Phi_{mp}\, f = \frac{E_2}{N_2} \tag{15}$$

Hence, the voltage ratio and turns ratio between the two circuits are the same [24]:

$$\frac{E_1}{N_1} = \frac{E_2}{N_2} \tag{16}$$

And [24]**:**

$$N_1 I_1 = N_2 I_2 \tag{17}$$

$$\frac{E_1}{E_2} = \frac{N_1}{N_2} = \frac{I_2}{I_1} \tag{18}$$

Where [24]:

I_1 = primary side current (A)

I_2 = secondary side current (A)

2.2 Transformer efficiency

Transformer efficiency is calculated as follows [24]:

$$\text{Efficiency } \% = \frac{P_{output}}{P_{output} + P_{loss}} \times 100 \tag{19}$$

$$P_{loss} = P_{no-load} + P_{load\ loss} \tag{20}$$

Where [24]:

P_{loss} = total transformer loss measured in watt (W)

$P_{load\ loss}$ = load loss or copper loss or winding loss (W)

$P_{no-load}$ = no-load loss or core loss (W)

P_{output} = output power (W)

2.3 Rated quantities

Single phase transformer's rated quantities are calculated using Ohm's law as follows [24]:

$$R_L = \frac{V}{I} \tag{21}$$

2.3.1 Single phase transformers

The apparent power for single phase transformers is calculated as follows [24]:

$$S = V_2 I_2 \tag{22}$$

Where [24]:

S = apparent power measured in volt-ampere (VA)

2.4 Voltage regulation

Voltage regulation of the transformer is calculated as follows [24]:

$$\%\ \text{Regulation} = \frac{E_2 - V_2}{E_2} \times 100 = \frac{I_2(R_2\cos\theta \pm X_2\sin\theta)}{E_2} \quad (23)$$

Where [24]:

θ = phase angle between V_2 and I_2

$\pm$ = positive implies power factor is lagging (inductive impedance) and negative implies power factor is leading (capacitive impedance)

2.5 No-load losses

No-load loss is the active power which consists of core losses (hysteresis losses), eddy current losses, stray losses, and anomalous losses [2], [25], [26], [27]. These losses are explained below.

Equation (24) to Equation (28) are used for no-load loss calculations. These are displayed below [24], [28]:

$$P_{no-load} = \frac{E^2}{R_c} \quad (24)$$

$$W_h = K_h f(B_{mp})^n \quad (25)$$

$$W_e = \frac{k_2 \times f^2 \times t^2 \times B_{eff}^2}{\rho} \quad (26)$$

$$W = \alpha L \int_0^{B_{max}} H.\,dB \quad (27)$$

$$\int H.\,dB = \text{Total area enclosed by Hysteresis Loop} \quad (28)$$

Where [24], [28]:

B_{eff} = flux density corresponding to rms value of applied voltage (T)
K_h = hysteresis constant, dependent on core lamination material
k_2 = material dependant constant
n = Steinmetz exponent, this varies between 2 to 2.6 for flux density between 1.45 T to 1.7 T
t = thickness of laminations (m)
W = total work done for a complete cycle of magnetism measured in joule (J)
W_e = eddy current losses measured in watt per kilogram (W/kg)
W_h = hysteresis losses (W/kg)
αL = volume measured in cubic metre (m^3)

From Equation (25) and Equation (26), W_h and W_e are lower for amorphous core transformers due to lower peak flux density.

2.5.1 Hysteresis losses

This is defined as the magnetisation and demagnetisation caused by the magnetic field alternating in the core laminations which creates frictional movements of magnetic domains. Hysteresis is lower for Silicon steel compared to normal steel; however, amorphous metal has lower hysteresis than Silicon steel. These losses are generally accountable for 50% to 70% of the no-load losses [20].

2.5.2 Eddy current losses

Fluctuating magnetic fields induces eddy currents in laminations resulting in heat been generated. Losses are decreased by thinner laminated sheets with a slim varnish layer. These losses are generally accountable for 30% to 50% of the no-load losses [20].

2.5.3 Stray and dielectric losses

These losses are marginal and occur in the transformer core and are responsible for 1% or less of the no-load losses [20].

2.5.4 Other methods of calculating no-load losses

Albach, Dürbaum and Brockmeyer in reference [29] proposed equations to provide an accurate and simple method to define core losses of the magnetic mechanisms for random

waveforms. Simulation tools enable currents through the magnetic equipment to be obtained and these can be used with the proposed equations to obtain magnetic losses if sufficient information is not provided.

Freitag, Kasti and Leibfried in reference [30] uses post processing algorithm in Matlab and Finite Element Model (FEM) simulation in Ansys Maxwell 2015 to estimate core losses in a transformer. This simulation result is compared to the measured result. The results are similar; hence the simulation can be used to estimate transformer core losses.

Nogueira, Facchinello and Ramos in reference [31] simulates open-circuit tests using numerical calculations and finite element Computer Aided Design (CAD) software to produce estimations of magnetising current waveshape for a given value of sinusoidal voltage supply of a single-phase shell-type transformer. Numerical calculations use the nonlinear magnetisation characteristic of the transformer's magnetic core to predict magnetisation currents. The results prove that the transformer under open-circuit condition behaves like a nonlinear reactor.

Hernandez, Olivares-Galvan, Georgilakis and Cañedo in reference [32] simulates core losses as well as excitation current for distribution transformers with wound core using FEM. Results from the simulation are compared to results using a lamination by lamination method. The differences were small. Hence, FEM software provides accurate results and is simpler.

2.6 Load losses

Load loss is the absorbed active power and it consists of winding losses (copper loss), eddy current losses and stray losses [2], [25], [27].

2.6.1 Copper losses

Also known as Ohmic loss. It happens in the windings of the transformer due to the resistance of the conductor. It is reduced by decreasing the length of the winding or having a bigger conductor (i.e. higher cross sectional area) [20].

Equation (29) and Equation (30) are used for load loss calculations. These are displayed below [28]:

$$P_{\text{load loss}} = I^2R = \text{copper loss} \quad (29)$$

Copper losses also include stray losses, therefore [28]:

$$P_{\text{load loss}} = I_2^2R_{eq} + \text{Stray loss} \quad (30)$$

Where [28]:
R_{eq} = equivalent resistance measured in ohms (Ω)

2.6.2 Eddy currents

Alternating currents creates magnetic fields which occur in the windings. It is decreased by smaller cross sectional area of conductor. Stranded conductors, made up of parallel windings and using a continuously transposed conductor (CTC), can attain the low resistance required as well as control the eddy current loss [20].

2.7 Construction of distribution transformers

Figure 2 - 5 displays a typical pole mounted transformer where 22 kV enters the bushing (which is the MV incomer to the transformer) and there are double surge arresters per phase since the transformer is installed in a high lightning area as per the Eskom standard [33].

Figure 2 - 5: 16 kVA transformer installed at a pilot site (Courtesy of Eskom)

2.7.1 Transformer core types

The transformer's core can be constructed in two common designs, namely closed core or shell core. Closed core is also referred to as core form. In this type, the windings get wound on the outside and they surround the ring of the core. The windings are wound inside the shell core, also referred to as shell type or shell form, such that a shell is formed [34].

The advantage of shell core is that the leakage flux is minimised since the two windings get wound along the centre limb or leg which is double the outer limb cross-sectional area. Hence, there are two closed paths for the magnetic flux to flow, thereby increasing the transformer's efficiency and decreasing the core losses [34].

There are two common shapes of transformer cores, namely rectangular or circular (cylindrical or oval) core. The core is made up of laminated core material. The windings are wound around the core limbs. Generally, transformers rated above 5 Mega volt amp (MVA) (used for industrial applications) have a circular core and transformer rated at 5 MVA and below (used for distribution applications) has a rectangular core [34], [35].

The transformer cores simulated in Chapter 4 is rectangular with a rectangular air core, which results in higher flux at the corners. Due to its shape, there will be non-uniform radial electromagnetic forces which occur around the coil edges which may alter the coil shape depending on the magnitude of the forces [10].

2.7.2 Transformer windings

Windings are conductors used to transport current. These conductors are wound around the transformer core. Since they are current carrying conductors, they are required to be insulated. As the supply current to the transformer increases, so does the temperature of the windings. Hence, it is necessary for the transformer to contain a cooling medium [36].

Transformer windings need to have the required electrical strength for over voltages and remain mechanically stable when forces result from short-circuits [37].

Generally, aluminium and copper are used for the windings. The disadvantage of aluminium is that it requires a larger cross section than copper to carry the same amount of current.

Silver-bearing copper may be used when extreme forces are experienced by transformers since they provide more strength [36].

Conductors are stranded with rectangular cross section. Sometimes they may be foil or sheet conductors. Continuously transposed cable is when a winding cable has lots of rectangular conductor strands. This technique decreases or eliminates circulating currents. Usually core-form transformer windings are concentrically arranged around a core leg. Interleaved arrangement is stacked individual coils separated by cooling ducts and insulating barriers. Circular windings have higher mechanical strength compared to rectangular windings [36].

Some winding types are [36]:

- **Pancake windings:** This arrangement consists of conductors being wound around in a rectangular form. Mainly used in shell-form transformers.
- **Layer (barrel) windings:** This arrangement consists of insulated conductors being wound around the spacers and cylinder right next to the other insulated conductors. Variations of this type of windings can be found in tap windings of transformers.
- **Helical windings:** This type of arrangement consists of many insulated strands (slightly above one hundred) being wound in parallel alongside the span of the drum. Spacers are inserted between the suitable transpositions and discs or adjacent turns to decrease circulating currents in the middle of the parallel strands. Mainly used for applications (lower voltage classes) requiring higher-current.
- **Disc windings:** This type of arrangement consists of insulated conductors with single or several strands being wound in a sequence of parallel horizontal orientation discs. These discs are connected by the inside disc or outside disc called a crossover point. Every disc contains many turns which is wound over the other turns and the crossovers alternate between the outside and inside.

Winding classes above and equal to 25 kV in core-form transformers are generally disc type because of high voltages. When this transformer is exposed to transient voltage surges, the stress between the discs and the turns close to the winding's end is high [36].

Circular shaped coils are considered to be very durable and have a small probability to distort during a fault. Rectangular shaped coils have a higher probability to distort their shape to circular when they are subjected to forces and this may result in insulation damage [35].

The primary side and secondary side windings' electrical centres need to be balanced. Helical windings provide the best way of doing this, since axial forces are limited by structures such as core clamping. In rectangular shaped coils, the electrical centres are not balanced well [35].

When transformers are subjected to forces, telescoping occurs. This is when the two windings are sliding against one another. This may result in transformer failure as the coils are being damaged. This can be prevented by appropriate insulation and design selection [35].

2.7.3 Transformer insulation

Paper is used as insulation for the transformer windings. Transformer oil is used as an insulation medium for the core [38], [39].

Types of transformer insulation are [38], [39]:

- **Transformer oil:** This is a cooling medium. The minimum temperature where heated oil exhales sufficient vapour in order to support combustion is called the oil flash point. It indicates volatility of oil and presence of contaminates.
- **Solid oil-impregnated paper insulation:** This is paper insulation around the windings.

2.7.4 Tap changer

Transformers contain tap changers to regulate output voltage. This is achieved by varying the turns ratio by altering the amount of turns in a winding. A transformer's tap changer can either be on-load tap changer (OLTC) or de-energised tap changer (DETC). Historically, transformer failures where mainly due to the tap changer. Tap changer tests are important as they provide information on its integrity [40].

Generally tap changers are on the higher voltage windings due to the current being lower and the lower voltage winding is sometimes wound inside this winding [41].

OLTC changes the turns ratio even though the transformer is in operation. DETC also known as no-load tap changer (NLTC), changes the turns ratio only when the transformer is switched off [40], [42].

Failures that may occur with OLTC's are classified as [40]:

- Dielectric failures as a result of poor oil quality.
- Thermal failures as a result of crimp problems.
- Mechanical failures as a result of lubrication problems.

2.8 Different types of tests done on transformers

After transformers are manufactured, they are tested to ensure that they met the necessary standards and limits as prescribed by the customer [2].

Below are explanations of the different tests.

Routine test: Every transformer has to be subjected to this test. It includes voltage ratio, short-circuit impedance, load loss, no-load loss, current and winding resistance measurements. Phase displacement is also checked [2], [25].

Type test: This refers to a test done on a transformer (not covered during routine tests), which represents other transformers that are manufactured using the same drawings, techniques, materials and by the same factory. This is done to validate that those transformers are compliant with specific requirements [2], [43].
Non-Routine test: A test which is outside the standards but used to identify phenomena that may be encountered in operation [2].

2.9 Amorphous core transformers

D. Li, Zhang, G. Li, Lu and Zhou in reference [44] experimented on the effects of increasing the content of boron in the amorphous core. This developed a technique of field annealing which decreased no-load losses in the core.

The magnetic and mechanical properties, viz: hardness and strength are different in amorphous alloys compared to conventional crystalline alloys. The core material resistivity

was increased by alloying iron and silicon; then cold-rolling the materials into thin laminated sheets of 7 millimetre (mm) to 12 mm thickness. This technique allows the iron atoms to be randomly oriented (i.e. core is annealed in a magnetic field). The process of a molten alloy of iron, silicon and boron is allowed to spill in a ribbon onto a rapidly rotating drum. This is where it is chilled at a rate of one million degrees per second. This allows the formation of a material that is glasslike ribbon about 1 mm thick without crystalline structure. These processes produce a material that has low inherent hysteresis losses, good magnetic properties and high resistivity. The eddy currents are reduced drastically because of the very thin laminations, which add to the high assembly cost due to their brittleness and difficulty in handling them. This core material exhibits less than twenty-five percent of losses per pound compared to the best high-grade silicon steel cores [20], [45].

The disadvantages of amorphous core materials are [20], [45]**:**

- Increased core cost.
- More difficult to manufacture.
- Lower saturation flux density.
- Windings are rectangular, which is not as strong as circular windings for short-circuits.

Their advantages are higher efficiency due to reduced transformer core losses (ranges from 65% to 90% compared to CRGO steel cores used in Europe under sinusoidal load conditions) [20], [45].

Lenke, Rohde, Mura and De Doncker in reference [46] calculated using typical values of an oil-cooled distribution transformer. Their results showed that it is feasible to use amorphous core in applications that have power electronics with maximum excitation frequency of 1 kilohertz (kHz).

AMDTs lightly loaded have low losses at higher frequencies compared to CRGO steel core transformers. This is because they are manufactured to have a consistent strip and are thinner, have small energy magnetic flux reversal and larger electrical resistivity [20].

2.10 Differences between AMDT and CRGO transformers

Amorphous material (2605SA1) is used in AMDTs and M-5 steel material is used in the CRGO transformers been investigated in this dissertation. Table 2 - 2 displays the differences between the core materials of typical transformers.

Table 2 - 2: Differences between AMDT and CRGO steel core transformers. Table drawn with information from these references [10], [20], [23], [45], [47], [48], [49], [50], [51] and [52]

	AMDT	**CRGO**
Electrical Properties		
Density measured in gram per cubic centimetre [g/cm^3]	7.15	7.65
Specific resistance	130	45
Saturation flux density (T)	1.56	2.08
Thickness (mm)	0.025	0.27
Space factor	0.86	0.97
Stacking factor	Lower	Higher
Brittleness	Higher	Lower
Annealing temperature measured in degree celsius (^{o}C)	360	810
Coefficient of rolling	94.8%	82%
Available form	Ribbon/foil	Sheet/Roll
Typical core loss [W/kg] (at 50Hz, 1.4 T)	0.2	0.9
Temperature coefficient of resistivity	Low	High
Short-circuit	Not so good and not so strong	Good and strong
Crystallisation	Must not take place during manufacturing	Silicon steel has crystalline structure
Excitation current	Lower	Higher
Inrush Currents	Higher	Lower
No-load loss	About one third of CRGO no-load loss	-
Operating temperature	Lower	Higher
Zero sequence current	Less	More
Noise	Less	More
Magnetisation current	Lower	Higher
Efficiency	Higher	Lower
Mechanical Properties		
Handling	Difficult due to brittleness	Not difficult
Requirements	Annealing in magnetic field	Thermos-mechanical grain orientation processing for best properties
Windings	Square or rectangular	Circular
Laminations	Thin, hence reduced eddy currents	Thicker
Assembly cost	Higher	Lower
Sensitivity to Mechanical stress	Very sensitive	Not very sensitive
Core structure	Medium rating transformers have square or rectangular core	Medium rating transformers have multi-stepped core

The magnetic flux density (B) verses magnetic field intensity (H) curve is commonly referred to as the B-H curve. The B-H curves for CRGO and AMDT are displayed in Figure

2 - 6. The operating peak flux density is generally about 10% to 20% below saturation flux density [23].

Definitions for the legend in Figure 2 - 6 are:

- Amorphous represents the B-H curve for AMDT.
- M-5 represents the B-H curve for CRGO.

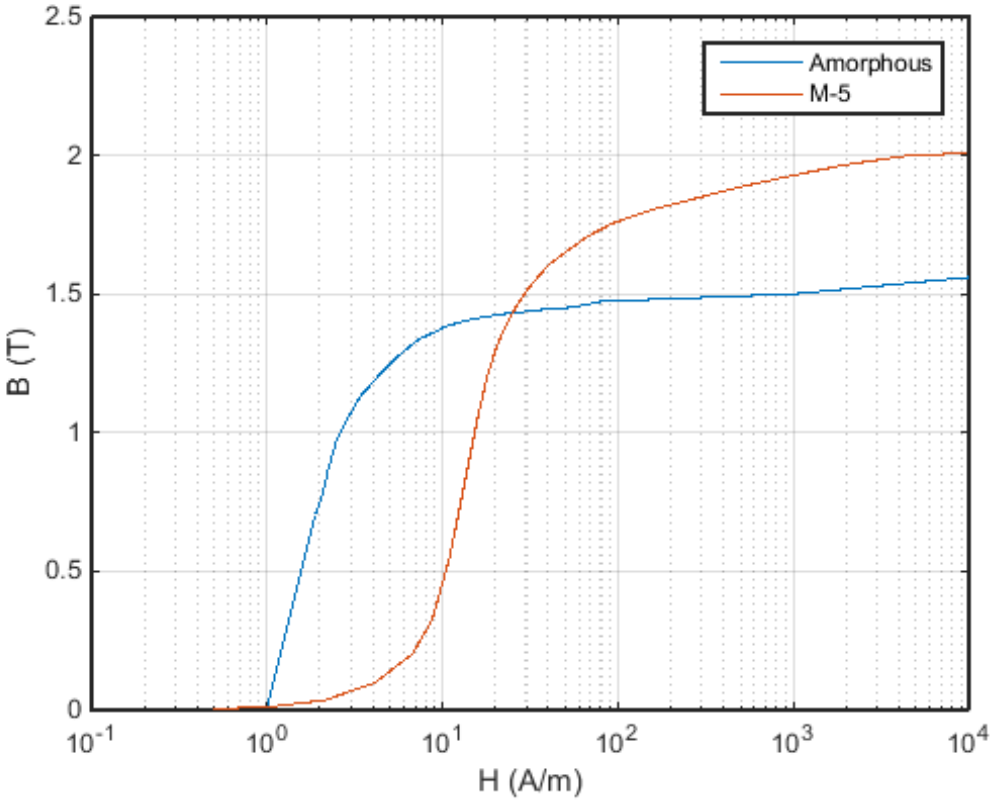

Figure 2 - 6: B-H curves for AMDT and CRGO transformer core materials

2.11 Other developments

Mohan and Singh in reference [53] compared the efficiency and cost of CRGO, amorphous core and Amorphous-CRGO core distribution transformers. Their results show that amorphous core cost more but is efficient. To reduce the cost, Amorphous-CRGO core can be used.

Yamamoto, Mori, Kawasaki, Tsutsui, Itoh and Yagisawa in reference [54] recommends that a composite core (Silicon-steel and amorphous core) is needed to achieve more strength in large wound cores.

Francoeur and Couture in reference [55] used a process called continuous fast-forward rapid thermal annealing (CFF-RTA) to produce rolled-up-core amorphous-metal distribution transformer kernels. This process allows the core to be easier to handle and less labour intensive.

3 INRUSH CURRENTS

Pole mounted transformers are in the outdoors; hence they are exposed to adverse weather conditions, overloading and faults (internal or external) through its lifespan. When they fail, they need to be replaced in order to restore electricity supply to customers. These transformers are protected by surge arrestors [6], [56].

A transformer is switched off in the following ways [5]:

- Incoming power supply is cut-off by the upstream protection equipment such as a breaker opening.
- The fuse connected on the primary side of the transformer melts due to an electrical fault.
- The operator manually opens the fuse links on the primary side of the transformer.

Inrush currents occur during start-up of the transformer. There are three factors that determine the transformer's energisation current [47]:

- The residual flux of transformer core (B_R). This is dependent on the point of the waveform that the transformer was switched off at and the length of time it has been off for.
- The point on the voltage wave at which the transformer is energised.
- The source impedance, the magnetising inductance and the air core inductance of the energised winding.

In a distribution system, the source impedance is very small compared to the impedance of the transformer [11].

Inrush currents have predominately second harmonics (i.e. frequency of 100Hz). This is one of the differences between inrush currents and fault currents. This causes nuisance tripping on some networks, but for the pole mounted distribution transformers, this is not the main issue. The inrush currents, however, may lead to forces and these are studied in Chapter 4 [27], [57], [58], [59].

3.1 Magnetic circuit for inrush currents

The transformer can be represented by the magnetic circuit illustrated in Figure 3 - 1. For a single phase three limb core, the reluctances are divided into several portions. Under normal no-load conditions the magnetising flux flows through $\mathcal{R}_{\mathrm{c}}$ as it has a lower reluctance than that of $\mathcal{R}_{\mathrm{air}}$. During abnormal conditions, the core saturates due to magnetic flux flowing through the core ($\mathcal{R}_{\mathrm{c}}$). Hence, the flux flowing through the air gap ($\mathcal{R}_{\mathrm{air}}$) is the total magnetic flux minus the magnetic flux saturation.

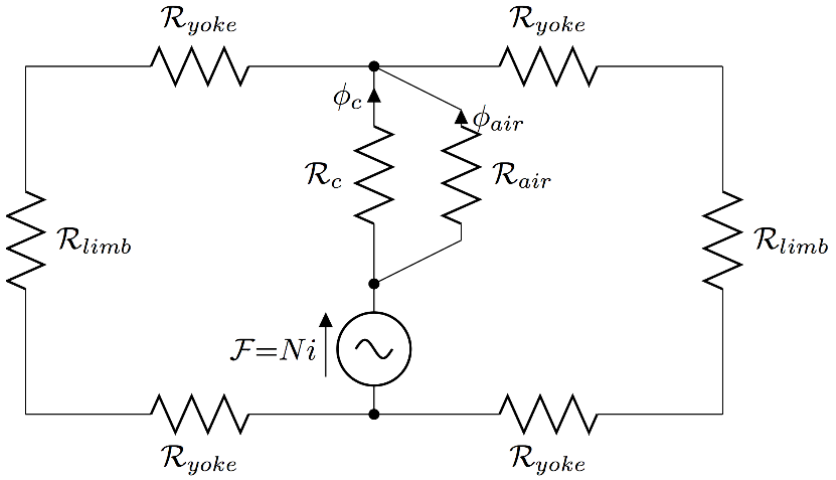

Figure 3 - 1: Magnetic circuit

Description for the symbols on Figure 3 - 1:

i = current measured in ampere (A)

N = number of turns

$\mathcal{F}$ = mmf = magnetomotive force measured in ampere turn (AT)

$\mathcal{R}_{\mathrm{air}}$ = magnetic reluctance of the air gap measured in ampere turn per weber (AT/Wb)

$\mathcal{R}_{\mathrm{c}}$ = magnetic reluctance of the core (AT/Wb)

$\mathcal{R}_{\mathrm{limb}}$ = magnetic reluctance of the limb measured in (AT/Wb)

$\mathcal{R}_{\mathrm{yoke}}$ = magnetic reluctance of the yoke (AT/Wb)

ϕ_{air} = magnetic flux in the air gap measured in weber (Wb)

ϕ_{c} = magnetic flux in the core (Wb)

The equivalent electrical representation of the transformer is shown in Figure 3 - 2. Only the primary is considered here as this is where the magnetising current is drawn from.

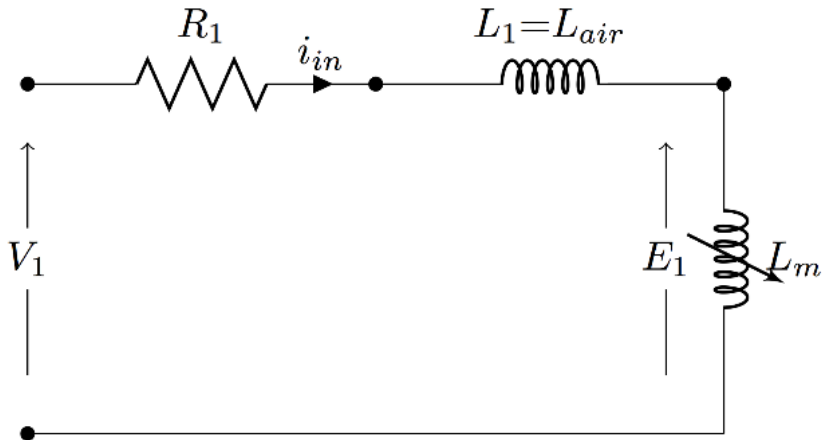

Figure 3 - 2: Electrical circuit

Description for the symbols on Figure 3 - 2:

E_1 = primary induced emf measured in volt (V)

i_{in} = inrush current (A)

L_m = magnetising inductance of the core measured in henry (H)

$L_1 = L_{air}$ = air core inductance of the winding (H)

R_1 = resistance in the primary winding measured in ohm (Ω)

V_1 = primary terminal voltage (V)

For an applied sinusoidal voltage [48]:

$$V_p(\omega t + \theta) = i_0 R_1 + N_1 \frac{d\Phi_m}{dt} \quad (31)$$

Where [48]:

i_0 = instantaneous value of magnetising current (A)

N_1 = primary winding turns

t = time measured in second (s)

V_p = peak value of the applied voltage (V)

θ = angle at which the voltage is switched on (degrees)

Φ_m = instantaneous value of flux at any time t (Wb)

ω = angular frequency measured in radian per second (rad/s)

ωt = angle related to frequency measured in radian (rad)

When the transformer is switched on, the flux may be higher due to a remnant flux and due to the switching angle of the source voltage.

The inrush flux in the core consists of the normal AC component as well as a DC component due to the switching angle and the residual flux in the core [48], [60]:

$$\Phi_m = \left(\Phi_{mp}\cos\theta \pm \Phi_r\right)e^{\frac{-R_1}{L_1}t} - \Phi_{mp}\cos(\omega t + \theta) \quad (32)$$

Where [48], [60]:
L_1 = leakage inductance of primary winding (H)
Φ_{mp} = instantaneous peak value of flux (Wb)
Φ_r = residual flux (Wb)

Since the source wave is a cosine wave, from Equation (32), it can be deduced that when the angle, θ is zero, the inrush current is the highest because flux is the highest.

The worst case of over-flux occurs at the zero crossing of the voltage, leading to a doubling of the flux which then drives the core into saturation [48].

Referring to Figure 3 - 1, the core saturates, causing the reluctance to increase, which forces the flux into the air core of the transformer winding. The flux in the air could be represented by [48]:

$$\Phi_{air} = \mu_0 H A_w = \left(2\Phi_{mp} + \Phi_r - B_{sat}A_c\right) \quad (33)$$

Where [48]:
A_c = net core area measured in square metre (m^2)
A_w = mean area enclosed by a winding turn (m^2)
B_{sat} = saturation flux density measured in tesla (T)
Φ_{air} = flux in air (Wb)
μ_0 = permeability of space = $4\pi \times 10^{-7}$ (H/m)

Referring to the equivalent electrical circuit in Figure 3 - 2, the flux causes saturation, the magnetising inductance decreases and the magnetising current increases. The current would be limited by the air core inductance of the magnetised winding [47], [60].

This is quite difficult to model using software due to the non-linearity of the core and the calculation of the air core inductance.

Daut, Hasan and Taib in reference [61] used a method to estimate the nonlinear core saturation with relation to magnetisation current, power factor and harmonic content. The results showed that magnetic flux density is proportional to magnetisation current, harmonic content and inversely proportional to power factor during saturation. The magnetising current's pattern and total harmonic distortion current percentage versus the magnetic flux density is similar to the magnetic material's B-H curve. Hence this method provides an estimation of the saturation flux density.

Girgis and teNyenhuis in reference [62] showed the impact of design on inrush currents, these are [62]:

1. Transformer cores consisting of high permeability CRGO and are domain refined electrical steels have a decrease in the peak inrush current's magnitude of 15% to 20%, however the least peak inrush current ratio or percentage second harmonic is 30% larger in comparison to regular grain oriented core transformers.
2. The magnitude of the peak inrush current is larger in transformer core with step-lap joint and has a least peak current ratio or percentage second harmonic compared to transformer cores with non-step-lap joint.

The theoretical single phase transformer inrush currents are given by [48], [63]:

$$i_{0max} = \frac{h_w H}{N_1} = \frac{h_w(2\Phi_{mp} + \Phi_r - B_{sat}A_c)}{\mu_0 A_w N_1} = \frac{h_w A_c(2B_{mp} + B_r - B_{sat})}{\mu_0 A_w N_1}$$
$$= i_{0\,max\,single\,phase} \quad (34)$$

Inductance of the magnetising branch (L_μ) of the transformer is calculated as follows [47]:

$$L_\mu = \frac{N^2 A_c \mu_0 \mu_r}{l} \quad (35)$$

$$\mu_0\mu_r = \frac{B}{H} \tag{36}$$

Where [47], [48], [63]:

B = flux density (T)

B_{mp} = maximum peak flux density (T)

B_r = residual flux density (T)

H = field intensity measured in ampere per metre (A/m)

h_w = height of the energised winding measured in metre (m)

i_{0max} = maximum first peak inrush current (A)

l = length of core (m)

L_μ = Inductance of the magnetising branch (H)

N = number of turns

μ_r = relative permeability, depends on B-H curve operating point

From Equation (36), permeability of material is proportional to the B to H ratio. After saturation, this ratio approaches zero. Equation (34) and Equation (36) explain how saturation impacts inrush currents [47].

3.2 ATP/EMTP models

Inrush currents are affected by residual flux in transformer core and source voltage angle switching [47].

In this section, the following parameters were changed to determine their effects on inrush currents:

- Source voltage switching angle.
- Winding resistance.
- Residual flux in transformer core.
- Air core inductance.
- Voltage drop on the network.

Alternative Transients Program/Electromagnetic Transients Program (ATP/EMTP) software was used to simulate the behaviour of CRGO and AMDTs under inrush currents [64].

ATP does not calculate the residual flux applied in the simulation. To ensure that the simulation is accurate, the residual flux was experimentally determined as outlined in Chapter 3.3 and manually entered in ATP.

ATP models with the following design flux densities are simulated:

- AMDT with design flux density of 1.2 T.
- AMDT with design flux density of 1.3 T.
- CRGO with design flux density of 1.3 T.
- CRGO with design flux density of 1.7 T.

3.2.1 Magnetising inductance

A Type 93 non-linear inductor is used to simulate the magnetising inductance. Values derived from the flux linkage against current curves displayed in Figure 3 - 3 are entered in the characteristics of this object. The disadvantage of this type of inductor type is that it does not account for hysteresis, however, it does account for residual flux.

Description for legend in Figure 3 - 3:

- Amorphous 1.2T depicts AMDT with design flux density of 1.2 T.
- Amorphous 1.3T depicts AMDT with design flux density of 1.3 T.
- M-5 1.3T depicts CRGO with design flux density of 1.3 T.
- M-5 1.7T depicts CRGO with design flux density of 1.7 T.

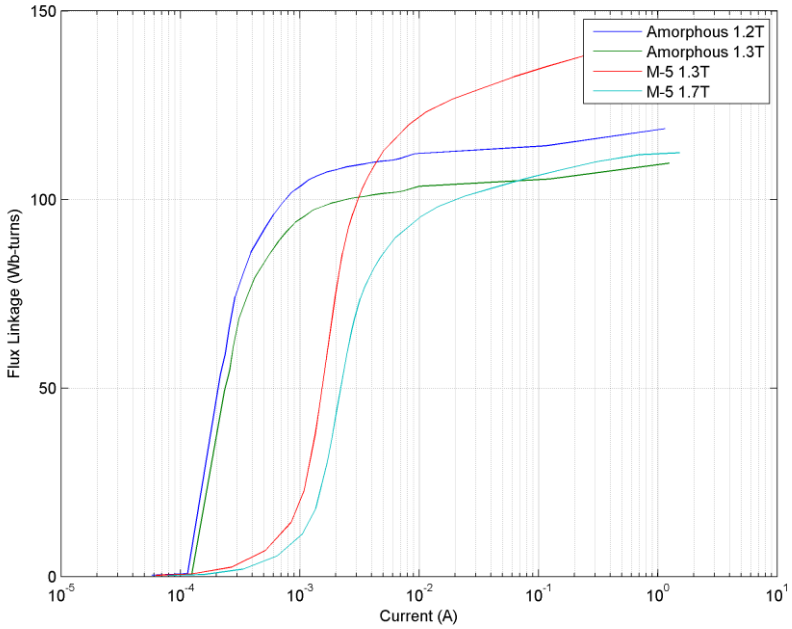

Figure 3 - 3: Flux linkage vs. current curves for AMDT and CRGO

Figure 3 - 3 illustrates the flux linkage vs. current curves for different design flux densities for AMDT and CRGO core materials.

3.2.2 Resistance

The winding resistance was kept the same for all the models, except when testing the effects of resistance on inrush currents.

3.2.3 Air core inductance

The inductance in the air core can be calculated as follows [58]:

$$L_{air} = \mu_0 N_1^2 \frac{A_1}{h_{eq1}} \tag{37}$$

Where [58]:

A_1 = mean area bounded by a winding turn for the primary winding (m^2)

h_{eq1} = equivalent primary winding height with fringing effects included (m)

In order to determine h_{eq1}, the winding height is divided by Rogowski factor, which is K_R. This factor must be less than one and is generally determined empirically. It's a function of radial width, height and mean diameter of a winding [58].

3.2.4 Source

The transformers used for this dissertation require a source voltage of 22 kV. Two sources are used per model in order to achieve 22 kV. The magnitude of the voltage per source is calculated as follows [65] :

$$V_s = \frac{V}{\sqrt{3}} = \frac{22\ \text{kV}}{\sqrt{3}} = 12.7\ \text{kV} \tag{38}$$

Where [65]:
V = source line voltage (V)
V_s = source peak voltage (V)

3.3 Validation of the model

Testing was done in a transformer testing facility. Its setup is displayed in Figure 3 - 4 in a single line diagram. A three phase 250 kVA generator is used to supply a 2 MVA 400 V/ 33 kV star-delta step-up transformer which supplies the test transformer, which is a single phase CRGO transformer. The output of the 2 MVA transformer was maintained at 22 kV. Switching the circuit breaker on and off was done to obtain the inrush currents.

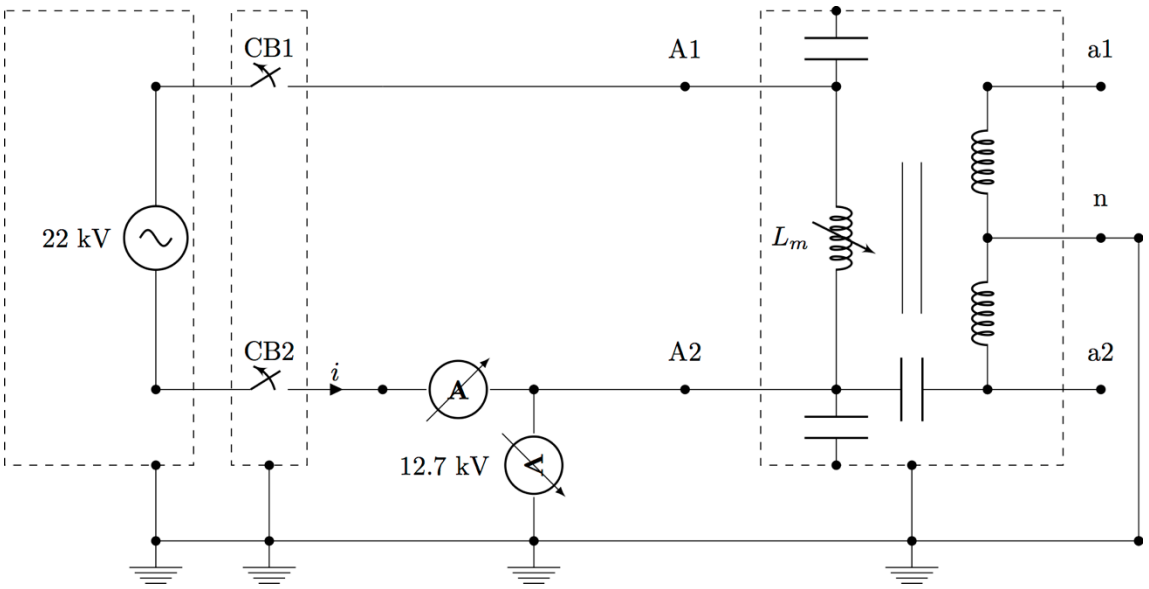

Figure 3 - 4: Single line diagram of the validation test

Description for the symbols in Figure 3 - 4:

CB1 = circuit breaker 1

CB2 = circuit breaker 2

A1 = one point on the HV winding

A2 = one point on the HV winding

Lm = magnetising inductance

a1 = one point on the LV winding

a2 = one point on the LV winding

n = neutral point

Table 3 - 1 contains the locations and details of the measuring equipment used in the experiment. The oscilloscope (Rigol 50 Megahertz (MHz)) was connected on the LV side of the transformer.

Table 3 - 1: Measuring equipment used for the experiment

Equipment	**Location**	**Type**
Voltage probe	A2	Tektronix P6015A 1:1000 Passive probe
Current probe	A2	Pearson x301 1:100 Rogowski probe

Figure 3 - 5 (a) to Figure 3 - 5 (d) displays the results when the circuit breaker is switched off and on. Switching off is important because the transformer residual flux before it is switched on can be estimated.

Description for legend in Figure 3 - 5 is:

- Blue curve represents the voltage (kV) curve.
- Red curve represents the current (A) curve.

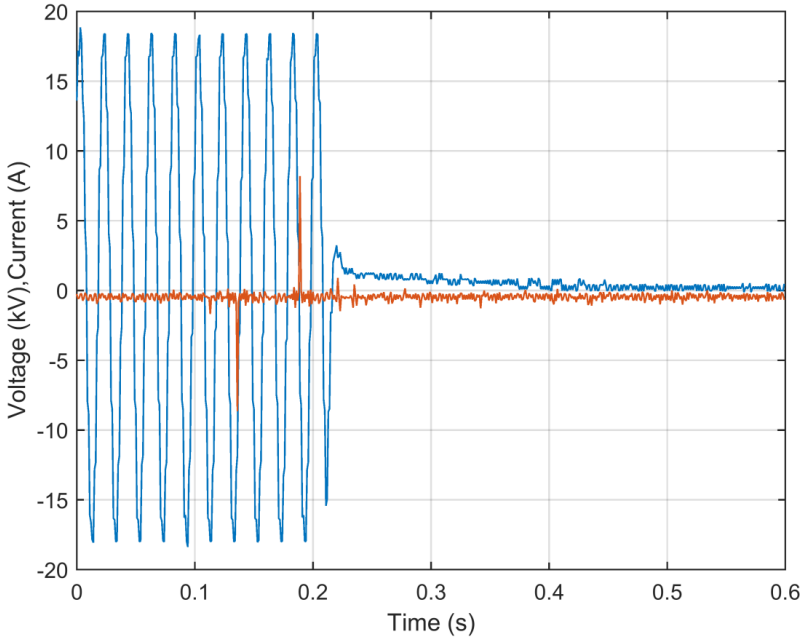

(a) Switch off at 2.5 kV on the waveform where the peak voltage is at 18.3 kV

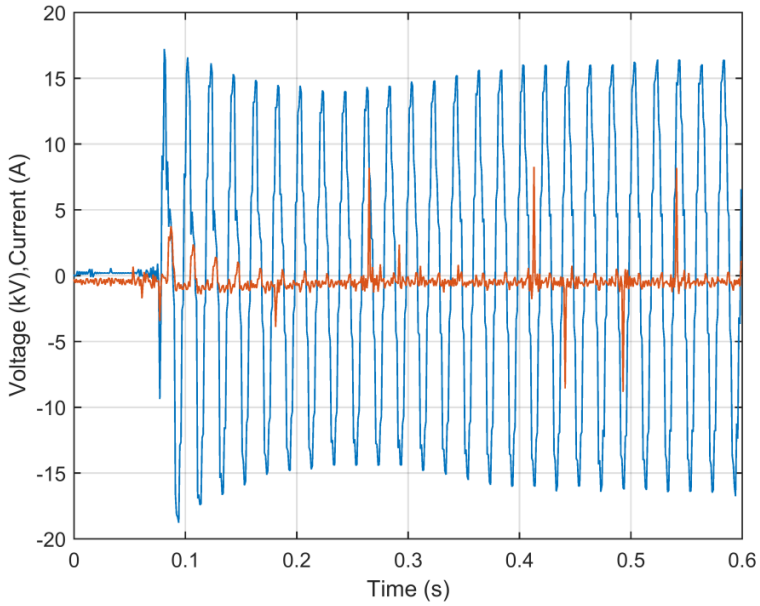

(b) Switch on at -9.54 kV on the waveform

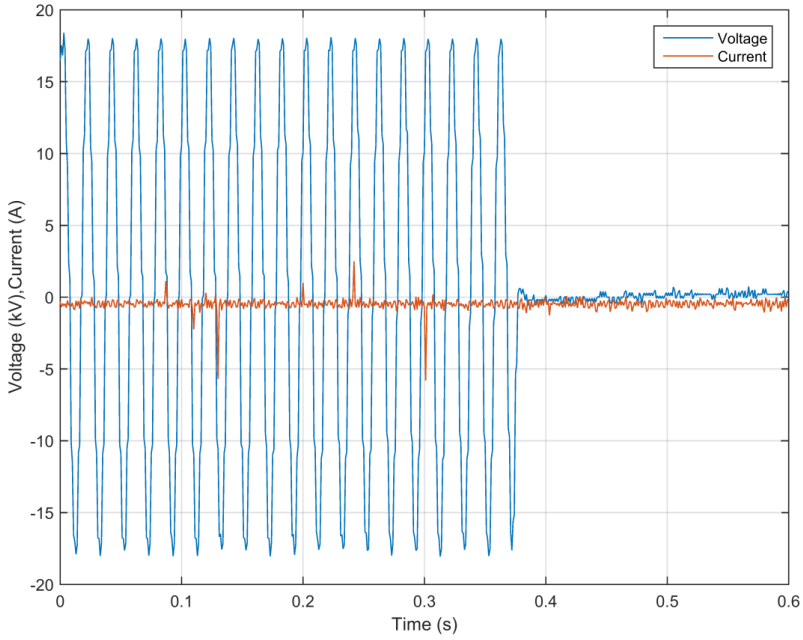

(c) Switch off at 1.1 kV on the waveform where the peak voltage is 18.3 kV

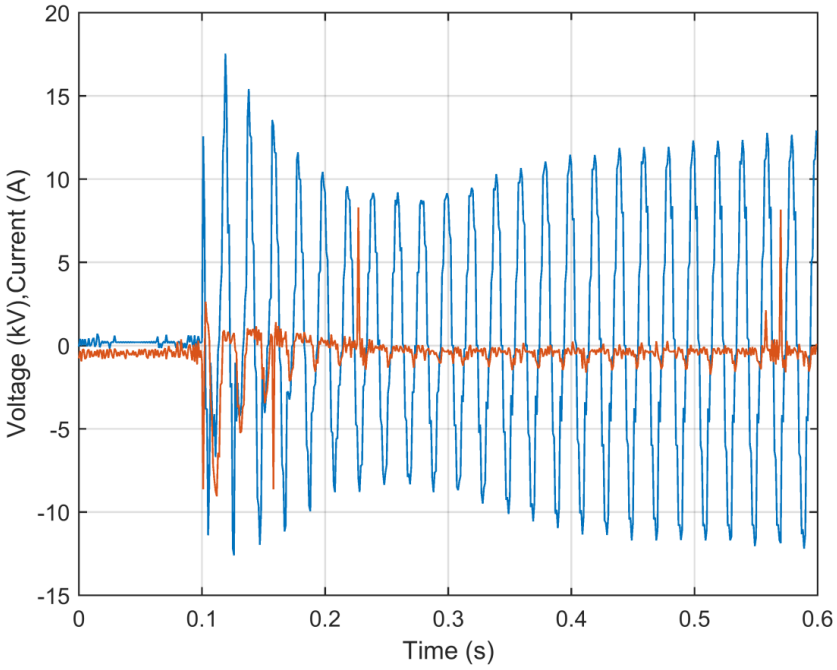

(d) Switch on at 13.3 kV on the waveform

Figure 3 - 5: Current into A2 and voltage measurement at A2

The transformer was energised after 0.22 seconds when the supply was interrupted by the circuit breakers opening. The voltage is approximately 2.5 kV when switched off in Figure 3 - 5 (a). This results in a flux linkage of 86% of the peak design flux linkage.

The transformer was re-energised after 0.08 seconds, when the circuit breakers were closed. In Figure 3 - 5 (b), the voltage is approximately -9.54 kV when switched on. This results in a 320 degree switching angle.

The transformer was then energised for 0.38 seconds. The circuit breakers were opened resulting in the voltage been approximately 1.1 kV when switched off in Figure 3 - 5 (c). This results in a flux linkage of 94% of the peak design flux linkage.

The transformer was re-energised at 0.1 seconds resulting in Figure 3 - 5 (d), where the voltage is approximately 13.3 kV. This results in a 126 degree switching angle.

The ATP model was simulated using the values in this experiment. The model is displayed in Figure 3 - 6.

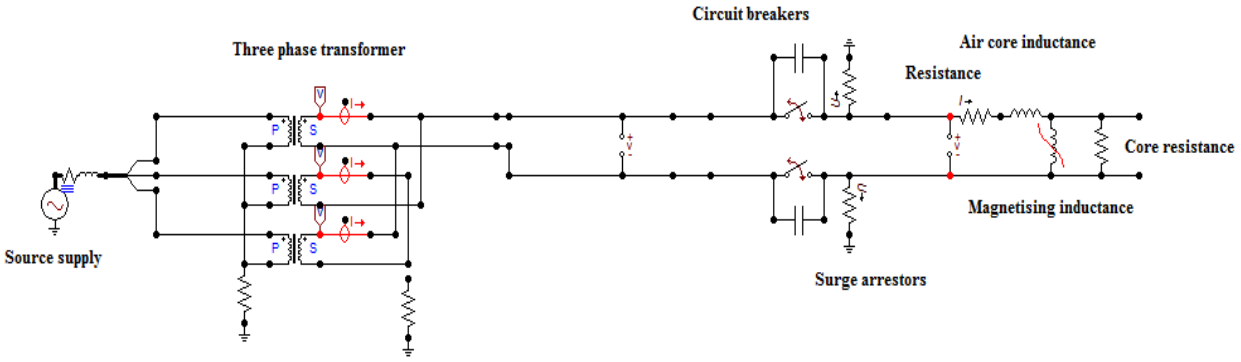

Figure 3 - 6: Validation model simulated on ATP

Description for the symbols in Figure 3 - 6 are:

P = primary side of transformer

S = secondary side of transformer

The simulation results are displayed in Figure 3 - 7 (a) to Figure 3 - 7 (d), where the residual flux used was calculated from the switch off voltage. These correlate with the experiment results even though there is a slight voltage dip on the measured results. The reason for this is the generator is only modelled as an impedance on ATP.

Description for legend in Figure 3 - 7 is:

- Blue curve represents the voltage (kV) curve.
- Red curve represents the current (A) curve.

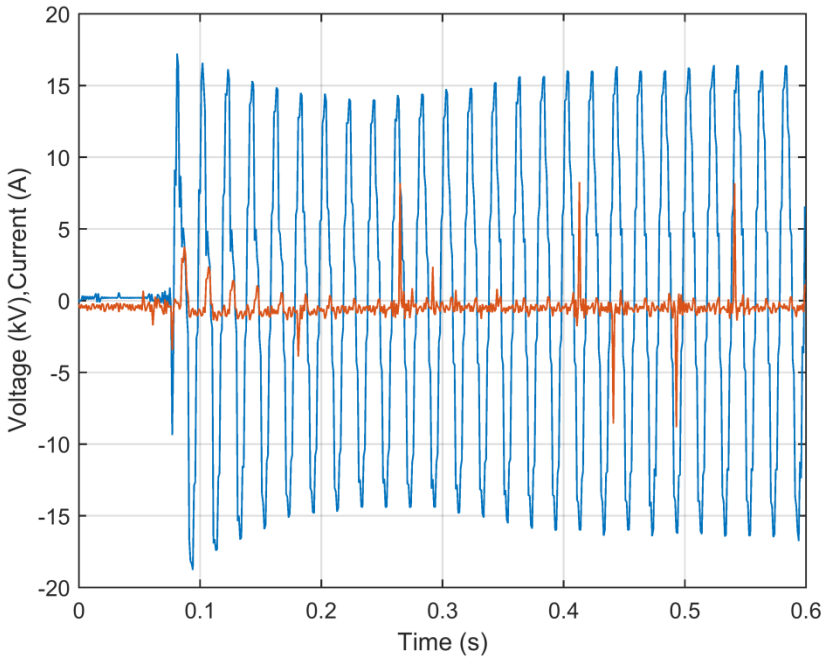

(a) Experimental results when switched on at -9.54 kV

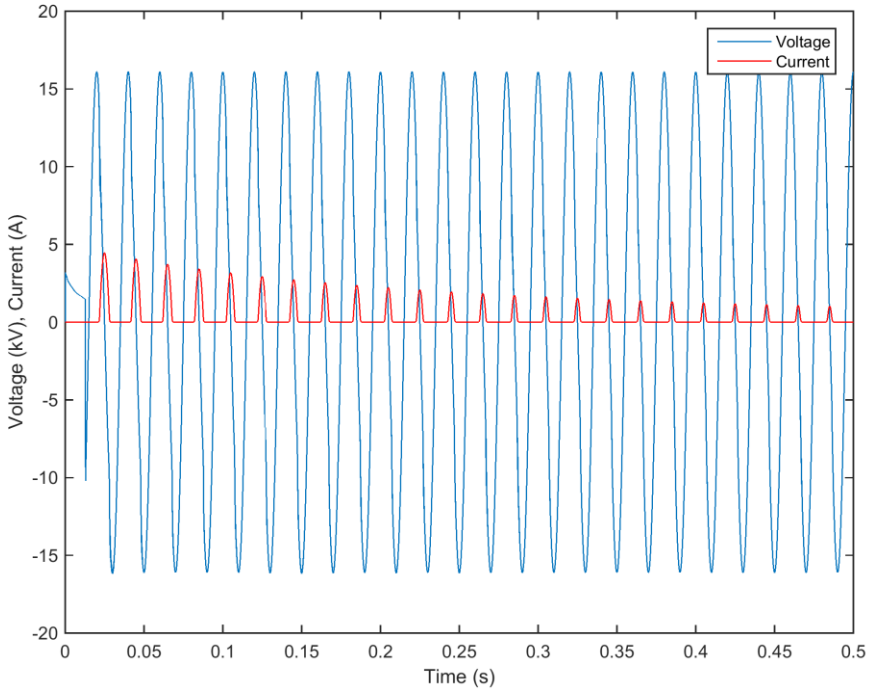

(b) Simulation results when switched on at -9.54 kV

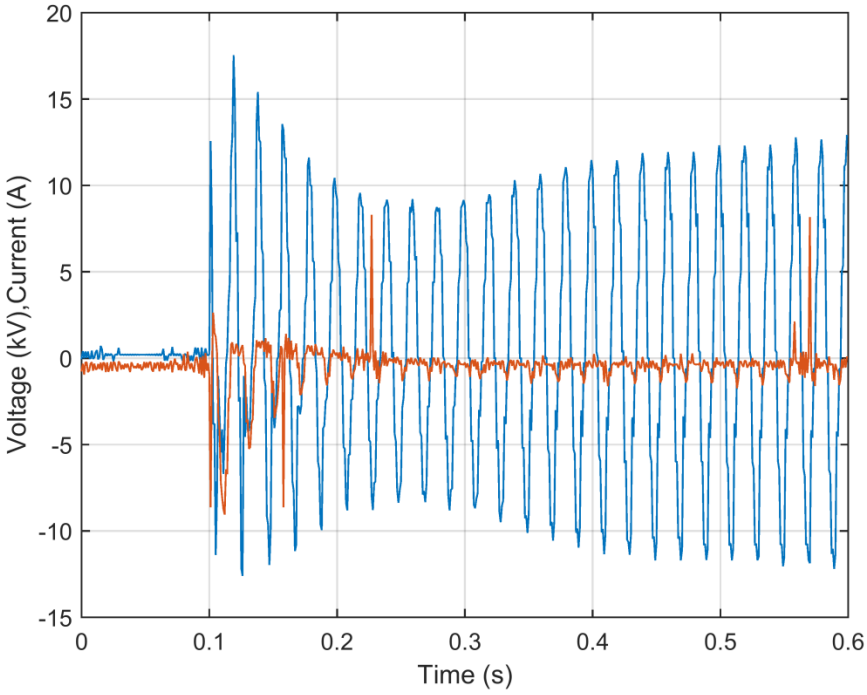

(c) Experimental results when switched on at 13.3 kV

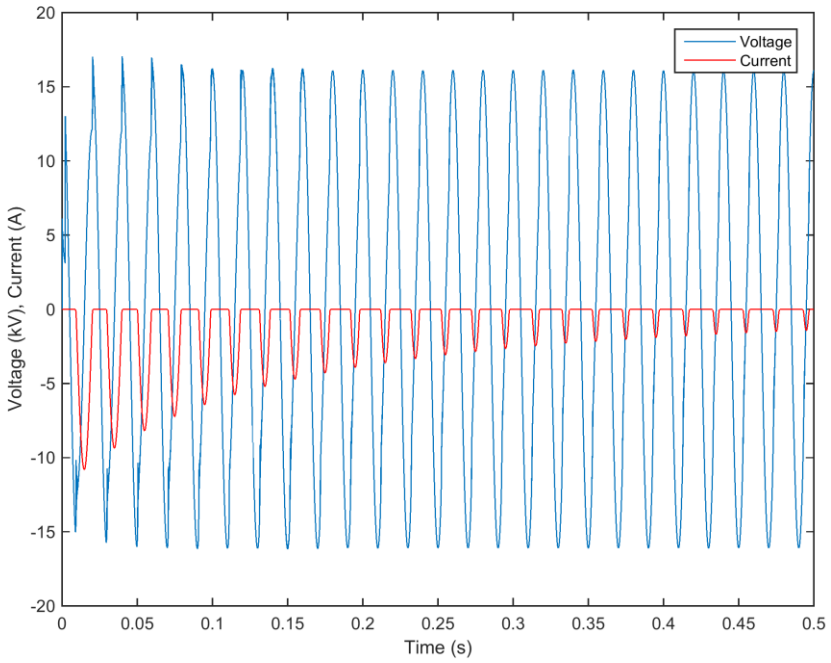

(d) Simulation results when switched on at 13.3 kV

Figure 3 - 7: ATP inrush current simulation results compared to the measurements

In Figure 3 - 7 (a), the transformer was energised at 0.08 seconds by closing the circuit breakers. The voltage was measured to be -9.54 kV when switched on which also results in a 320 degree switching angle.

Using this residual flux in the ATP model produces the results in Figure 3 - 7 (b). The results are similar to that in Figure 3 - 7 (a).

In Figure 3 - 7 (c), the transformer was re-energised at 0.1 seconds and switched on by closing the circuit breakers. The effect was the voltage being approximately 13.3 kV when switched on and this result in a 126 degree switching angle.

Using this residual flux in the ATP model produces the results in Figure 3 - 7 (d). The results are similar to that in Figure 3 - 7 (c).

3.4 Results

The ATP models for the different designed flux density and core material where simulated. The models were built using the same equipment, however their characteristics and values where different. Figure 3 - 8 displays the ATP model. The model types and parameters are in Table 3 - 2.

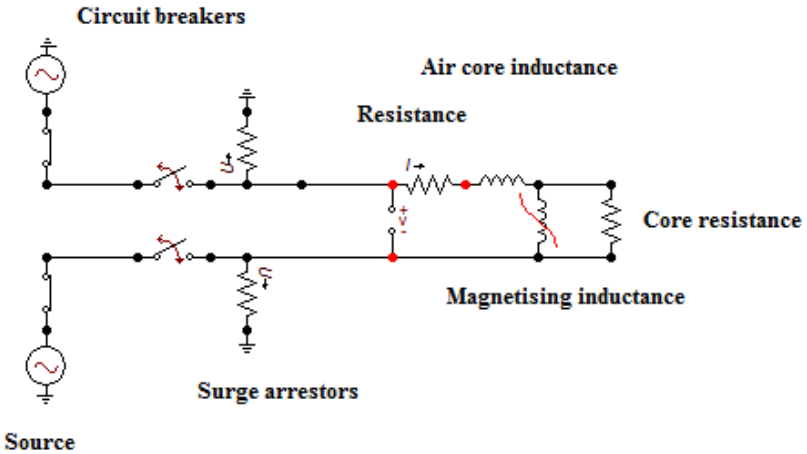

Figure 3 - 8: ATP model

In Table 3 - 2 to Table 3 - 12 and Figure 3 - 9, the following indicates:

- AMDT2 implies AMDT with design flux density at 1.2 T.
- AMDT3 implies AMDT with design flux density at 1.3 T.
- CRGO3 implies CRGO with design flux density at 1.3 T.
- CRGO7 implies CRGO with design flux density at 1.7 T.

Table 3 - 2: Model types and parameters

Model type	**Value**
Source	
Magnitude (rms value)	12.7 kV
Frequency (measured in hertz (Hz))	50 Hz
Circuit breaker measured in millisecond (ms)	tc (ms). Circuit breaker time is controlled
Surge arrestors measured in megaohm (MΩ)	1 MΩ
Resistance (Ω)	300 Ω
Air core inductance calculated using Equation (37) (H)	
AMDT with design flux density at 1.2 T (AMDT2)	13 H
AMDT with design flux density at 1.3 T (AMDT3)	12 H
CRGO with design flux density at 1.3 T (CRGO3)	12 H
CRGO with design flux density at 1.7 T (CRGO7)	7 H
Magnetising inductance	As per flux linkage verse current curves depicted in Figure 3 - 3
Residual flux for magnetising inductance measured in Weber turns (Wb.turns)	0 Wb.turns
Core resistance (MΩ)	100 MΩ

3.4.1 Switching angle

The aim of this test is to demonstrate the effects of source voltage switching angle on inrush currents. The circuit breaker time (tc) is controlled; the model parameters are the same as in Table 3 - 2, besides the circuit breaker time which is varied. The results are displayed in Table 3 - 3.

Table 3 - 3: Circuit breaker start time effects on inrush current

tc (ms)	Current for AMDT3 (A)	Current for CRGO3 (A)	Current for AMDT2 (A)	Current for CRGO7 (A)
0	-0.0024	-0.0031	-0.00076	-0.01953
1	-1.533	-0.0396	-0.9288	-2.3012
2	-3.2	-1.4293	-2.4734	-5.3348
3	-4.352	-2.864	-3.56	-7.44
4	-5.13	-3.82	-4.2829	-8.836
5	**-5.39**	**-4.13**	**-4.52**	**-9.28**
6	-5.0772	-3.7514	-4.2316	-8.727
7	-4.25	-2.736	-3.4599	-7.2457
8	-2.9754	-1.1615	-2.2725	-4.9426
9	-1.36	-0.0202	-0.7673	-1.98
10	0.003985	0.0032	0.00083	0.0256
11	1.62	0.0493	1.01	2.46
12	3.19	1.43	2.47	5.333
13	4.4	2.925	3.6	7.52
14	5.15	3.85	4.308	8.87
15	**5.4**	**4.133**	**4.522**	**9.282**
16	5.075	3.75	4.23	8.725
17	4.25	2.7341	3.46	7.24
18	3.0467	1.2518	2.34	5.07
19	1.446	0.0298	0.848	2.14
20	-0.00239	-0.00309	-0.00076	-0.01953

The results from Table 3 - 3 are displayed graphically in Figure 3 - 9.

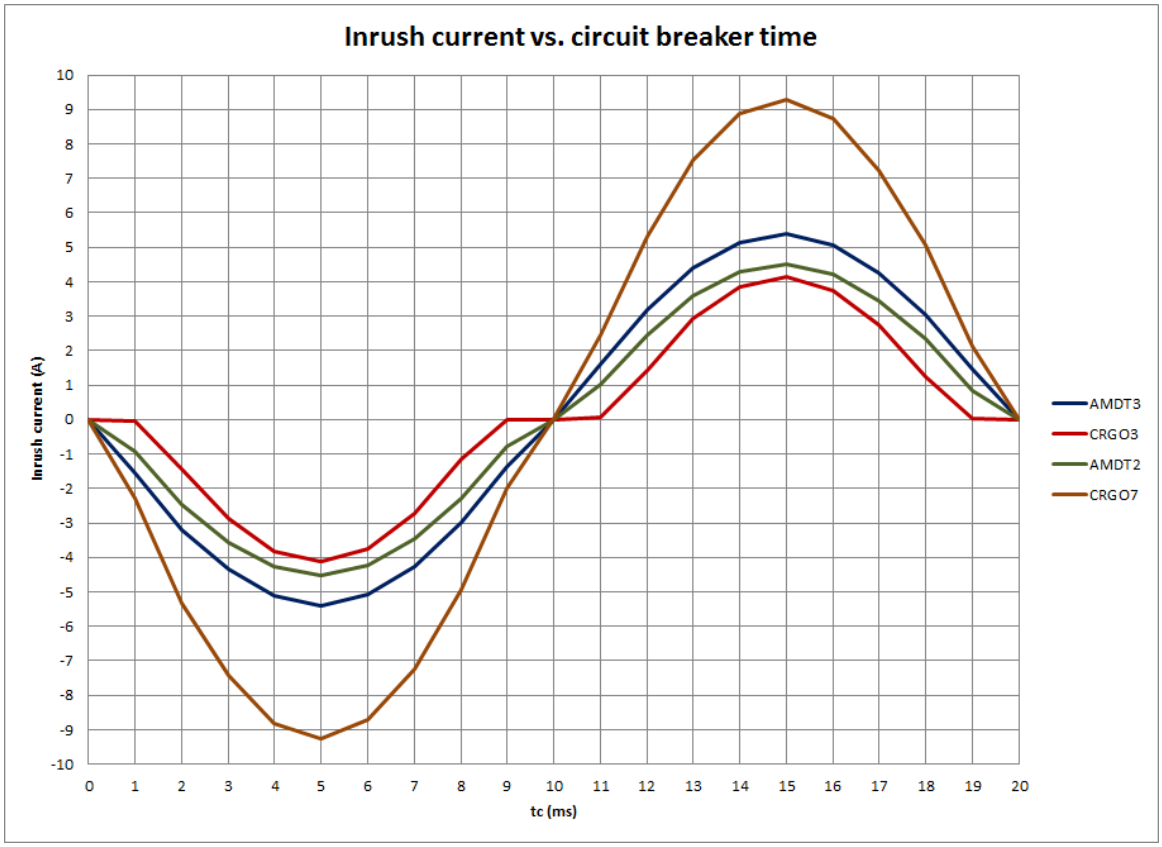

Figure 3 - 9: Graph of inrush current vs. circuit breaker time

From the graph in Figure 3 - 9, it can be seen that the higher the designed flux density, the higher the inrush current. CRGO designed at 1.3 T still has a lower inrush current peak compared to AMDT designed at 1.2 T. It is evident that AMDT has a higher inrush current compared to CRGO at the same designed flux density.

Inrush currents can have magnitudes up to eight times greater than the full load current for AMDT and up to six times greater for CRGO.

The zero crossing of the source voltage is at 5 ms and 15 ms. The is due to the flux being the highest. For the remainder of tests, tc will be set to 15 ms since this results in the highest positive peak.

Moon and Dhatrak in reference [66], examined the performance of inrush currents and revealed when a transformer operated at a 90 degree angle, the inrush current was minimum, when operated at 0 degree angle, it was maximum. However, the source voltage type of the curve was not clear.

3.4.2 Resistance

This test is done at tc = 15 ms. The parameters are kept the same as in the Table 3 - 2 except for the resistance. The resistance is varied between 100 Ω and 500 Ω. The results are displayed in Table 3 - 4.

Table 3 - 4: Resistance effects on inrush currents

Resistance (Ω)	Current for AMDT3 (A)	Current for CRGO3 (A)	Current for AMDT2 (A)	Current for CRGO7 (A)
100	5.57	4.27	4.66	9.8971
200	5.48	4.2	4.6	9.57
300	5.4	4.133	4.522	9.282
400	5.3	4.05	4.45	9
500	5.2	4	4.38	8.7

From Table 3 - 4, it can be seen that as the resistance increases, the peak inrush current decreases.

When varying a value using percentages in Table 3 - 5 to Table 3 – 10; a positive percentage implies addition to the calculated value and negative percentage implies subtracting the calculated value. For example: 50% of calculated value means that it is 50% extra of calculated value and if it is -50% of calculated value, it means 50% less of calculated value.

3.4.3 Residual flux for magnetising inductance

This test is done at tc = 15 ms. The parameters are kept the same as in the Table 3 - 2 except for the residual flux. The residual flux is varied between -100% to 100% of its calculated value to display the effects of residual flux on inrush currents. The calculated residual flux values are rounded up and displayed in Table 3 - 5 to Table 3 - 7.

3.4.3.1 AMDT and CRGO designed at 1.3 T

For these transformers, the residual flux = 91 Wb.turns. Table 3 - 5 displays the inrush current peak values when the residual flux for the magnetising inductor is varied for AMDT and CRGO designed at 1.3 T.

Table 3 - 5: Residual flux effects on inrush currents for cores with design flux density = 1.3 T

Percentage of calculated value	Residual flux (Wb.turns)	Current for AMDT3 (A)	Current for CRGO3 (A)
-100%	0	5.4	4.133
-75%	23	6.4	4.35
-50%	46	7.576	4.97
-25%	69	8.7	5.86
Calculated value	91	9.538	6.72
25%	114	9.7	7.38
50%	137	9.45	7.55
75%	160	9.02	7.53
100%	183	8.47	7.388

3.4.3.2 AMDT designed at 1.2 T

For this transformer, the residual flux = 91 Wb.turns. Table 3 - 6 displays the inrush current peak values when the residual flux for the magnetising inductor is varied for AMDT designed at 1.2 T.

Table 3 - 6: Residual flux effects on inrush currents for AMDT with design flux density = 1.2 T

Percentage of calculated value	Residual flux (Wb.turns)	Current for AMDT2 (A)
-100%	0	4.522
-75%	23	5.48
-50%	46	6.6
-25%	69	7.67
Calculated value	91	8.58
25%	114	9
50%	137	8.9
75%	160	8.57
100%	183	8.17

3.4.3.3 CRGO designed at 1.7 T

For this transformer, the residual flux = 95 Wb.turns. Table 3 - 7 displays the inrush current peak values when the residual flux for the magnetising inductor is varied for CRGO designed at 1.7 T.

Table 3 - 7: Residual flux effects on inrush currents for CRGO with design flux density = 1.7 T

Percentage of calculated value	Residual flux (Wb.turns)	Current for CRGO7 (A)
-100%	0	9.282
-75%	24	9.35
-50%	48	9.85
-25%	71	10.69
Calculated value	95	11.36
25%	119	11.44
50%	143	11.2
75%	166	10.637
100%	190	10

From the results in the Table 3 - 5 to Table 3 - 7, as the residual flux increases, so do the inrush currents.

3.4.4 Air core inductance

This test is done at tc = 15 ms. The parameters are kept the same as in the Table 3 - 2 except for the air core inductance. This is varied between -20% to 20% of its calculated value to determine its effects on inrush currents.

3.4.4.1 AMDT and CRGO designed at 1.3 T

The calculated air core inductance using Equation (37) is 12 H. Table 3 - 8 displays the inrush current peak values when the air core inductance is varied for AMDT and CRGO designed at 1.3 T.

Table 3 - 8: Air core inductance effects on inrush currents for cores with design flux density = 1.3 T

Percentage of calculated value	Inductance (H)	Current for AMDT3 (A)	Current for CRGO3 (A)
-20%	9.6	6.25	4.97
-15%	10.2	6.01	4.73
-10%	10.8	5.79	4.51
-5%	11.4	5.58	4.316
Calculated value	12	5.4	4.133
5%	12.6	5.2	3.9652
10%	13.2	5.04	3.81
15%	13.8	4.88	3.66
20%	14.4	4.73	3.5359

3.4.4.2 AMDT designed at 1.2 T

The calculated air core inductance using Equation (37) is 13 H. Table 3 - 9 displays the inrush current peak values when the air core inductance is varied for AMDT designed at 1.2 T.

Table 3 - 9: Air core inductance effects on inrush currents for AMDT with design flux density = 1.2 T

Percentage of calculated value	Inductance (H)	Current for AMDT2 (A)
-20%	10.4	5.252
-15%	11.05	5.0484
-10%	11.7	4.86
-5%	12.35	4.68
Calculated value	13	4.522
5%	13.65	4.37
10%	14.3	4.2275
15%	14.95	4.0947
20%	15.6	3.97

3.4.4.3 CRGO designed at 1.7 T

The calculated air core inductance using Equation (37) is 7 H. Table 3 - 10 displays the inrush current peak values when the air core inductance is varied for CRGO designed at 1.7 T.

Table 3 - 10: Air core inductance effects on inrush currents for CRGO with design flux density = 1.7 T

Percentage of calculated value	Inductance (H)	Current for CRGO7 (A)
-20%	5.6	10.88
-15%	5.95	10.43
-10%	6.3	10
-5%	6.65	9.63
Calculated value	7	9.282
5%	7.35	8.95
10%	7.7	8.65
15%	8.05	8.36
20%	8.4	8.09

From the results in Table 3 - 8 to Table 3 - 10, an increase in air core inductance results in a decrease in inrush currents.

3.4.5 Effect of supply voltage on inrush currents

Referring to Figure 3 - 10, as the installation site moves further away, the voltage decreases because of voltage drop on the network.

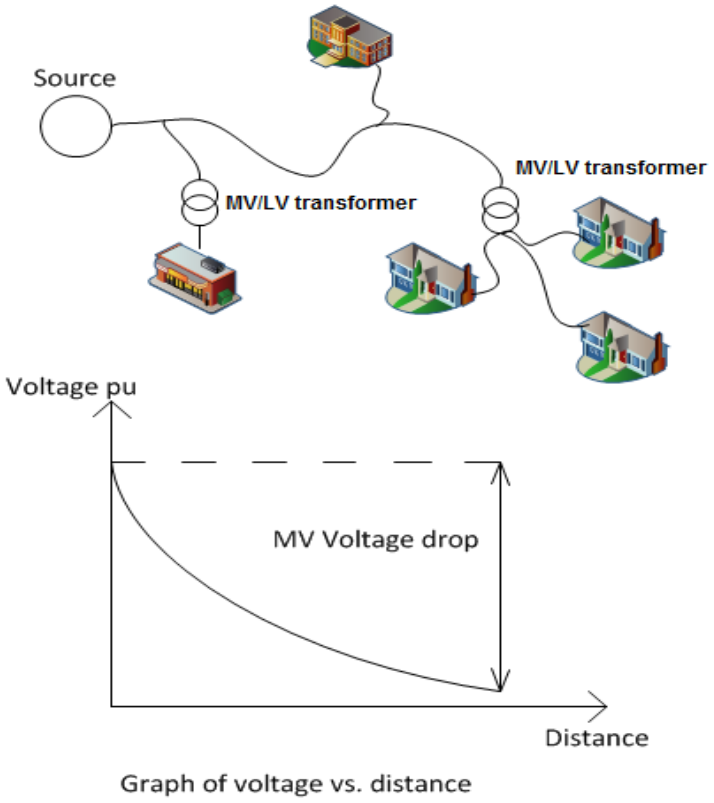

Figure 3 - 10: Illustration of the effects of voltage drop on a network

From Eskom's Distribution voltage regulation and apportionment limits in reference [67]; in Eskom the percentage voltage (%V) maximum limit is 106% and minimum limit is 85% for distribution networks. Each network has a normal and abnormal minimum and maximum %V limits that need to be adhered to depending on the class and tap zone that each network is classified as. The %V for the majority type of networks within Eskom's distribution grid during abnormal conditions for percentage minimum voltage (%Vmin) is 93.5% or 91% and percentage maximum voltage (%Vmax) is 105%. At Eskom the voltage source for distribution networks is simulated at %V. As the installation site moves further down the source, a voltage drop is seen.

The reason percentage voltage was chosen and not distance was due to the diverse scattering of customers connected to networks. Hence, percentage voltage can be universally applied to overcome the diversity of customer placements on distribution networks.

The models were simulated under various voltage drop conditions to determine the inrush currents.

This test is done at tc = 15 ms. The parameters are kept the same as in the Table 3 - 2 except for the source voltage (Vs measured in kV). Equation (38) was used to calculate the voltage split per source. The results are displayed in Table 3 - 11.

In Table 3 - 11, 22 kV is nominal voltage expressed as 100%.

Table 3 - 11: Voltage drop effects on inrush current

Percentage of calculated value	Source voltage (kV)	Current for AMDT3 (A)	Current for CRGO3 (A)	Current for AMDT2 (A)	Current for CRGO7 (A)
105%	23.1	5.95	4.82	5.05	10.28
100%	22	5.4	4.133	4.522	9.282
95%	20.9	4.83	3.45	4	8.27
90%	19.8	4.25	2.75	3.477	7.25
85%	18.7	3.7	2.076	2.95	6.24
80%	17.6	3.13	1.377	2.43	5.2

From Table 3 - 11, as the voltage decreases, so does the peak inrush current. This is expected as a higher voltage results in a higher flux in the core.

3.4.6 Comparison between calculated and simulation results

Equation (34) is used to calculate the peak inrush currents for the single phase transformers. The calculated results are compared to the ATP simulated results when tc = 15 ms. The results are displayed in Table 3 - 12. The ATP results are assumed to be more accurate than the calculated results as it accounts for flux leakage around the winding and the damping resistance of the circuit.

Table 3 - 12: Calculated vs. simulated results for inrush currents

	Current for AMDT3 (A)	Current for CRGO3 (A)	Current for AMDT2 (A)	Current for CRGO7 (A)
Calculated	10.6115	7.3464	9.0417	13.6254
Simulation	5.4	4.133	4.522	9.282

3.5 Discussion and conclusion

The peak flux occurs at the zero crossing of the voltage. AMDT designed with 1.3 T experiences a higher inrush current compared to CRGO designed with 1.3 T.

The following parameters are proportional to inrush currents:

- Residual flux: AMDT and CRGO with design flux density of 1.3 T experienced the highest peak inrush current of 8.47 A and 7.388 A respectively when the residual flux was the highest (100% of the calculated value).
- Source voltage: AMDT and CRGO with design flux density of 1.3 T experienced the highest peak inrush current of 5.95 A and 4.82 A respectively when the source voltage was the highest (105% of the nominal voltage).

The following parameters are inversely proportional to inrush currents:

- Resistance: AMDT and CRGO with design flux density of 1.3 T experienced the highest peak inrush current of 5.57 A and 4.27 A respectively when the resistance was the lowest (100 Ω).
- Air core inductance: AMDT and CRGO with design flux density of 1.3 T experienced the highest peak inrush current of 6.25 A and 4.97 A respectively when the air core inductance was the lowest (-20% of the calculated value). The air core inductance is dependent on the number of turns. The higher the magnetic flux density design point, the lower the turns and the inductance.

The conclusions from this chapter indicate how the above mentioned parameters impact on inrush currents of single phase transformers with AMDT and CRGO cores. Hence, by changing certain transformer parameters, it is possible to design a transformer that may experience lower inrush currents.

4 ELECTROMAGNETIC FORCES

When a transformer is subjected to forces, the coils are stressed. Axial forces are due to the unbalance in the electrical centres of the windings and this causes the coils of the two windings to slide against each other which may result in transformer failure [35].

Electromagnetic forces have the ability to do the following [68]:

- The inner winding radius reduces.
- The outer winding radius increases.
- The height of the winding reduces due to the axial forces.
- Axial component of leakage flux results in forces created in the radial direction.
- Radial component of leakage flux results in forces created in the axial direction.

The windings and internal structures of the transformer are exposed to mechanical forces because of the inrush currents and short-circuit currents. These forces are axial and radial forces and they are related to magnetic flux interactions and current. The forces, depending on magnitude, may lead to winding displacement and subsequent dielectric failure [15].

This chapter investigates the forces on the windings of the transformer using Finite Element Method Magnetics (FEMM), where inrush and short-circuit currents are simulated and compared for AMDT and CRGO transformers. Matlab code was written to extract the data from the FEMM models to obtain graphs for the axial and radial forces.

Steurer and Fröhlich in reference [69] investigated mechanical stresses of inrush and short-circuit currents on high voltage power transformers. The authors' showed that the axial forces due to inrush currents are higher than short-circuit currents. This was done using a two dimensional model (magnetic field calculations) and comparing the results with a three dimensional model (done using FEM).

Chapter 3 concluded that the peak inrush currents can have magnitudes up to eight times greater than the full load current for AMDT and up to six times greater for CRGO. AMDT has a higher inrush current compared to CRGO with the same design flux density.

4.1 Forces experienced by transformer windings

Mechanical forces occur in the windings. This is due to interactions of current in the windings as well as the magnetic flux distribution. The force experienced by a current carrying conductor is given by [69]:

$$\vec{F} = \int \vec{J} \times \vec{B} dV \tag{39}$$

Where [69]:

$\vec{B}$=flux density measured in tesla (T)

$\vec{F}$= force measured in newton (N)

$\vec{J}$=current density in the coil measured in ampere per square metre (A/m^2)

V = volume of the coil measured in cubic metre (m^3)

Equation (39) can be broken into radial and axial forces illustrated in Figure 4 - 1 and Figure 4 – 2. The equations are [15], [69]:

$$F_r = B_a \times J \times V \tag{40}$$

$$F_a = B_r \times J \times V \tag{41}$$

Where [15], [69]:

B_a = axial flux (T)

B_r = radial flux (T)

F_a = axial force (N)

F_r = radial force (N)

J = current density in the coil (A/m^2)

V = volume of the conductor (m^3)

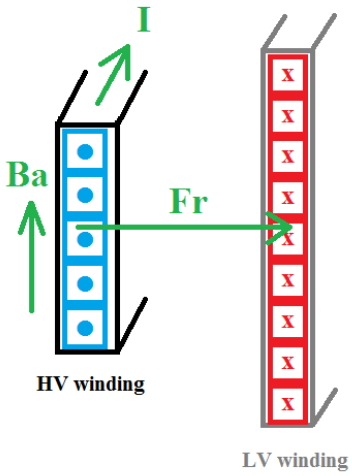

Figure 4 - 1: Radial force

The sum of all the electromagnetic forces on the winding is the radial force. Failures due to radial forces are [68]:

- Inner winding buckling.
- Outer winding diameter increases.
- Spiralling occurs when the end turn tips in the helical type winding make a tangential shift.

Compressive stress results in the inner winding when the radial forces are inwards. Tensile stress results in the outer winding when the radial forces are outwards. The mean value across the winding may be used for the withstand analysis [68].

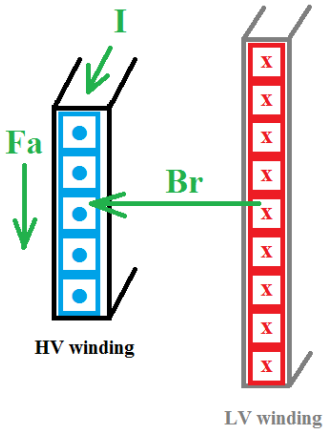

Figure 4 - 2: Axial force

The axial force of each conductor as displayed in Figure 4 - 3 consists of an electromagnetic force as well as the electromagnetic forces exerted by the adjacent conductors.

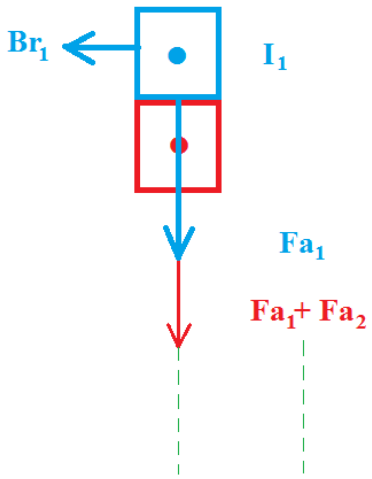

Figure 4 - 3: Forces experienced per conductor

Failures due to axial forces are [68]:

- The conductors tilt.
- Axial bending occurs between the spacers.
- The end turn tips of the helical type windings spiral.
- Mechanical withstand of core clamps, spacers and yoke insulation decreases.

Axial forces occur as a result of load tap changer or de-energised tap changer in HV winding operation since it changes the distribution of the ampere turn [15].

The windings for both transformer core types tested were rectangular shaped and layer type.

Chapter 2.7.2 explains that rectangular or square windings are not as strong as circular windings for short-circuits.

Winding arrangement and core shape affects leakage flux. Winding depth, length and size affects copper losses and mutual flux in transformers [70].

Flux distribution has an impact on the forces experienced by transformers. During short-circuit current conditions; current density exists in both high voltage (HV) and LV windings.

This causes the magnetic field intensity to be very high between both windings. The flux flowing in the core is the design flux and there is leakage flux between the HV and LV windings as seen Figure 4 - 4. The black arrows indicate the direction of the flux density.

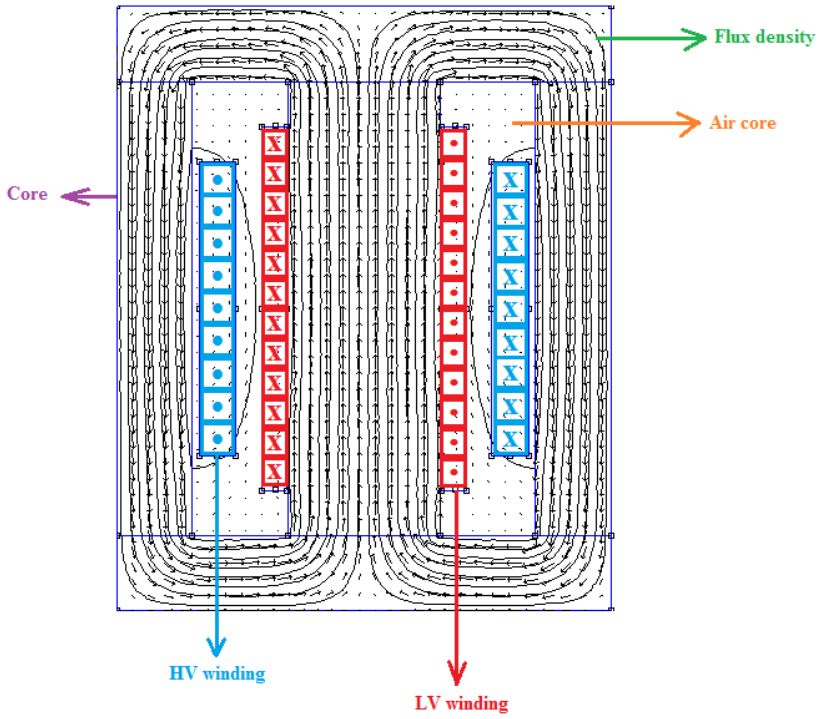

Figure 4 - 4: Illustration of flux in the core during short-circuit current conditions

Short-circuit current results in [68]:

- A mechanical force as a result of the interaction between the current and flux.
- An increase in the temperature of the transformer if the short-circuit current is sustained for a few seconds or longer. This heat contributes to the losses of the transformer.

The International Electrotechnical Commission (IEC) recommends the following criteria for short-circuit test, these are [68]:

- Short-circuit impedance varied.
- Routine test been repeated with successful results.
- Active parts must not have noticeable physical damages throughout the test.
- Low voltage impulse and frequency response analysis are additional recommendations.

During inrush current conditions, current density only exists in the HV winding. This causes the magnetic field intensity to be slightly higher around the HV windings compared to the surroundings. The flux saturates in the core and thus is forced out of the core as seen in Figure 4 - 5 and explained in Chapter 3.1. The black arrows indicate the direction of the flux density.

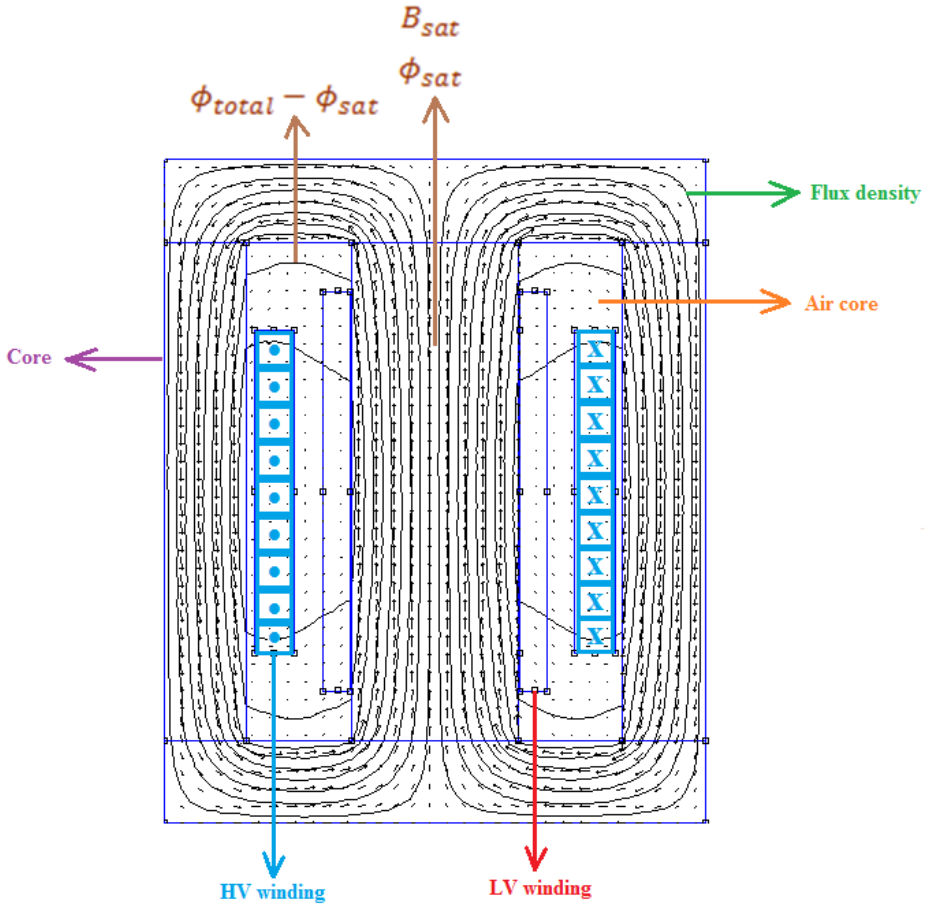

Figure 4 - 5: Illustration of flux in the core during inrush current conditions

The following govern fault current [68]:

- Source impedance.
- Open-circuit voltage.
- The instant of the fault onset.

The risk for short-circuit failure mainly depends on [68]:

- Source impedance.
- The instant of the fault onset.

Generally, transformers in service might not experience the maximum force. There is a possibility that transformers may experience forces of about 20% to 40% of the peak theoretical force [68].

Equation (42) to Equation (44) demonstrate the relationship between the force and current [68]:

$$F \propto IB \tag{42}$$

$$B \propto I \tag{43}$$

Equation (42) and Equation (43) result in the following [68]:

$$F \propto I^2 \tag{44}$$

Equation (44) proves that the force is proportional to the square of the instantaneous current [68].

Where [68]:
B = flux density (T)
F = force (N)
I = current measured in ampere (A)

4.2 Finite element model

Finite element is commonly used to determine the flux distributions in the transformer models. Other uses are solving axisymmetric and two dimensional planar problems [71].

de Azevedo, Delaiba, de Oliveira, Carvalho and de Souza Bronzeado in reference [72] proposed a method (time domain approach) to calculate mechanical stresses which occur under short-circuit conditions in the windings. The results were compared to a finite elements software based model. The investigation was carried out for stresses and radial forces. In conclusion, time domain approach is acceptable to achieve the internal forces of the transformer and stress evaluation.

de Azevedo, Rezende, Delaiba, de Oliveira, Carvalho and de Souza Bronzeado in reference [73] investigated transformer internal electromagnetic forces due to external faults (short-circuit conditions). Finite element method (FEM) was used to model and simulate a three-phase transformer. The simulated results were compared to the calculated results obtained from using mechanical and electrical equations. Both results were similar. The FEM model showed that using tap sections may result in huge changes in magnetic flux distribution, which causes higher radial magnetic field density and axial force inside the transformer. Axial force is accountable for damages to the structures that support the windings in the transformer. High currents created by an external short-circuit have a huge effect on flux path, which causes higher radial forces due to increase in the axial leakage field. Axial forces are responsible for causing a more damaging effect on transformers.

The single phase AMDT and CRGO transformers were simulated using FEMM to determine the magnetic flux density distribution in the windings for inrush and short-circuit currents.

The voltage ratio and turns ratio were calculated based on the transformer parameters. The inrush currents were determined in the ATP simulation as described in Chapter 3.

The B-H curves used in the FEMM simulations for CRGO and AMDT are displayed in Figure 2 - 6 in Chapter 2.10. Both models were simulated at a design flux density of 1.3 T. The boundary condition types for the models were set to zero so that FEMM confides the simulations to the working area, which are models only. Models were set-up to a certain depth.

The FEMM models are confined to the core, windings and space between the windings of the transformers (also called air core). The spaces are defined as air which does not conduct and has a relative permeability of one; this is the same for oil.

The air core corners of the core are curved and not rectangular like in FEMM. Unfortunately, the corners could only be drawn rectangular. This rectangular air core results in higher flux at the corners. According to [10], this shape causes non-uniform radial electromagnetic forces which may alter the coil shape depending on the magnitude of the forces.

A cubic spline line is used by FEMM to interpolate between the entered B-H curve data points. The disadvantage is that this function is problematic for the sharp ‘knee’ point of the

B-H curve. Hence, FEMM uses a three-point moving average filter to obtain a single-valued curve. If there are still problems, then extra points by the 'knee' point can be added. Adding extra points by the 'knee' point is more beneficial since FEMM extrapolates the end of the entered B-H curve linearly if out of range flux density or field intensity levels are encountered making the material appear more permeable compared to reality at high flux densities [74], [75].

During short-circuit conditions; the B-H curve is a nonlinear curve since there is no additional flux in the core.

When modelling and simulating the inrush current on FEMM, only the high voltage winding is simulated with current.

For the AMDT and CRGO designed at 1.3 T, the transformer details are as follows:

- N_1= 5168 turns (primary winding turns).
- N_2= 60 turns (secondary winding turns).

The turns ratio for these two models are kept the same to keep the models as similar as possible. The rated primary current (I_{rated}) is 0.73 Ampere (A) and primary voltage is 22 kV for both transformers. The secondary voltage is controlled using the tap changer position.

From the above details, the secondary current (I_2) can be calculated from Equation (17) in Chapter 2.1.2**.**

The flux density (|B|) for the models is determined by drawing a horizontal contour line in the centre of the core from the front of one HV winding to the other as displayed in Figure 4 - 6.

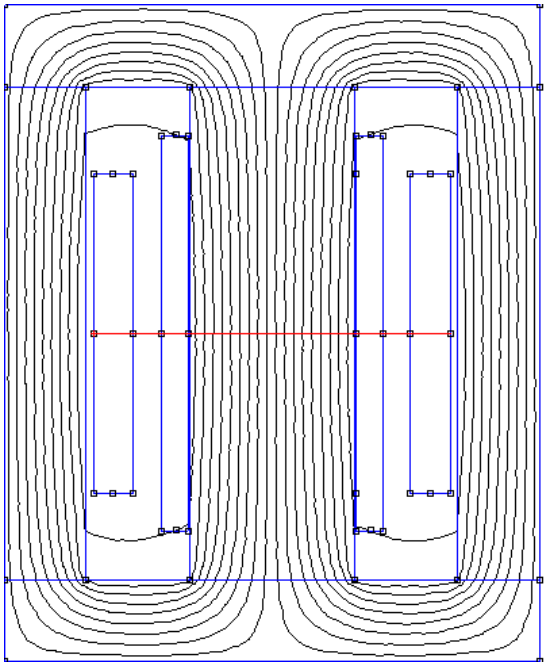

Figure 4 - 6: Obtaining peak flux density

The maximum flux density for the models in this chapter is higher than the peak flux density values in Table 4 - 1 to Table 4 - 6. The reason is the peak flux density displayed on the tables is the maximum flux density from the outside of the HV winding through to the opposite side of the HV winding as displayed by the red contour line in Figure 4 - 6.

The models are tested using 10 A and 5 A for the primary windings for short-circuit and inrush current models. These values were selected from the range of inrush current results in Chapter 3. One disadvantage with AMDT compared to CRGO with the same design flux density is that the inrush currents are higher in AMDT.

4.3 FEMM models for no-load test

This test is done to validate the FEMM model. The secondary current is set to zero and the primary current is increased from zero such that the peak supply voltage magnitude is reached. Supply voltage is 22 kV. Hence, the primary current to achieve this is called the magnetisation current. |B| determined in these models is the designed flux. Table 4 - 1 displays the input values and simulation results.

Table 4 - 1: Data for no-load simulations

Symbol	AMDT	CRGO
$I_1 = I_{mag}$	0.758 mA	28.325 mA
V_1	31 112.1 V	31 113.2 V
$\|B_p\|$	1.305 T	1.302 T

Where:

$|B_p|$ = peak flux density (T)

I_{mag} = magnetisation current (A)

I_1 = primary current (A)

V_1 = peak primary voltage measured in volt (V)

Figure 4 - 7 and Figure 4 - 8 displays the magnetic flux density distribution of the no-load models for AMDT and CRGO where the upper limit is ~1.4 T. The AMDT model has a higher and more evenly distribution of magnetic flux density in the core compared to the CRGO model.

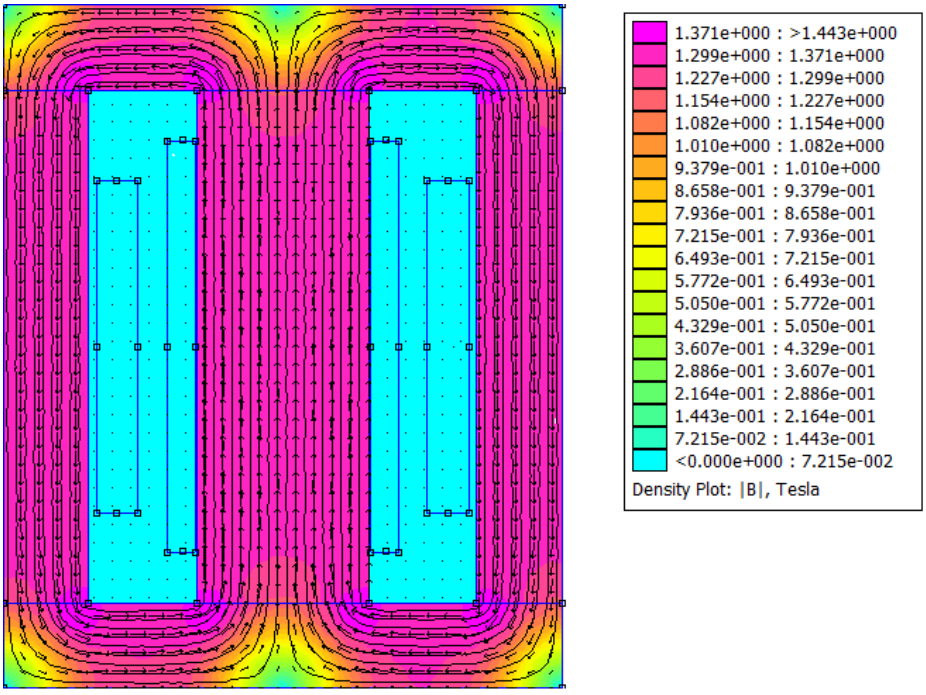

Figure 4 - 7: Magnetic flux density for no-load AMDT model

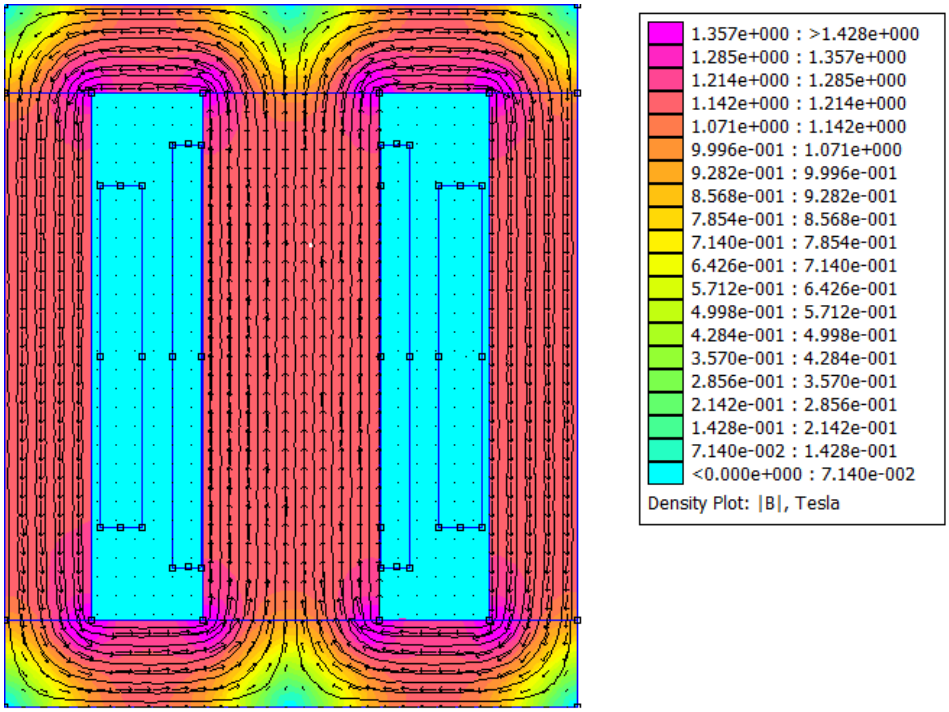

Figure 4 - 8: Magnetic flux density for no-load CRGO model

4.4 FEMM models for full load test

This test is done using the rated current and magnetisation current. The primary voltage should be as close as possible to the peak supply voltage (31 113 V). Using Equation (17) in Chapter 2.1.2, the secondary current was calculated. For these models, the input parameters were the primary and secondary currents. Table 4 - 2 displays their values and simulation results.

Table 4 - 2: Data for full load simulations

Symbol	AMDT	CRGO
$I_1 = I_{rated} + I_{mag}$	0.730758 A	0.758325 A
V_1	30 764.5 V	31 338.6 V
I_2	-62.88 A	-62.88 A
$\|B_p\|$	1.28 T	1.27 T

Where:

I_2 = secondary current (A)

Figure 4 - 9 and Figure 4 - 10 displays the magnetic flux density distribution of the full load models for AMDT and CRGO where the upper limit is ~1.4 T. The AMDT model has a higher and more evenly distribution of magnetic flux density in the core compared to the CRGO model.

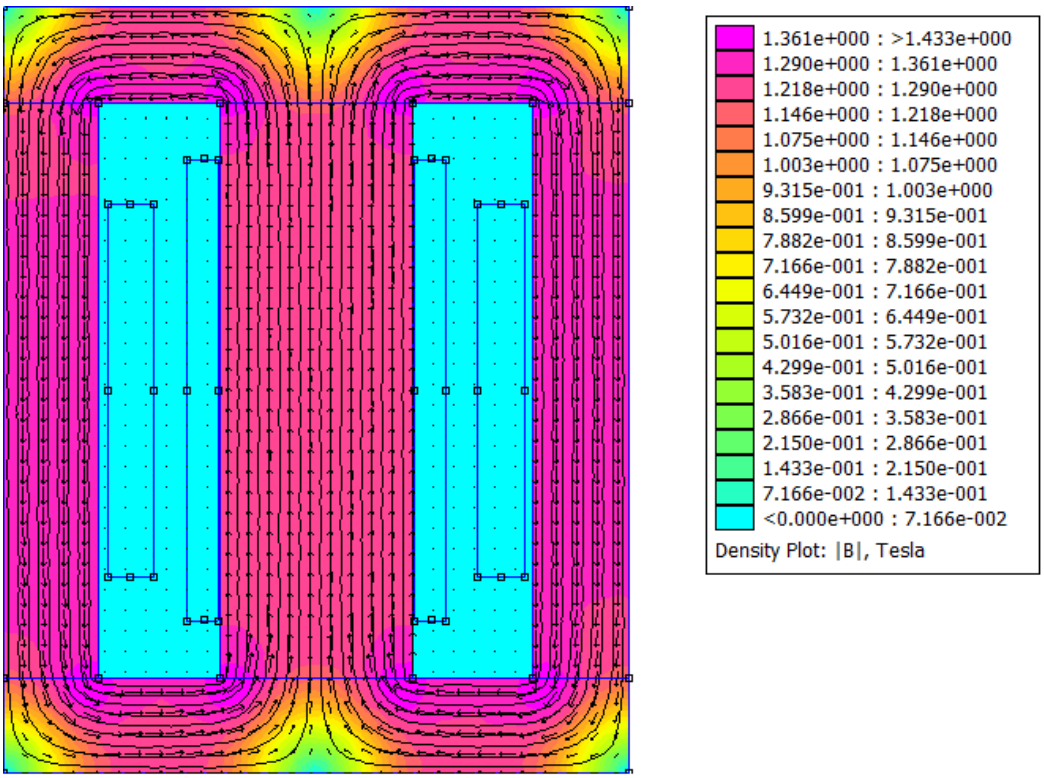

Figure 4 - 9: Magnetic flux density for full load AMDT model

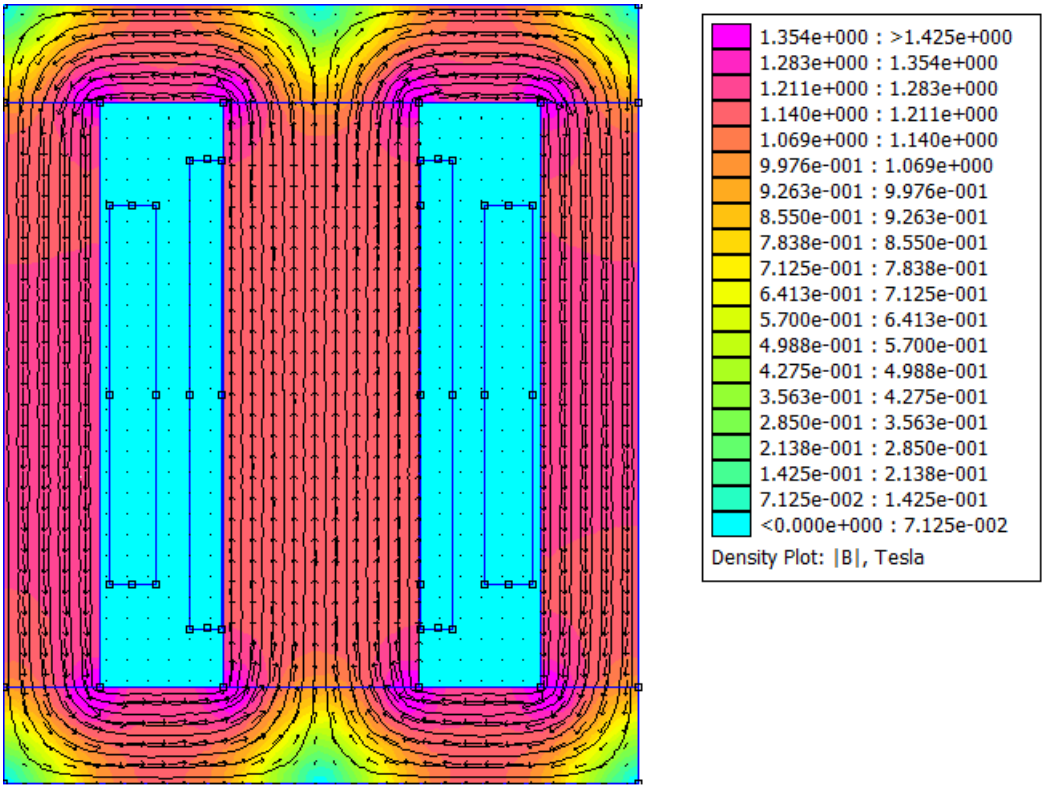

Figure 4 - 10: Magnetic flux density for full load CRGO model

4.5 FEMM models for short-circuit test

This test is done to determine the flux density during short-circuit conditions and is simulated using the short-circuit FEMM model. The short-circuit test is performed on the models when the primary current is 10 A and 5 A. Using Equation (17) in Chapter 2.1.2, the secondary current is calculated.

4.5.1 10 A FEMM models short-circuit test

For these models, the input parameters were the primary and secondary currents. Table 4 - 3 displays their values and simulation results.

Table 4 - 3: Data for 10 A short-circuit simulations

Symbol	AMDT	CRGO
$I_1 = I_1 + I_{mag}$	10.000758 A	10.028325 A
V_1	35 693.2 V	38 089 V
I_2	-861.324 A	-860.6 A
$\|B_p\|$	1.305 T	1.305 T

Figure 4 - 11 and Figure 4 - 13 displays the magnetic flux density distribution for AMDT and CRGO under short-circuit conditions for a primary current of 10 A. Figure 4 - 12 and Figure 4 - 14 displays the magnetic field intensity for AMDT and CRGO under short-circuit conditions for a primary current of 10 A.

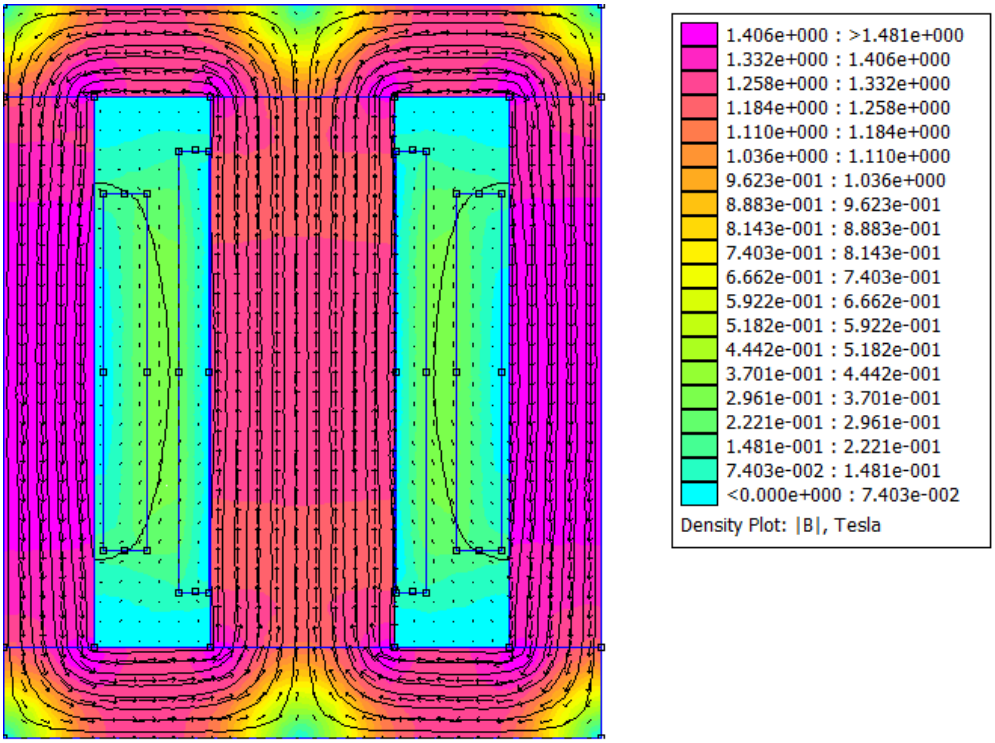

Figure 4 - 11: Magnetic flux density for 10 A short-circuit AMDT model

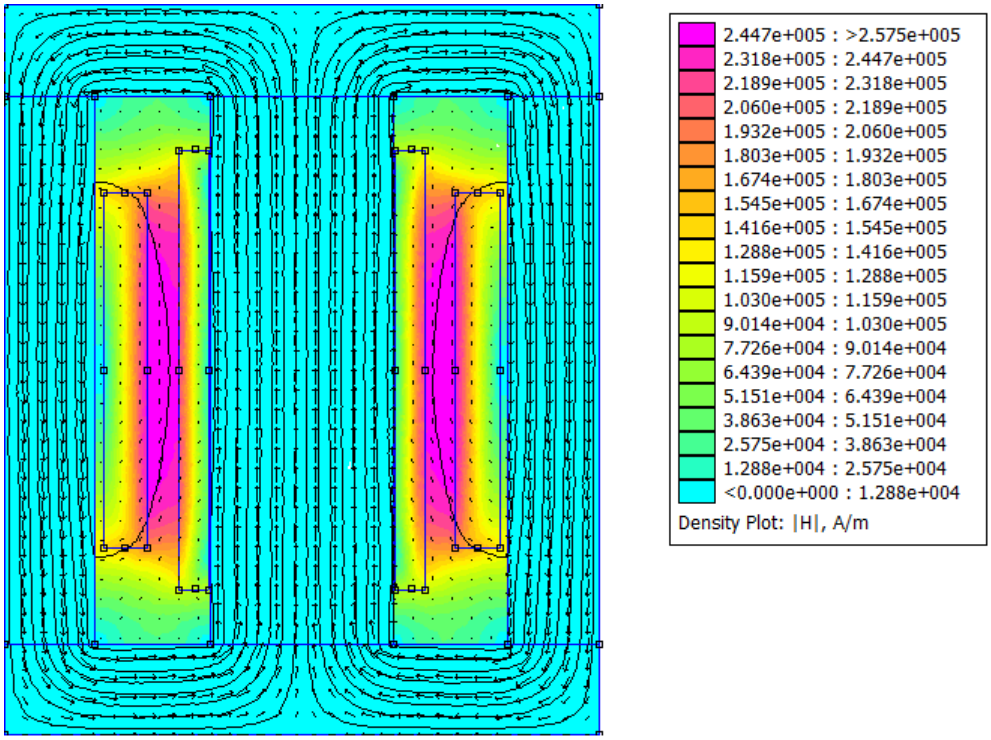

Figure 4 - 12: Magnetic field intensity for 10 A short-circuit AMDT model

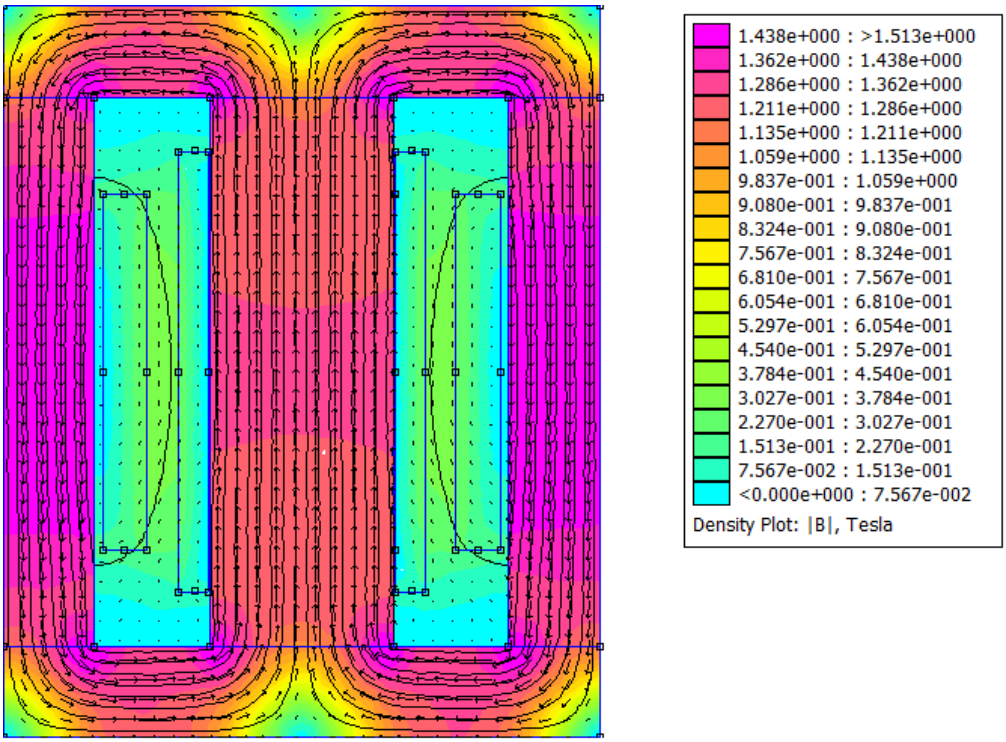

Figure 4 - 13: Magnetic flux density for 10 A short-circuit CRGO model

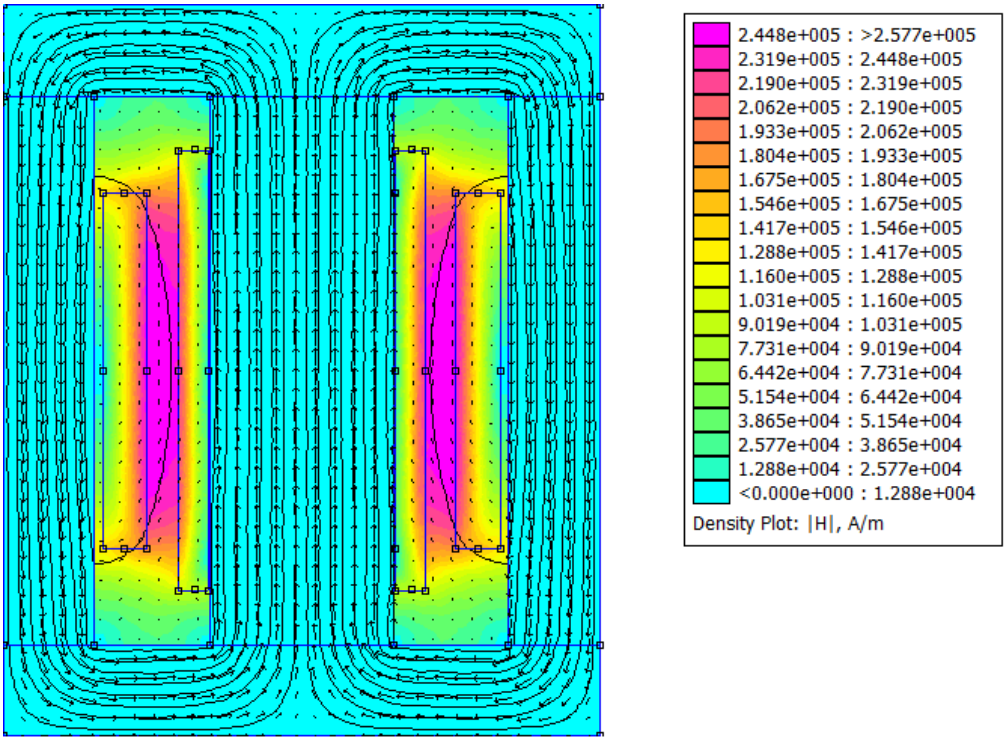

Figure 4 - 14: Magnetic field intensity for 10 A short-circuit CRGO model

4.5.2 5 A FEMM models short-circuit test

For these models, the input parameters were the primary and secondary currents. Table 4 - 4 displays their values and simulation results.

Table 4 - 4: Data for 5 A short-circuit simulations

Symbol	AMDT	CRGO
$I_1 = I_1 + I_{mag}$	5.000758 A	5.028325 A
V_1	29 064.2 V	35 931.4 V
I_2	-430.796 A	-430.12 A
$\|B_p\|$	1.30674 T	1.30467 T

Figure 4 - 15 and Figure 4 - 17 displays the magnetic flux density distribution for AMDT and CRGO under short-circuit conditions for a primary current of 5 A. Figure 4 - 16 and Figure 4 - 18 displays the magnetic field intensity for AMDT and CRGO under short-circuit conditions for a primary current of 5 A.

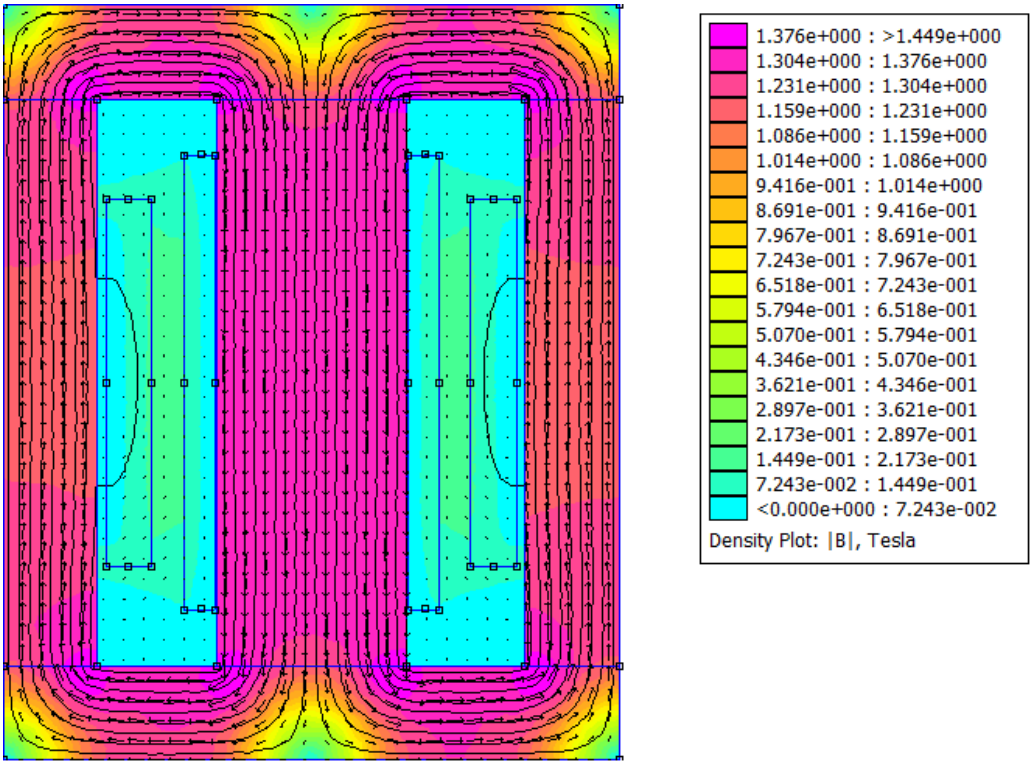

Figure 4 - 15: Magnetic flux density for 5 A short-circuit AMDT model

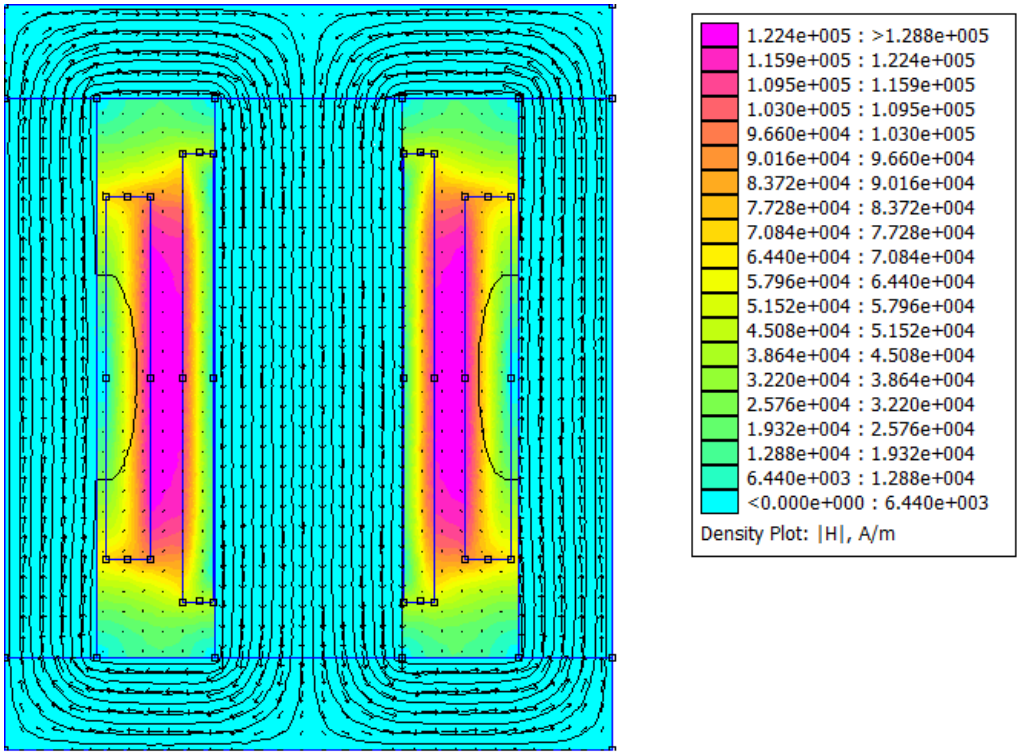

Figure 4 - 16: Magnetic field intensity for 5 A short-circuit AMDT model

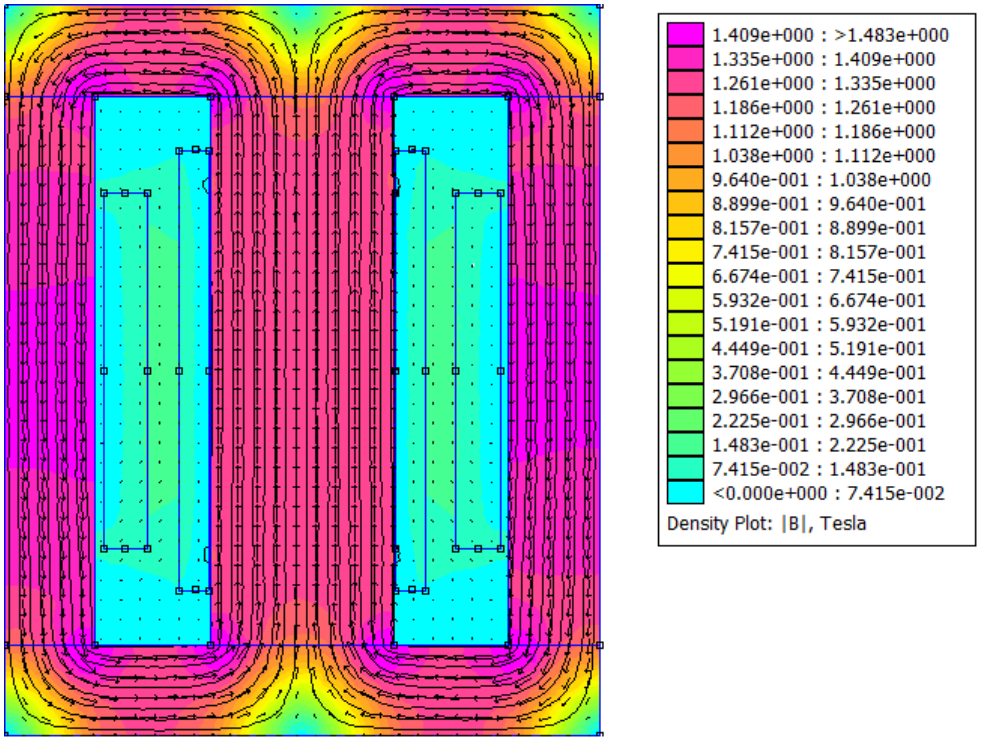

Figure 4 - 17: Magnetic flux density for 5 A short-circuit CRGO model

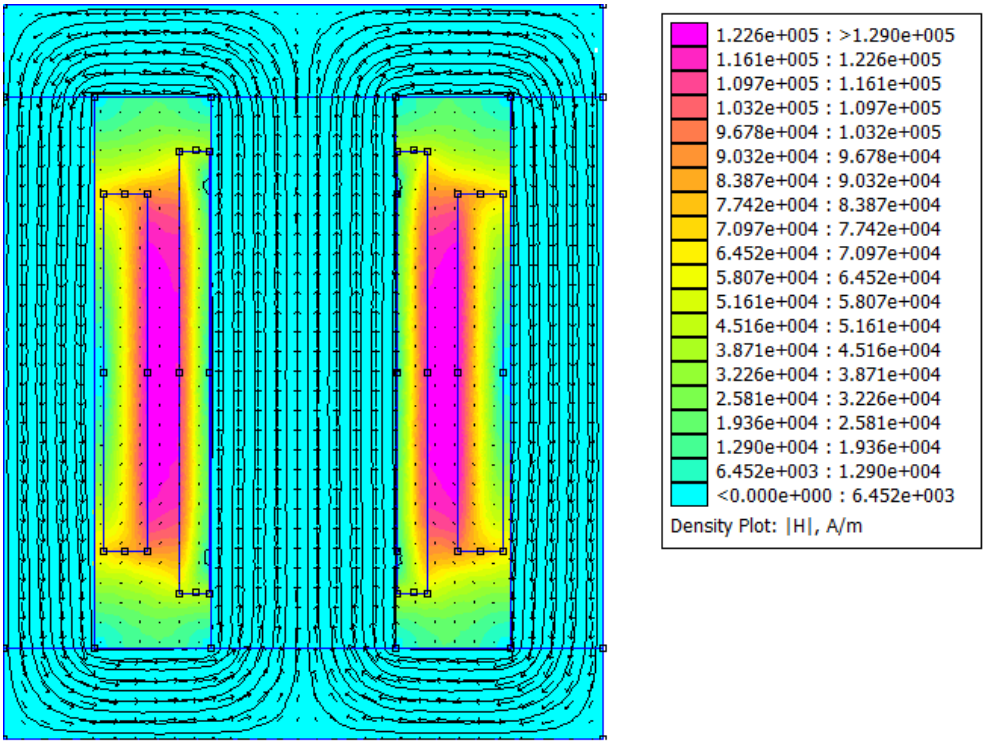

Figure 4 - 18: Magnetic field intensity for 5 A short-circuit CRGO model

4.6 FEMM models for inrush current test

The disadvantage of FEMM is that it does not simulate the saturation region well. FEMM is based on currents and not voltages. During inrush current conditions, the core saturates and FEMM does not allow for extrapolation correctly. The B-H curve used is a linear curve, it is not exactly correct but the model gives an acceptable distribution of the flux. The relative permeability was set to ensure that the flux in the core does exceed the saturation point for the inrush currents and to make sure that the correct magnetic flux is flowing through the windings. Using equations in Chapter 2 and Chapter 3, an equation to calculate the relative permeability for these models was derived as follows [23], [47], [48] :

$$\mu_r = \frac{l_c}{\mu_o}\frac{B_s}{N_1 i_{in}} \tag{45}$$

Where [23], [47], [48]:
B_s = saturation flux density (T)
l_c = length of the core measured in metre (m)
i_{in} = inrush current (A)
N_1 = number of turns for the primary winding
μ_o = permeability of space = $4\pi \times 10^{-7}$ (H/m)
μ_r = relative permeability

This test is done to determine the flux density during inrush current conditions. This test is simulated using the inrush current FEMM model. The inrush current test is performed on the models when primary current is 10 A and 5 A. During inrush current conditions, there is no current in the secondary windings; hence $I_2 = 0$ A. Equation (45) is used to calculate the relative permeability used in these models.

From Table 2 - 2 in Chapter 2.10, the saturation flux density is 1.56 T for AMDT and 2.08 T for CRGO.

4.6.1 10 A FEMM models inrush current test

For these models, the input parameters were relative permeability, primary and secondary currents. Table 4 - 5 displays their values and simulation results.

Table 4 - 5: Data for 10 A inrush current simulations

Symbol	AMDT	CRGO
$I_1 = I_1 + I_{mag}$	10.000758 A	10.028325 A
I_2	0 A	0 A
μ_r	17.79	25.85
$\|B_p\|$	1.558 T	2.075 T

Figure 4 - 19 and Figure 4 - 21 displays the magnetic flux density distribution for AMDT and CRGO under inrush current conditions for a primary current of 10 A. Figure 4 - 20 and Figure 4 - 22 displays the magnetic field intensity for AMDT and CRGO under inrush current conditions for a primary current of 10 A.

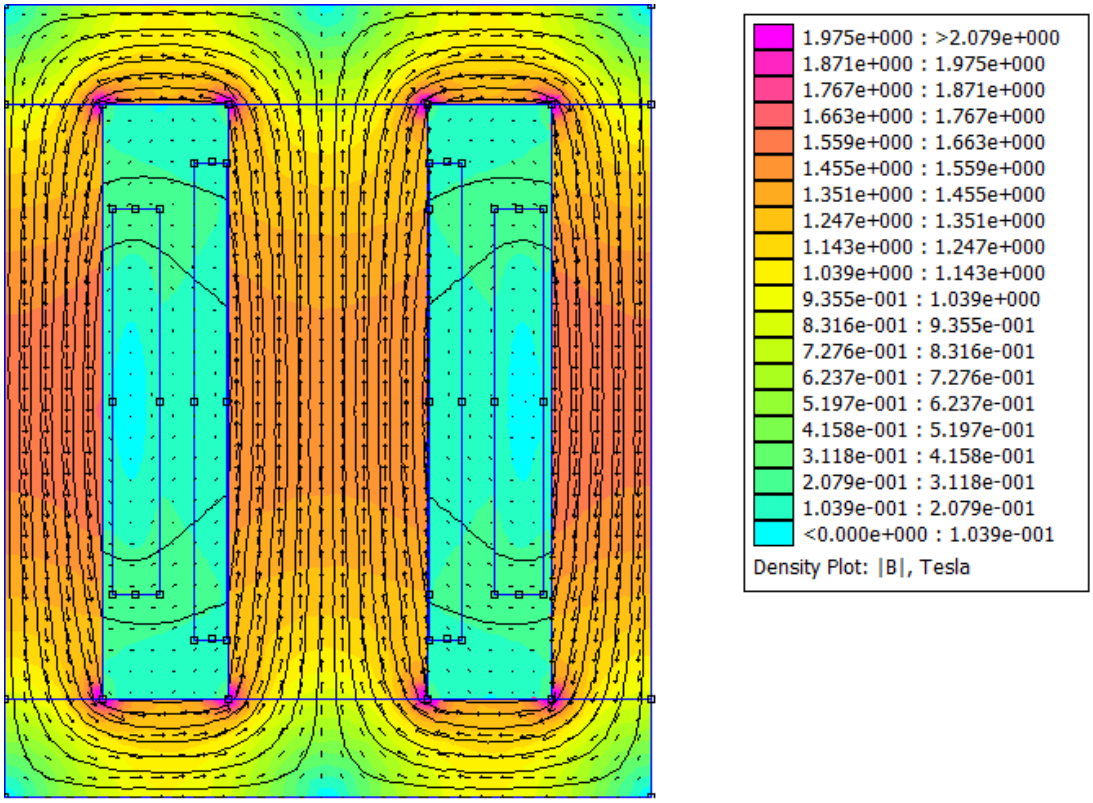

Figure 4 - 19: Magnetic flux density for 10 A inrush current AMDT model

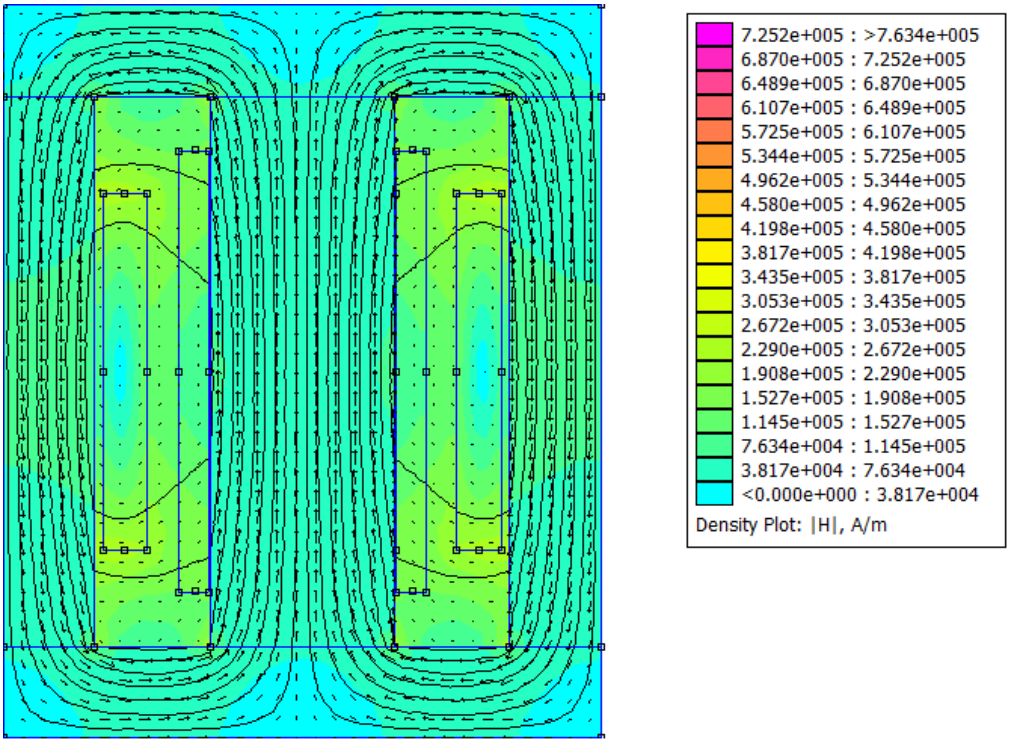

Figure 4 - 20: Magnetic field intensity for 10 A inrush current AMDT model

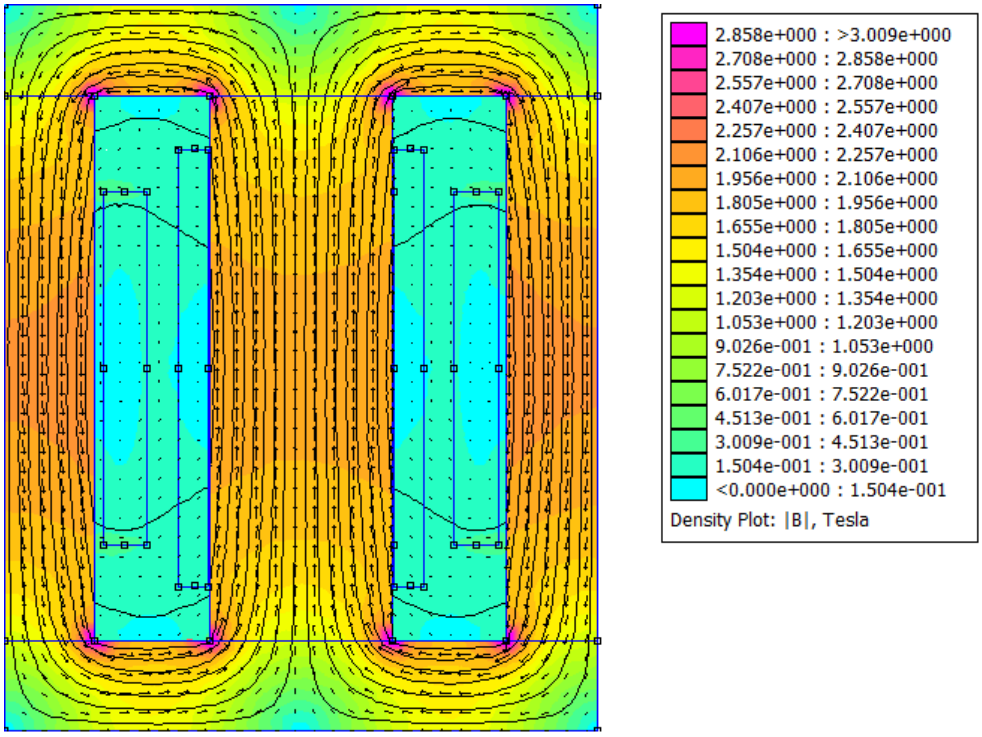

Figure 4 - 21: Magnetic flux density for 10 A inrush current CRGO model

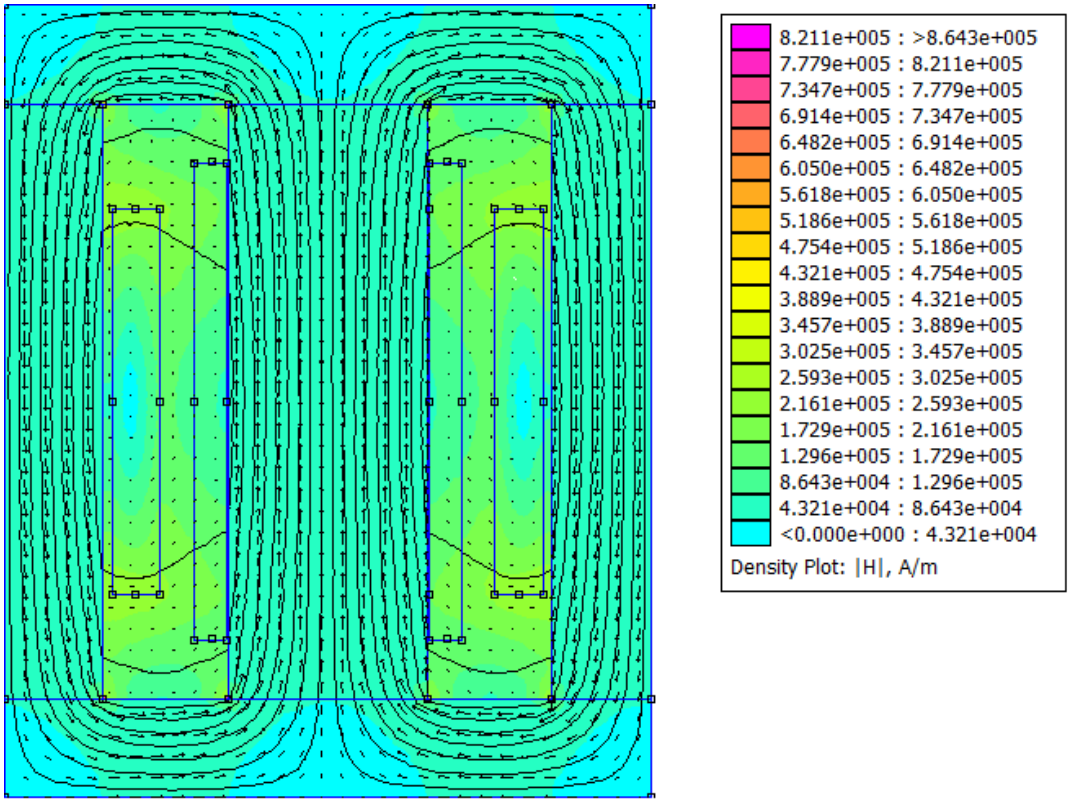

Figure 4 - 22: Magnetic field intensity for 10 A inrush current CRGO model

4.6.2 5 A FEMM models inrush current test

For these models, the input parameters were relative permeability, primary and secondary currents. Table 4 - 6 displays their values and simulation results.

Table 4 - 6: Data for 5 A inrush current simulations

Symbol	AMDT	CRGO
$I_1 = I_1 + I_{mag}$	5.000758 A	5.028325 A
I_2	0 A	0 A
μ_r	38.4	54.85
$\lvert B_p \rvert$	1.558 T	2.07533 T

Figure 4 - 23 and Figure 4 - 25 displays the magnetic flux density distribution for AMDT and CRGO under inrush current conditions for a primary current of 5 A. Figure 4 - 24 and

Figure 4 - 26 displays the magnetic field intensity for AMDT and CRGO under inrush current conditions for a primary current of 5 A.

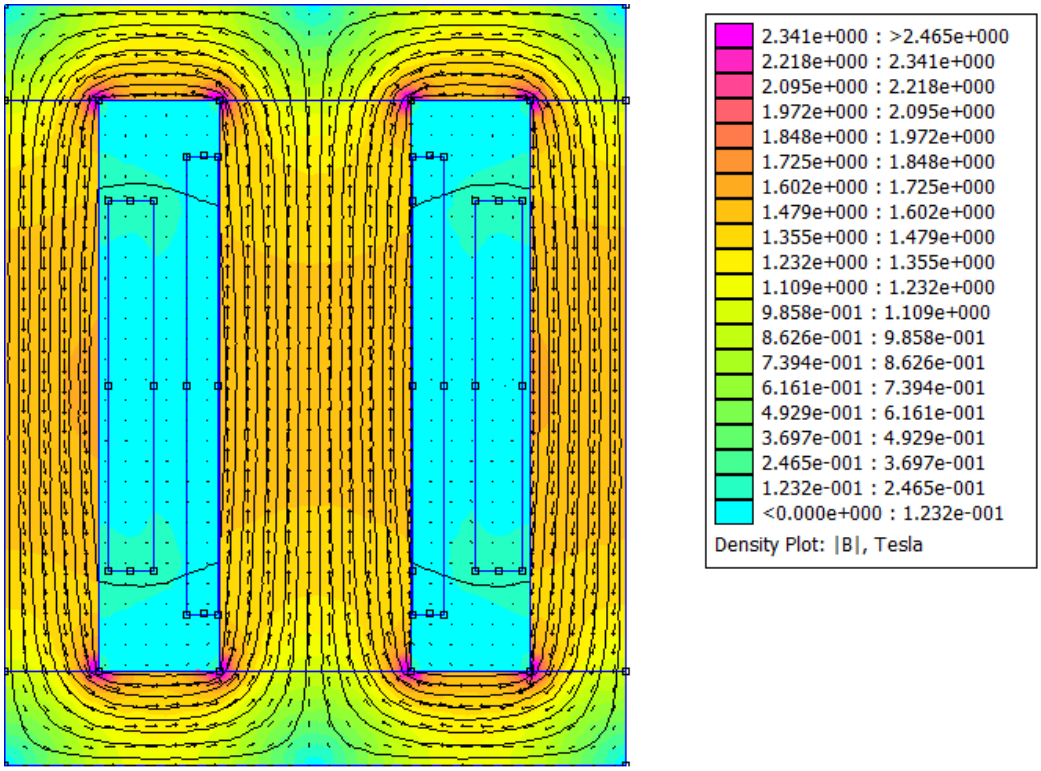

Figure 4 - 23: Magnetic flux density for 5 A inrush current AMDT model

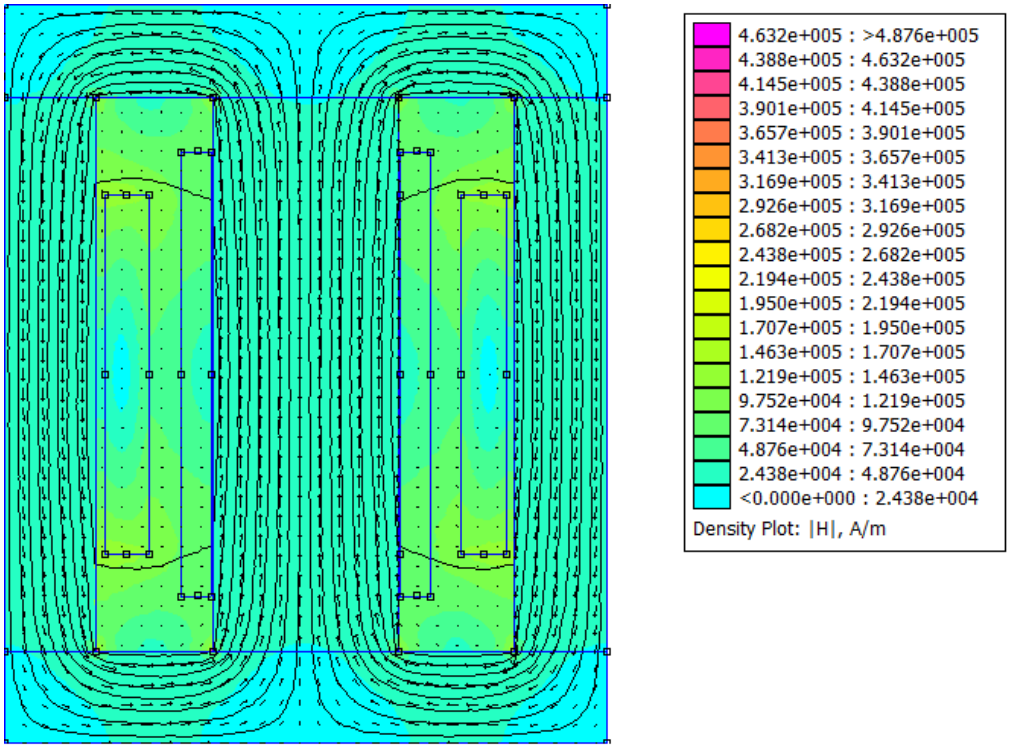

Figure 4 - 24: Magnetic field intensity for 5 A inrush current AMDT model

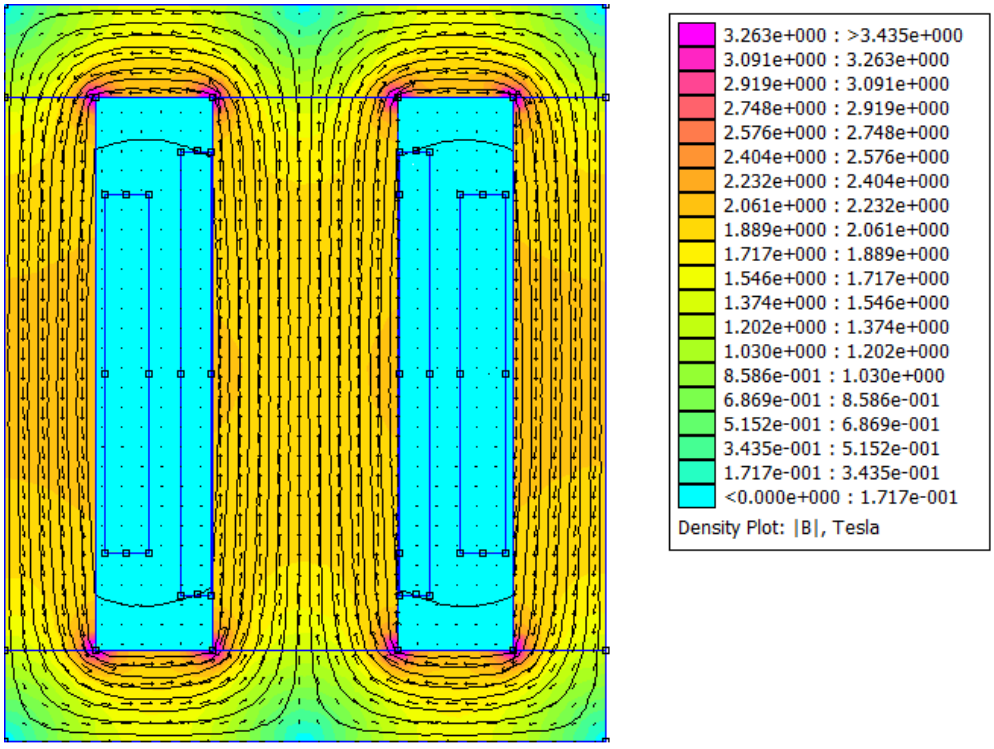

Figure 4 - 25: Magnetic flux density for 5 A inrush current CRGO model

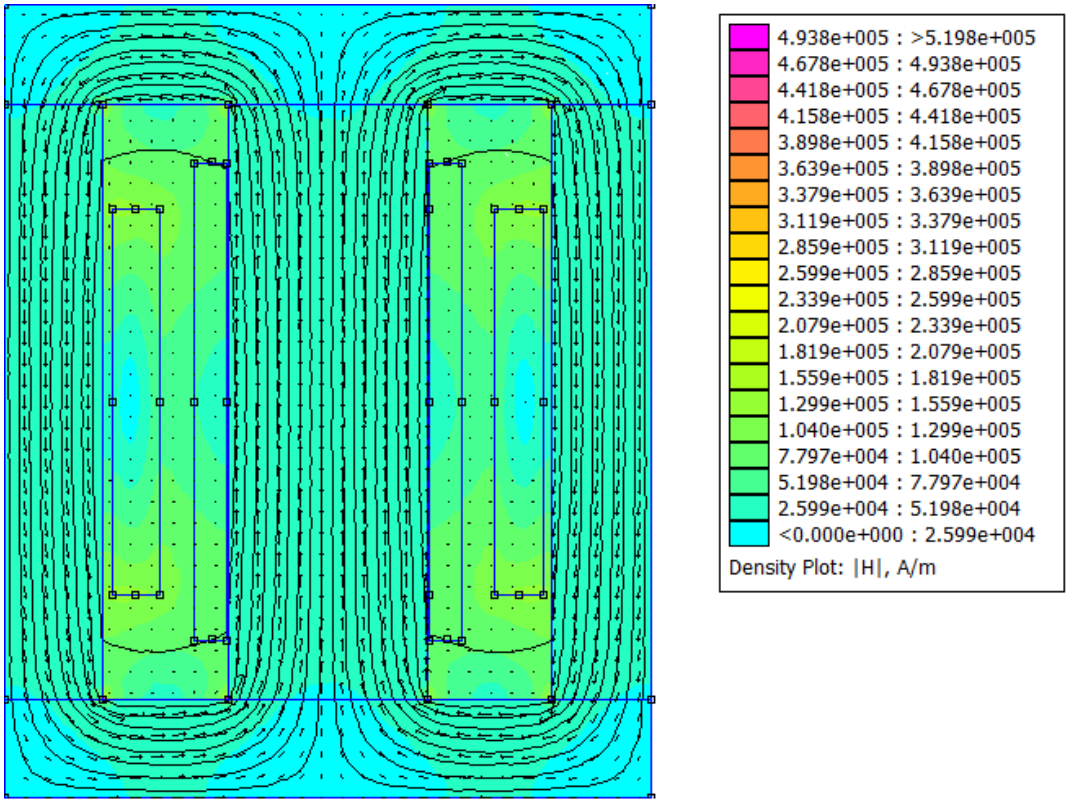

Figure 4 - 26: Magnetic field intensity for 5 A inrush current CRGO model

4.7 Short-circuit and inrush current models comparison

Looking at Figure 4 – 11 to Figure 4 – 26, the following is observed:

- The magnetic flux density is lower during short-circuit conditions.
- The magnetic field intensity is higher during inrush current conditions.
- During short-circuit conditions; there is an interaction between the windings since current flows in both HV and LV windings.
- During inrush current conditions; current flows in the HV winding only, the core saturates and more flux flows through the air core of the windings.

4.8 Comparison of the forces experienced on the windings

Code written in Matlab enabled the extraction of data from the FEMM models. Matlab calculated the force for each layer of the winding in order to determine the radial forces and axial forces were calculated for each sectional layer of the windings. The Matlab code can be found in Appendix A.

The assumption is that the transformer winding is square shaped and when a force occurs; the flux distribution is no longer uniform.

The position of the tap changer windings have an impact on the flux distribution during inrush and short-circuit conditions. Currently, they are installed at the end of the HV winding which results in a flux distribution that is unsymmetrical when forces are experienced. If the tap changer windings were installed at the centre of the HV winding, the magnitude of the forces might be lower due to a more symmetrical flux distribution.

The transformer core sees the arrestors in series, hence the capacitance of the surge arrestors are higher. A neutral surge arrestor is connected on the LV side of the transformers to one phase and straight to ground. Capacitance affects the current and hence the magnitude of the forces. Surge arrester size affects the short-circuit withstand capability [76]**.**

Both AMDT and CRGO core materials' were tested with the same design flux density of 1.3 T. It has been established in Chapter 3.4.1 that AMDT has a higher inrush current compared to CRGO.

4.8.1 Forces experienced by AMDT and CRGO with primary current of 10 A

This section discusses the forces experienced by AMDT and CRGO during short-circuit and inrush current conditions with a primary current of 10 A. Hence, these FEMM models were used.

Definitions for the legend in Figure 4 - 27 to Figure 4 - 30:

- Amorphous IR indicates AMDT inrush current condition.
- Amorphous SC indicates AMDT short-circuit current condition.
- M-5 IR indicates CRGO inrush current condition.
- M-5 SC indicates CRGO short-circuit current condition.

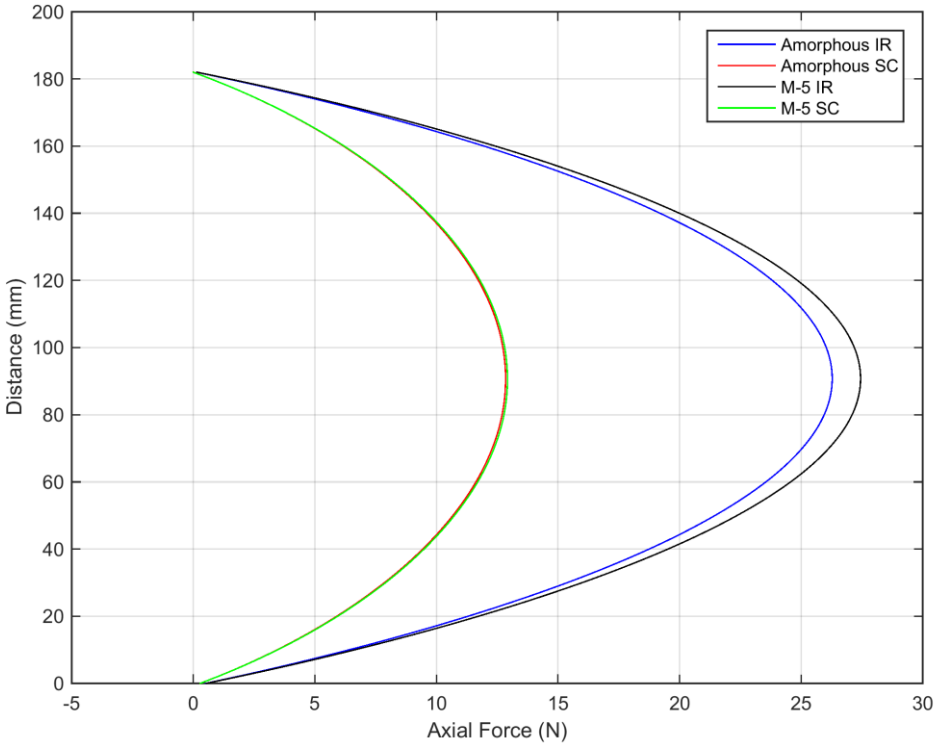

Figure 4 - 27: Average axial force of a layer of the HV winding for models with primary current of 10 A

Figure 4 - 27 displays that the top and bottom ends of the HV winding is cancelled out because the axial force is an accumulation of the forces of each conductor on each layer of the winding as displayed on Figure 4 - 3 in Chapter 4.1.

The axial force during inrush current conditions is about twice that of the axial force during short-circuit conditions. The axial force for CRGO during inrush currents is slightly higher than that of AMDT.

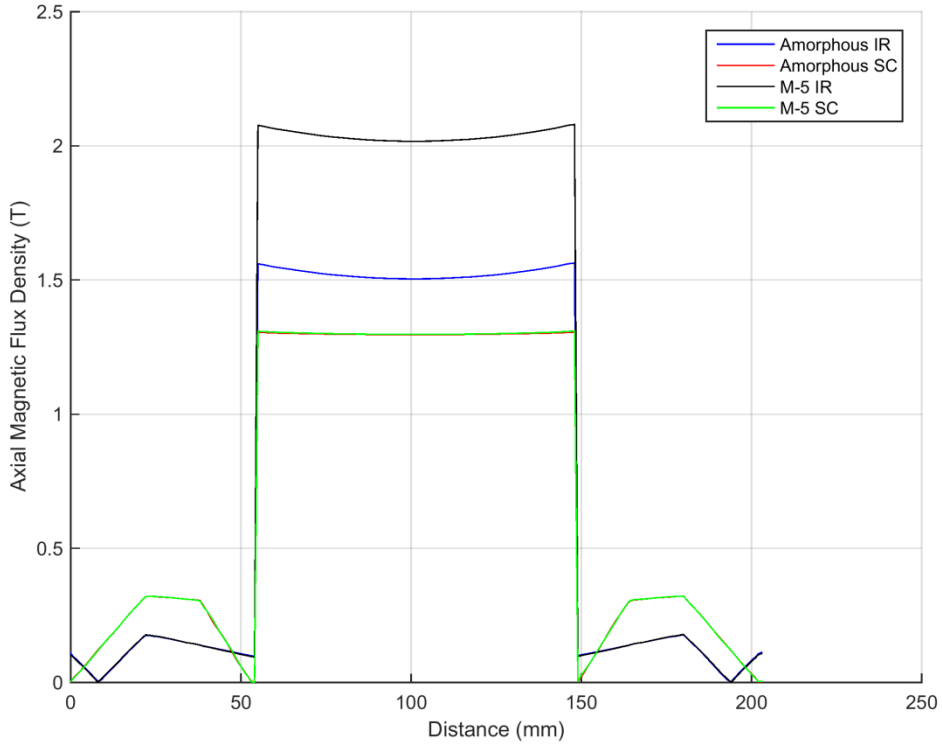

Figure 4 - 28: Magnetic flux density through the centre of the windings and core for models with primary current of 10 A

Figure 4 - 28 displays the magnetic flux density from the outside of the HV winding through to the opposite side of the HV winding with the contour defined in Figure 4 - 6 in Chapter 4.2.

CRGO has a higher axial magnetic flux density peak compared to AMDT during inrush currents even though the design flux density is the same and AMDT has a higher inrush current compared to CRGO.

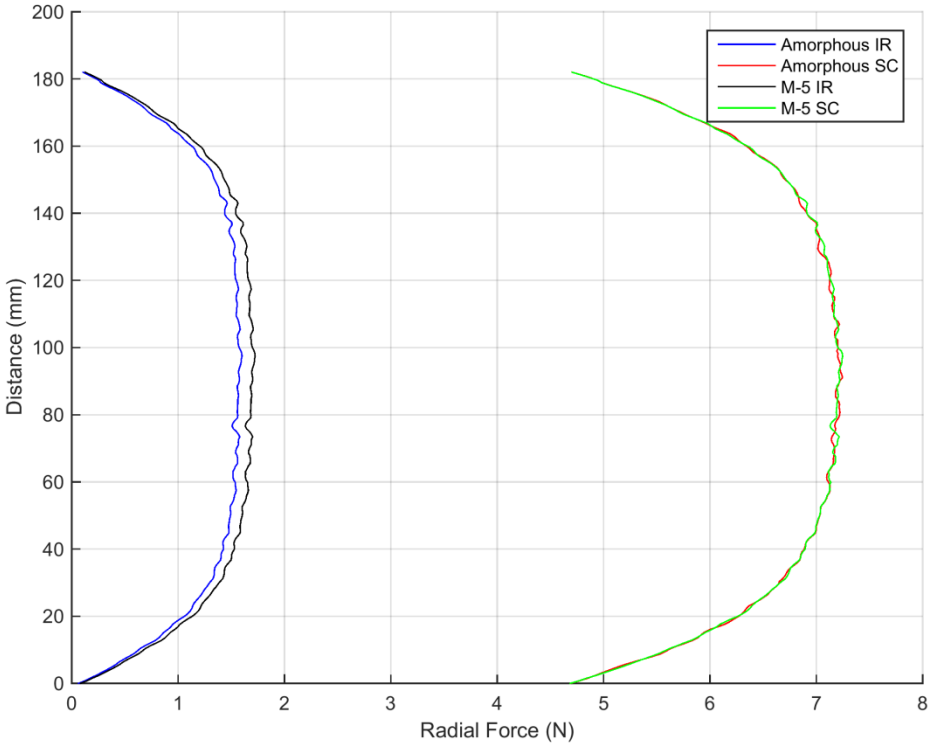

Figure 4 - 29: Net radial forces experienced on the HV windings for models with primary current of 10 A

In Figure 4 - 29, the radial forces experienced during inrush current conditions is much lower than the radial forces experienced during short-circuit conditions. The radial force for CRGO during inrush currents is slightly higher than AMDT.

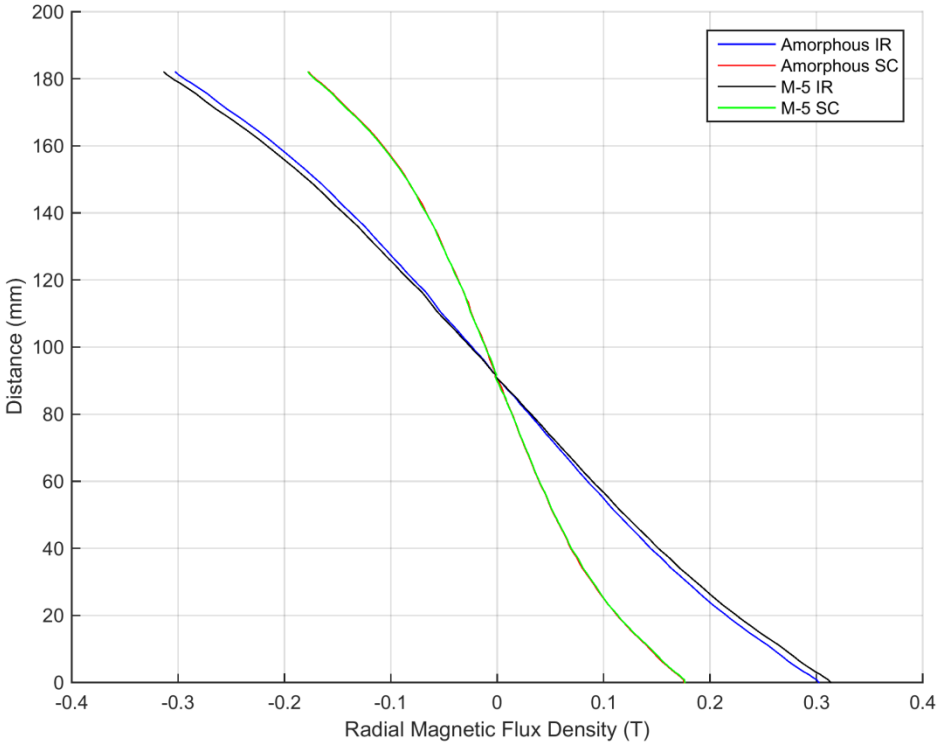

Figure 4 - 30: Radial magnetic flux density of the HV windings for models with primary current of 10 A

Figure 4 - 30 displays the magnetic flux density for the outer layer of the HV winding from top to bottom. The highest magnetic flux density is by the ends of the windings. At the centre of the windings, the magnetic flux density is such that the electrical force is cancelled so there is no radial magnetic flux density in the centre. The radial magnetic flux densities are different between the inrush currents and short-circuit currents because the flux density in the core is saturated during inrush current conditions causing the additional flux to be pushed out.

4.8.2 Forces experienced by AMDT with primary current of 10 A and 5 A

From Figure 4 - 31 to Figure 4 - 34, the AMDT FEMM models with primary current of 10 A (base case) is compared to the AMDT FEMM models with primary current of 5 A during short-circuit and inrush current conditions.

Definitions for the legend in Figure 4 - 31 to Figure 4 - 34:

- 5 A inrush indicates the inrush current condition with a primary current of 5 A.
- 5 A Short Circuit indicates the short-circuit condition with a primary current of 5 A.
- 10 A inrush indicates the inrush current condition with a primary current of 10 A.
- 10 A Short Circuit indicates the short-circuit condition with a primary current of 10 A.

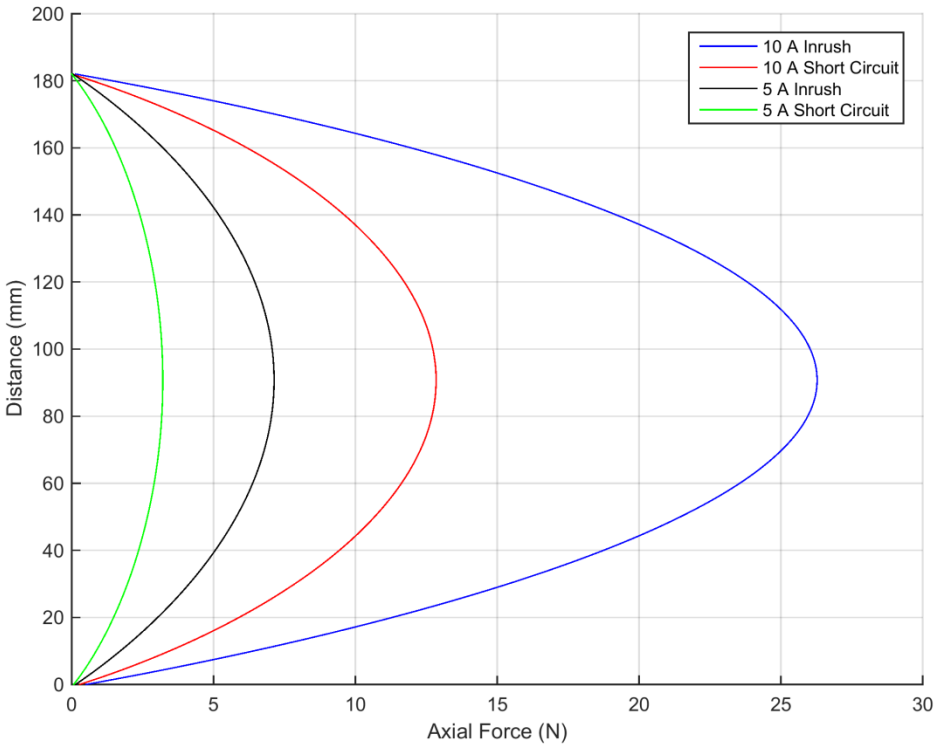

Figure 4 - 31: Average axial force of a layer of the HV winding for models with primary current of 10 A and 5 A

Figure 4 - 31 displays that the axial forces during short-circuit and inrush current conditions. The 10 A short-circuit and inrush current axial forces are almost four times higher than that of the 5 A short-circuit and inrush current axial forces.

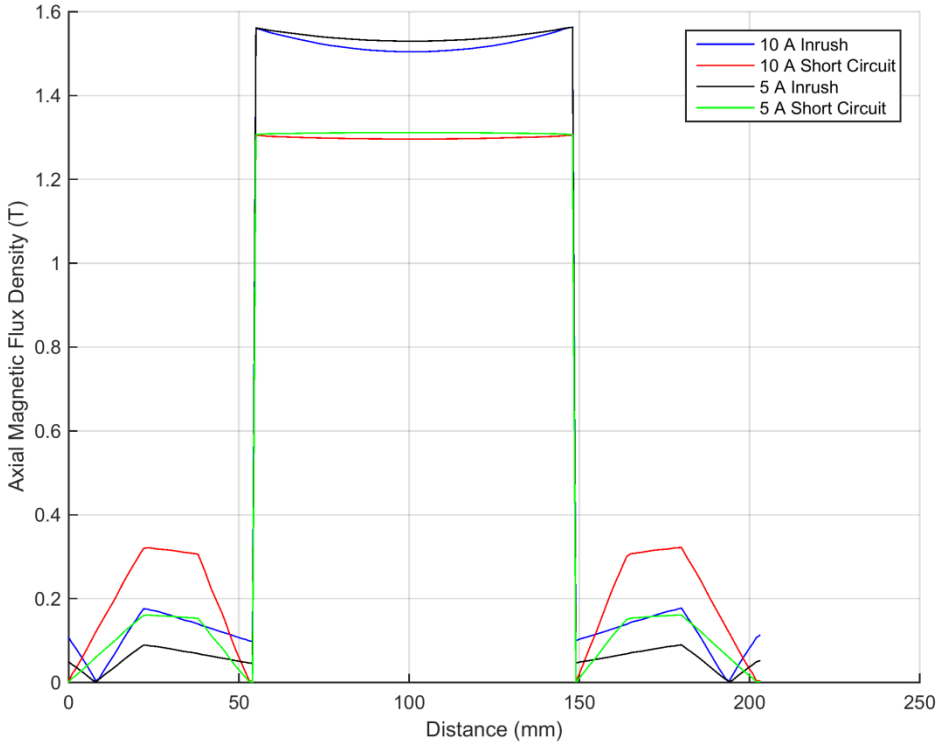

Figure 4 - 32: Magnetic flux density through the centre of the windings and core for models with primary current of 10 A and 5 A

In Figure 4 - 32, the axial magnetic flux density during short-circuit conditions between the HV and LV windings in the 10 A model is almost doubled when compared to that of the 5 A model. However, the peak axial magnetic flux density is almost similar for both models under short-circuit and inrush current conditions by the core.

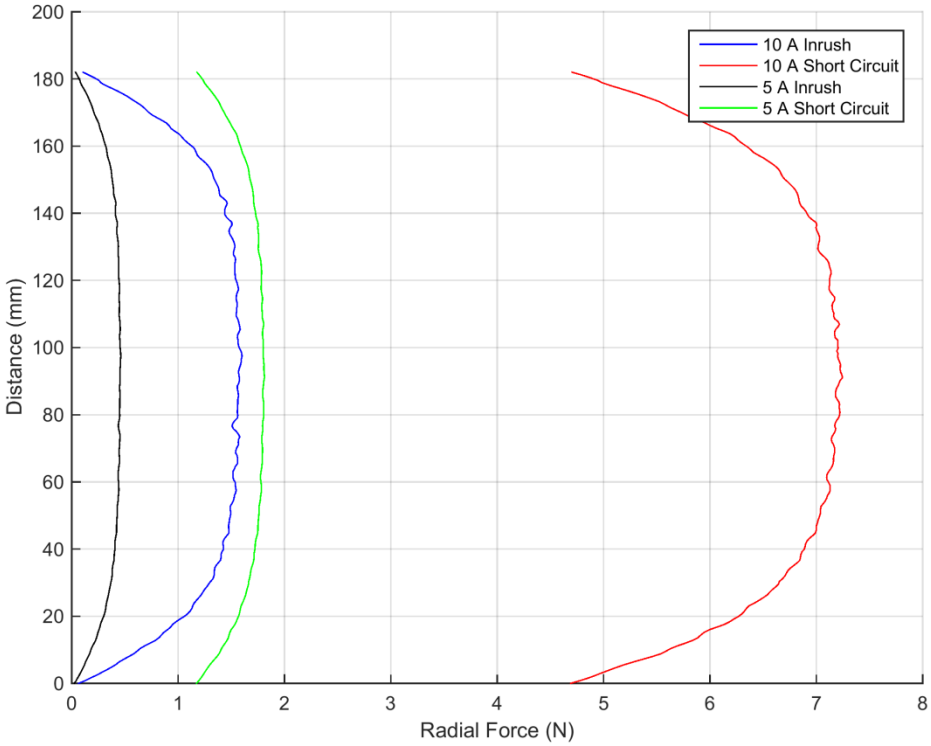

Figure 4 - 33: Net radial forces experienced on the HV windings for models with primary current of 10 A and 5 A

There is a huge difference in the radial forces during short-circuit conditions between the 10 A and 5 A models in Figure 4 - 33. During inrush currents, the 10 A model experiences a higher radial force compared to the 5 A model. This is a result of the different currents simulated in the windings.

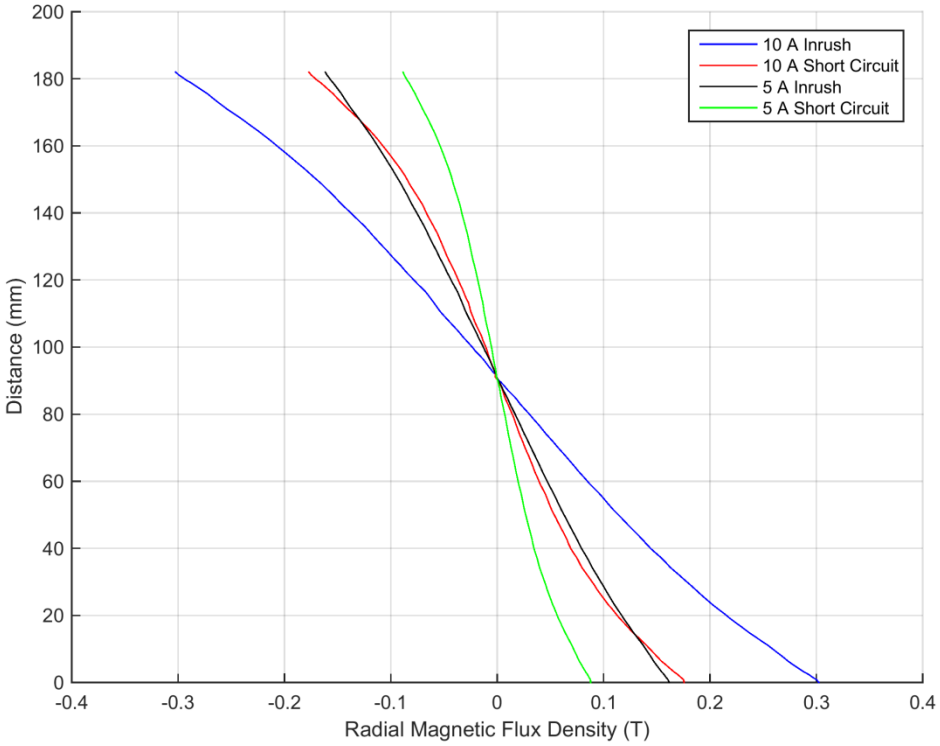

Figure 4 - 34: Radial magnetic flux density for models with primary current of 10 A and 5 A

The radial magnetic flux density curves in Figure 4 - 34 for the 10 A and 5 A models under short-circuit and inrush current conditions are different because of the different currents simulated in the windings.

4.9 Positioning of the tap changer winding

Forces experienced by conductors in the windings of transformers are based on the current density and magnetic flux density. Equation (39) to Equation (41) as well as Figure 4 - 1 to Figure 4 - 3 explain in detail how forces are calculated.

Definitions for the legend in Figure 4 - 35 to Figure 4 - 36:

- Tap Changer IR represents the tap changer winding under inrush current condition.
- Tap Changer SC represents the tap changer winding under short-circuit current condition.
- Winding IR represents winding under inrush current condition.
- Winding SC represents winding under short-circuit current condition.

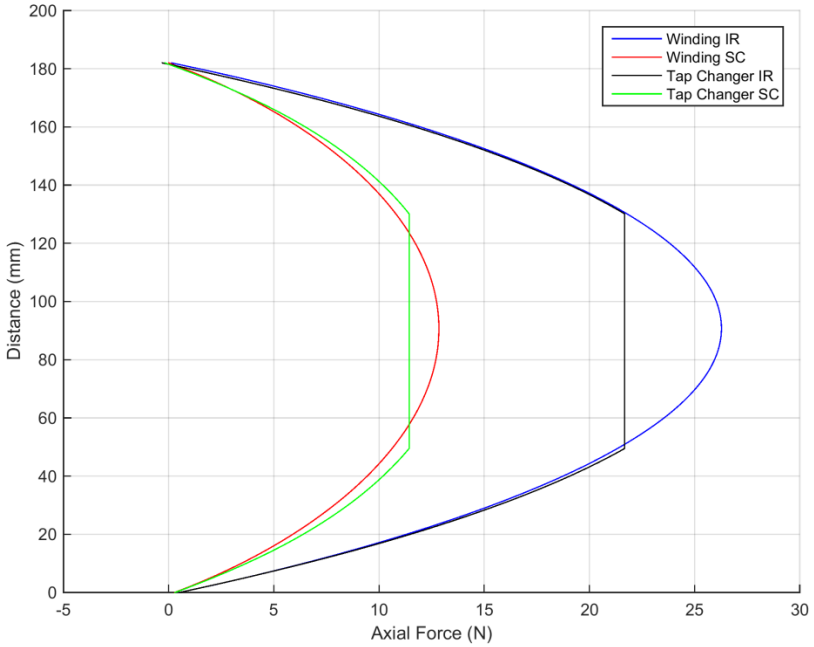

(a) Symmetrical winding distribution

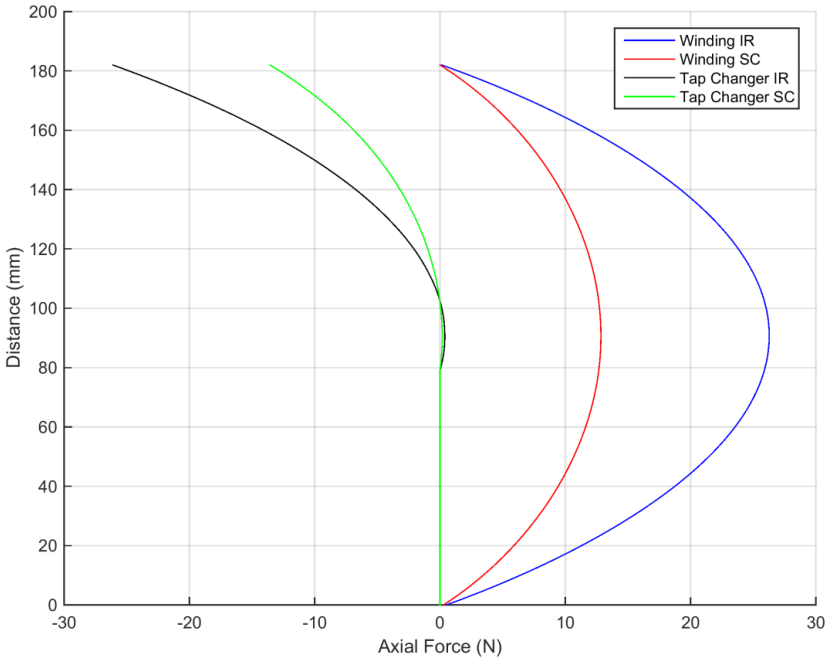

(b) Unsymmetrical winding distribution

Figure 4 - 35: Axial force that each conductor experiences on a single layer of the HV winding and tap changer winding

The position of the tap changer on the windings is displayed in Figures 4 – 35 (a) and Figure 4 – 35 (b) with the Tap Changer IR and Tap Changer SC curves. It can be clearly seen that when the tap changer position has a symmetrical arrangement (Figure 4 – 35 (a)), the net force exerted on the layer will be zero. In the unsymmetrical figure (Figure 4 – 35 (b)), it can be seen that the net force on the winding is non-zero. This may cause the layer to experience a force unnecessarily. In Figure 4 – 35 (a), the axial force is higher during inrush currents compared to short-circuit conditions. Figure 4 – 35 (b) displays that when there is a force, it is negative for the tap changer winding during inrush current and short-circuit conditions.

The axial force causes the conductor to move upwards and downwards, if the force is high enough, it could push the ends of the conductors out of place. If the tap windings were centrally located, the result is symmetrical flux distribution when the transformer is energised and minimum vertical forces due to short-circuit [77].

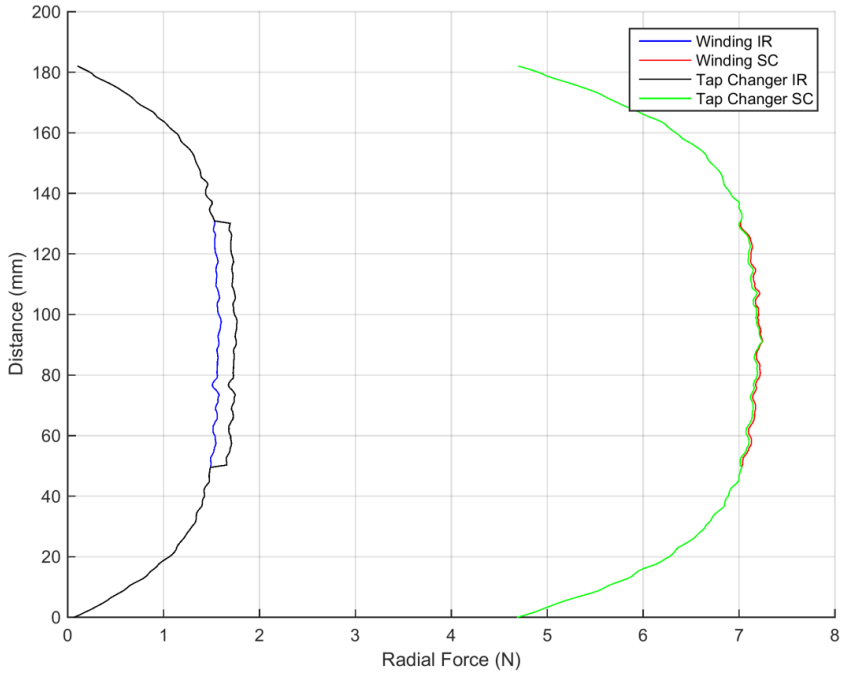

(a) Symmetrical winding distribution

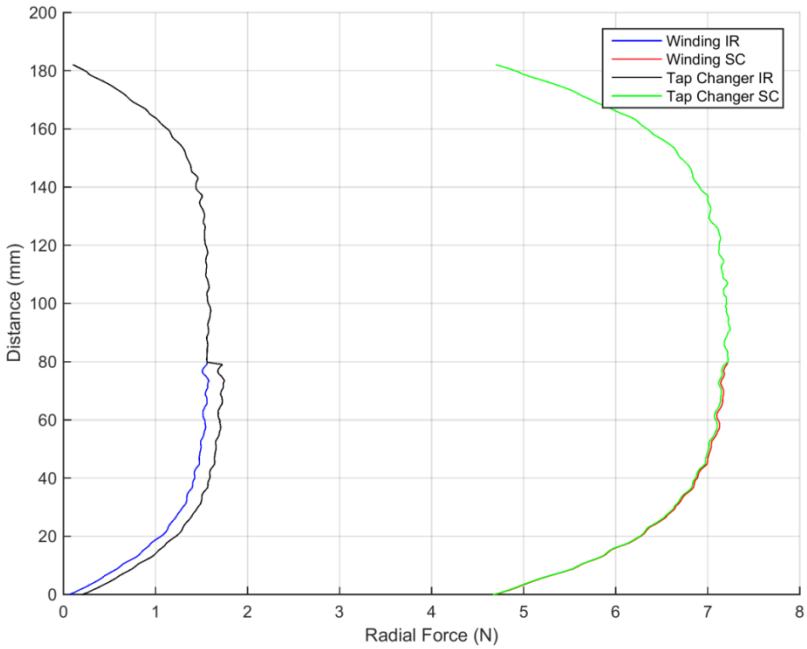

(b) Unsymmetrical winding distribution

Figure 4 - 36: Radial force on HV tap changer winding

Figure 4 - 36 displays that the radial force is higher under short-circuit conditions compared to inrush current conditions. This is due to both HV and LV windings having current under short-circuit conditions. The forces experienced in both Figure 4 - 36 (a) and Figure 4 - 36 (b) does not seem to be very sensitive to the tap changer position on the winding.

4.10 Discussion and conclusion

During inrush current conditions the core saturates and the flux is forced to go through the air unlike during short-circuit conditions. Inrush currents only occur during start-up of the transformer.

The axial force for inrush current conditions is higher than short-circuit conditions. The radial force for short-circuit conditions is higher than inrush current conditions. AMDT and CRGO experience similar axial and radial forces.

When any non-current carrying tap changer windings are symmetrically arranged in the centre and when the entire layer in the HV windings carries current, the net axial force will be zero.

When any non-current carrying tap changer winding is unsymmetrical, the net axial force is non-zero. This has the potential to impact on the mechanical integrity of the winding, especially during inrush current conditions.

5 CONCLUSION

The simulations and tests conducted established that the peak current occurs at the zero crossing of the voltage due to the flux been the highest at this point.

Based on the simulations and tests conducted, AMDTs experience higher inrush currents than CRGO even though they have the same design flux density. This is due to the lower saturation point of the AMDT.

The primary inrush current can be reduced according to the results in Chapter 3, these are explained further below.

The following parameters are proportional to inrush currents:

- Residual flux: AMDT and CRGO with design flux density of 1.3 T experienced the highest peak inrush current of 8.47 A and 7.388 A respectively when the residual flux was the highest (100% of the calculated value).
- Source voltage: AMDT and CRGO with design flux density of 1.3 T experienced the highest peak inrush current of 5.95 A and 4.82 A respectively when the source voltage was the highest (105% of the nominal voltage).

The following parameters are inversely proportional to inrush currents:

- Resistance: AMDT and CRGO with design flux density of 1.3 T experienced the highest peak inrush current of 5.57 A and 4.27 A respectively when the resistance was the lowest (100 Ω).
- Air core inductance: AMDT and CRGO with design flux density of 1.3 T experienced the highest peak inrush current of 6.25 A and 4.97 A respectively when the air core inductance was the lowest (-20% of the calculated value).

The axial force for inrush current conditions is higher than short-circuit conditions. The radial force for short-circuit conditions is higher than inrush current conditions. However in Chapter 4.8.1, the axial and radial forces AMDT and CRGO with design flux density of 1.3 T experienced are almost the same. In order to decrease the magnitude of the forces experienced, the primary current must be decreased.

The tap changer position on the HV windings also influences the forces. When any non-current carrying tap changer windings are symmetrically arranged in the centre and when the entire layer in the HV windings carries current, the net axial force will be zero.

When any non-current carrying tap changer winding is unsymmetrical, the net axial force is non-zero. This has the potential to impact on the mechanical integrity of the winding, especially during inrush current conditions.

The hypothesis is valid for this dissertation since AMDT experiences a higher inrush current than CRGO with the same design flux density, but the forces they experience as a result of inrush currents and short-circuit currents are similar.

In conclusion, AMDTs are a suitable replacement for CRGO. AMDTs are known for having lower no-load losses. According to Table 2 - 2, AMDTs may have approximately one third of CRGO no-load losses. This is an important technology that may be used to decrease losses on the distribution network.

REFERENCES

[1] Eskom, “Eskom awaits NERSA decision on regulatory clearing account (RCA) balance,” Eskom Holdings SOC Ltd , 2016. [Online]. Available: http://www.eskom.co.za/news/Pages/RCAmediastatement.aspx. [Accessed 11 November 2016].

[2] SABS, Composer, *South African National Standards (SANS) 60076-1:2011 Power Transformers; Part 1: General*. [Sound Recording]. South African Bureau of Standards (SABS); Standards Division. Edition 2, 2011.

[3] Wikipedia, “Transformer,” A wikimedia project powered by MediaWiki, 03 July 2016. [Online]. Available: https://en.wikipedia.org/wiki/Transformer. [Accessed 04 July 2016].

[4] Eskom, “Company information overview,” Eskom Holdings SOC Ltd, 2016. [Online]. Available: http://www.eskom.co.za/OurCompany/CompanyInformation/Pages/Company_Information.aspx. [Accessed 04 July 2016].

[5] Wikipedia, “Distribution transformer,” A wikimedia project powered by MediaWiki, 30 June 2016. [Online]. Available: https://en.wikipedia.org/wiki/Distribution_transformer. [Accessed 04 July 2016].

[6] TasNetworks Delivering your power, “Pole Mounted Transformers - Distribution,” *Asset Management Plan*, vol. Record number: R260428, no. 1, October 2015.

[7] electrcial4u.com, “Transformer Test | Type Test and Routine Test of Transformer,” electrical4u, 2011-2016. [Online]. Available: http://www.electrical4u.com/transformer-testing-type-test-and-routine-test-of-transformer/. [Accessed 26 July 2016].

[8] V. Pangonilo, “IEC 60076-5 Transformer Impedances,” Facebook Auto Publish Powered by: XYZScripts.com, 12 August 2011. [Online]. Available: https://pangonilo.com/2011/08/iec-60076-5-transformer-impedance.html. [Accessed 26 July 2016].

[9] Eskom, Composer, *Transformer specification for Amorphous Core Pilot Project*. [Sound Recording]. Eskom. 2012.

[10] M. Mohan, “An Overview on Amorphous Core Transformers,” *Journal of Emerging Trends in Engineering and Applied Sciences (JETEAS)*, no. ISSN: 2141-7016, 2012.

[11] J. Naidoo and A. Swanson, “A simulation study of the inrush current performance of

amorphous core and c.r.g.o transformers," *South African Universities Power Engineering Conference; Vaal University of Technology*, no. ISBN 978-1-77012-386, 2016.

[12] EE publishers, "Reducing SA's electrical distribution transformer losses," EE Publishers (Pty) Ltd, 20 November 2014. [Online]. Available: http://www.ee.co.za/article/reducing-sas-electrical-distribution-transformer-losses.html. [Accessed 26 July 2016].

[13] Wikipedia, "Inrush current," A wikimedia project powered by MediaWiki, 14 July 2016. [Online]. Available: https://en.wikipedia.org/wiki/Inrush_current. [Accessed 26 July 2016].

[14] Wikipedia, "Short circuit," A wikimedia project powered by MediaWiki, 18 July 2016. [Online]. Available: https://en.wikipedia.org/wiki/Short_circuit. [Accessed 26 July 2016].

[15] Electrical Engineering Portal, "When a transformer has stomach pain and wants to…," 2016 EEP; powered by CsanyiGroup, 08 May 2016. [Online]. Available: http://electrical-engineering-portal.com/when-transformer-has-a-stomach-pain-and-wants-to. [Accessed 11 November 2016].

[16] Wikipedia, "Electric power distribution," A wikimedia project powered by MediaWiki, 10 July 2016. [Online]. Available: https://en.wikipedia.org/wiki/Electric_power_distribution. [Accessed 26 July 2016].

[17] Wikipedia, "Electric power transmission," A wikimedia project powered by MediaWiki, 27 November 2016. [Online]. Available: https://en.wikipedia.org/wiki/Electric_power_transmission. [Accessed 28 November 2016].

[18] Eskom Holdings SOC Limited, "Integrated report: Being customer-centric," Eskom, 2014. [Online]. Available: http://integratedreport.eskom.co.za/bec-customer.php. [Accessed 07 January 2016].

[19] J. P. Navani, N. K. Sharma and S. Sapra, "Technical and non-technical losses in power system and its economic consequence in Indian economy," *International Journal of Electronics and Computer Science Engineering (IJECSE),* vol. 1, no. 2, ISSN: 2277-1956.

[20] Polish Copper Promotion Centre and European Copper Institute in collaboration with SEEDT Partners with the support of the European Commission, "Selecting Energy

Efficient Distribution Transformers; A Guide for Achieving Least-Cost Solutions," *Prepared for Intelligent Energy Europe Programme; Strategies for Development and Diffusion of Energy Efficient Distribution Transformers (SEEDT),* no. Project Number EIE/05/056/SI2.419632, 2008.

[21] Schneider Electric, "Power and Distribution Transformers," *Low Voltage and Medium Voltage Products Catalogue,* no. NRJED315628EN, 2015.

[22] Copper Development Association Inc, "Temperature Rise and Transformer Efficiency," Copper Development Association Inc; A Copper Alliance Member, 2016. [Online]. Available: http://www.copper.org/environment/sustainable-energy/transformers/education/trans_efficiency.html. [Accessed 07 January 2016].

[23] R. M. Del Vecchio, B. Poulin, P. T. Feghali, D. M. Shah and R. Ahuja, Transformer Design Principles, With Applications to Core-Form Power Transformers, Second ed., CRC Press, LLC; CRC Press is an imprint of Taylor & Francis Group, an Informa business, 2010.

[24] Eskom Holdings Ltd and ABB Powertech Transformers, (Eskom Power Series, Volumne 5) Theory, design, maintenance and life management of power transformers, Johannesburg: Y-Land Design, Print and Promotions, 2008.

[25] ABB, Transformer Handbook, Zürich, Switzerland: ABB, 2004.

[26] M. Digalovski, K. Najdenkoski and G. Rafajlovski, "Prediction of Core Losses of Three-Phase Distribution Transformer," *Journal of Energy and Power Engineering*, no. 7, 2013.

[27] E. I. Amoiralis, M. A. Tsili and P. S. Georgilakis, "The state of the art in engineering methods for transformer design and optimization: A survey," *Journal of Optoelectronics and advanced materials,* vol. 10, no. 5, 2008.

[28] electrical4u, "Hysteresis Eddy Current Iron or Core Losses and Copper Loss in Transformer," electrical4u, 2011-2016. [Online]. Available: http://www.electrical4u.com/hysteresis-eddy-current-iron-or-core-losses-and-copper-loss-in-transformer/. [Accessed 15 December 2015].

[29] M. Albach, T. Dürbaum and A. Brockmeyer, "Calculating Core Losses in Transformers for Arbitrary Magnetizing Currents, A Comparison of Different Approaches," in *Power Electronics Specialist Conference*, Baveno, Italy, 1996.

[30] C. Freitag, J. Kasti and T. Leibfried, "New approch to calculate core losses in power transformers based on combination of FEM simulation and post processing algorithm,"

in *The 19th International Symposium on High Voltage Engineering*, Pilsen, Czech Republic, 2015.

[31] A. F. L. Nogueira, G. G. Facchinello and L. A. Ramos, "Prediction of magnetizing currents in power transformers using numerically simulated open-circuit tests," *IJRRAS; www.arpapress.com/Volumes/Vol17Issue2/IJRRAS_17_2_01.pdf*, vol. 17, no. 2, 2013.

[32] I. Hernandez, J. C. Olivares-Galvan, P. S. Georgilakis and J. M. Cañedo, "Core loss and excitation current model for wound core distribution transformers," *International Transactions on Electrical Energy Systems; Int. Trans. Electr. Energ. Syst. 2014; 24:30–42*, no. Published online 4 September 2012 in Wiley Online Library (wileyonlinelibrary.com). DOI: 10.1002/etep.1687; Copyright © 2012 John Wiley & Sons, Ltd., 2012.

[33] G. Stanford, Composer, *Insulation co-ordination on MV/ LV shared wood structures*. [Sound Recording]. Eskom. 2004.

[34] Electronics Tutorials, "Transformer Construction," AspenCore, Inc., 2016. [Online]. Available: http://www.electronics-tutorials.ws/transformer/transformer-construction.html. [Accessed 07 October 2016].

[35] Solomon Corporation, "Circular Vs. Rectangular Windings | Part 2," Solomon Corporation, 25 March 2014. [Online]. Available: http://www.solomoncorp.com/circular-vs-rectangular-windings-part-2/. [Accessed 07 October 2016].

[36] Electrical Engineering Portal, "Power Transformer Construction – Windings," 2016 EEP; powered by CsanyiGroup, 24 August 2016. [Online]. Available: http://electrical-engineering-portal.com/power-transformer-construction-windings. [Accessed 06 October 2016].

[37] Electrical Engineering Assignment, "Transformer Windings," Electrical Engineering Assignment, 2012-13. [Online]. Available: http://www.electrical-engineering-assignment.com/transformer-windings. [Accessed 06 October 2016].

[38] Eskom, Composer, *Specification for mineral insulating oils (uninhibited and inhibited): Purchase, management, maintenance and testing*. [Sound Recording]. Eskom. 2014.

[39] R. Liao, C. Lv, L. Yang, Y. Zhang, Wu, Weiqiang and C. Tang, "The Insulation Properties of Oil-Impregnated Insulation Paper Reinforced with Nano-TiO2," *Journal of Nanomaterials*, vol. 2013, 2013.

[40] Megger, “Tap changers,” Megger, 2016. [Online]. Available: http://en.megger.com/applications/transformers/tap-changers. [Accessed 06 October 2016].

[41] Electrical Engineering Portal, “4 Essential Features of Transformer On-Load Tap Changer (OLTC),” 2016 EEP; powered by CsanyiGroup, 28 January 2016. [Online]. Available: http://electrical-engineering-portal.com/4-essential-features-of-transformer-on-load-tap-changer-oltc. [Accessed 06 October 2016].

[42] electrical4u.com, “On Load and No Load Tap Changer of Transformer | OLTC and NLTC,” electrical4u, 2011-2016. [Online]. Available: http://www.electrical4u.com/on-load-and-no-load-tap-changer-of-transformer-oltc-and-nltc/. [Accessed 06 October 2016].

[43] SABS, Composer, *South African National Standard (SANS) 60076-18:2013 Power transformers; Part 18: Measurement of frequency response*. [Sound Recording]. South African Bureau of Standards (SABS); Standards Division. Edition 1, 2013.

[44] D. Li, L. Zhang, G. Li, Z. Lu and S. Zhou, “Reducing the core loss of amorphous cores for distribution transformers,” *Chinese Materials Research Society; Progress in Natural Science: Materials International*, 2012.

[45] G. Stanford, G. Jones and S. Whiting, “Low Loss Distribution Transformers in a South African Context,” in *63rd AMEU Convention, Powertech Transformers*, Kempton Park, South Africa, 2012.

[46] R. U. Lenke, S. Rohde, F. Mura and R. W. De Doncker, “Characterization of Amorphous Iron Distribution Transformer Core for Use in High-Power Medium-Frequency Applications,” *IEEE Energy Conversion Congress and Exposition*, 2009.

[47] S. Hodder, B. Kasztenny, N. Fischer and Y. Xia, “Low Second-Harmonic Content in Transformer Inrush Currents – Analysis and Practical Solutions for Protection Security,” in *67th Annual Conference for Protective Relay Engineers*, College Station, USA, 2014.

[48] S.V.Kulkarni and S.A.Khaparde, Transformer Engineering; Design and Practice, Mumbai, India: Marcel Dekker, Inc, 2004.

[49] P. R. Barnes, J. W. Van Dyke, B. W. McConnell, S. M. Cohn and S. L. Purucker, “The feasibility of replacing or upgrading utility distribution transformers during routine maintenance,” *Power Systems Technology Program, Oak Ridge National Laboratory for the U.S. Department of Energy*, no. contract DE-AC05-84OR21400, 1995.

[50] R. Hasegawa, *Energy Efficiency of Amorphous Metal Based Transformers*, USA: Metglas, Inc, 2004.

[51] P. G. Vasile, C. Mircea, B. Radu, G. Călin-Octavian, G. Daniel and V. Răzvan, "Reducing losses in electrical distribution systems using amorphous transformers," *Journal of Sustainable Energy; ISSN 2067 – 5534*, vol. 1, no. 4, 2010.

[52] TATUNG, *Amorphous Distribution Transformer; Products range*, Taipei City, Taiwan: Power Business Group, 2013.

[53] M. Mohan and P. K. Singh, "Distribution transformer with amorphous-crgo core: An effort to reduce the cost of amorphous core distribution transformer," *Asian Research Publishing Network (ARPN) Journal of Engineering and Applied Sciences; ISSN 1819-6608*, vol. 7, no. 6, 2012.

[54] M. Yamamoto, T. Mori, T. Kawasaki, K. Tsutsui, T. Itoh and T. Yagisawa, "A design study of amorphous core transformer," *IEEE Transactions and Magnetics*, Vols. MAG-20, no. 5, 1984.

[55] B. Francoeur and P. Couture, "Low-Cost Amorphous-Metal Rolled-up-Core Distribution Transformer," in *IEEE PES Transmission and Distribution Conference and Exposition (T&D)*, Orange County, USA, 2012.

[56] Emerson Network Power, "Surge Current, Short-Circuit and Fault Current Overview," *White Paper; Power switching and controls for Business-Critical Continuity TM*, no. WP-30020 Rev.1 1/13, 2011.

[57] L. Šušnjić, S. Vlahinić and I. Mužić, "Prediction of the Transformer Inrush Current Forces," *Strojarstvo*, no. ISSN 0562-1887, 2010.

[58] N. Chiesa, Composer, *Power Transformer Modeling for Inrush Current Calculation*. [Sound Recording]. Thesis for the degree of Philosophiae Doctor; Norwegian University of Science and Technology; Faculty of Information Technology, Mathematics and Electrical Engineering; Department of Electric Power Engineering; NTNU. 2010.

[59] C. E. Lin, C. L. Cheng, C. L. Huang and J. C. Yeh, "Investigation of Magnetizing Inrush Current in Transformers; Part I - Numerical Simulation," *IEEE Transactions on Power Delivery*, vol. 8, no. 1, 1993.

[60] electrical4u, "Magnetizing Inrush Current in Power Transformer," electrical4u, 2011-2016. [Online]. Available: http://www.electrical4u.com/magnetizing-inrush-current-in-power-transformer/. [Accessed 10 November 2015].

[61] I. Daut, S. Hasan and S. Taib, “Magnetizing Current, Harmonic Content and Power Factor as the Indicators of Transformer Core Saturation,” *Journal of Clean Energy Technologies*, vol. 1, no. 4, 2013.

[62] R. S. Girgis and E. G. teNyenhuis, “Characteristics of Inrush Current of Present Designs of Power Transformers,” in *IEEE Power Engineering Society General Meeting*, Florida, USA, 2007.

[63] University of Idaho College of Engineering, “ECE 524: Lecture 35 - Transformer Examples,” Transients in Power Systems, 2014. [Online]. Available: www.ece.uidaho.edu/ee/power/ECE524/spring14/Lectures/L35/L35.pdf. [Accessed 04 October 2015].

[64] L. Prikler and H. K. Høidalen, ATPDraw version 5.6 Users' Manual, Trondheim: ATP, 2009.

[65] Electronics Tutorials, “Three Phase Transformers,” AspenCore, Inc., 2016. [Online]. Available: http://www.electronics-tutorials.ws/transformer/three-phase-transformer.html. [Accessed 28 October 2016].

[66] R. Moon and R. K. Dhatrak, “A Study of Effect of Magnetizing Inrush Current on Different Ratings Of Transformers,” *International Journal of Advanced Research in Electrical, Electronics and Instrumentation Engineering*, vol. 3, no. 4, 2014.

[67] Eskom, Composer, *Distribution voltage regulation and apportionment limits*. [Sound Recording]. Eskom. 2013.

[68] ABB, "*Transformers for reliable power quality*" *Short-circuit withstand capabilty*, ABB, 2012.

[69] M. Steurer and K. Fröhlich, “The Impact of Inrush Currents on the Mechanical Stress of High Voltage Power Transformer Coils,” *IEEE Transactions on Power Delivery*, vol. 17, no. 1, 2002.

[70] J. B. Calvert, “Inside transformers,” J B Calvert; University of Denver, 09 June 2011. [Online]. Available: http://mysite.du.edu/~jcalvert/tech/transfor.htm. [Accessed 09 August 2016].

[71] David Meeker (FEMM), “Finite Element Method Magnetics: MagneticsTutorial,” FEMM, 14 December 2013. [Online]. Available: http://www.femm.info/wiki/MagneticsTutorial. [Accessed 9 August 2016].

[72] A. C. de Azevedo, A. C. Delaiba, J. C. de Oliveira, B. C. Carvalho and H. de Souza Bronzeado, “Transformer mechanical stress caused by external short-circuit: a time

domain approach," in *International Conference on Power Systems Transients (IPST)*, Lyon, France, 2007.

[73] A. C. de Azevedo, I. Rezende, A. C. Delaiba, J. C. de Oliveira, B. C. Carvalho and H. de Souza Bronzeado, "Investigation of Transformer Electromagnetic Forces Caused by External Faults Using FEM," in *IEEE PES Transmission & Distribution Conference and Exposition*, Caracas, Venezuela, 2006.

[74] Meeker, David (FEMM), Finite Element Methods Magnetics; Version 3.4; User's Manual, FEMM, 2005.

[75] Meeker, David (FEMM), "Re: [femm] Metglas square loop BH curves," FEMM, 22 November 2000. [Online]. Available: http://www.femm.info/list/msg00278.html. [Accessed 09 August 2016].

[76] V. Hinrichsen, Metal-Oxide Surge Arresters in High-Voltage Power Systems; Fundamentals, vol. 3rd edition, Darmstadt; Germany: Siemens (Siemens AG), 2011.

[77] Electrical Engineering Portal, "Using Tap Changers to Match the System Voltage," 2016 EEP; powered by CsanyiGroup, 31 August 2012. [Online]. Available: http://electrical-engineering-portal.com/using-tap-changers-to-match-the-system-voltage. [Accessed 9 August 2016].

APPENDIX A1: MATLAB CODE 1

This code in conjunction with the code in Appendix A2 was used for extracting the data from FEMM, as well as analysing and plotting the graphs in Chapter 4.8 and Chapter 4.9.

```
I = 10;
mua = 4.2;
Na = 5168;
mub = 3.88;
Nb = 5600;
muc = 5.6;
Nc = 5168;
mud = 7.04;
Nd = 4115;

openfemm;
%try
%    vv=ver;
%    opendocument([cd,'/Trans_single_acore_IR.fem']);
%catch
   opendocument('Trans_single_acore_IR_10.fem');
%    opendocument('Trans_single_acore_IR.fem');
%end
mi_saveas('temp.fem');
mi_analyze;
mi_loadsolution;

[Fx1,Fy1,Bx1,By1,Br1,x1,y1] = force_ex(I);
[Fx5,Fy5,Bx5,By5,Br5,x5,y5] = force_tc(I);
closefemm;

openfemm;
% try
%     vv=ver;
%     opendocument([cd,'/Trans_single_acore_SC_10.fem']);
```

```
% catch
   opendocument('Trans_single_acore_SC_10.fem');
%end
mi_saveas('temp.fem');
mi_analyze;
mi_loadsolution;

[Fx2,Fy2,Bx2,By2,Br2,x2,y2] = force_ex(I);
[Fx6,Fy6,Bx6,By6,Br6,x6,y6] = force_tc(I);
closefemm;

openfemm;
% try
%     vv=ver;
%     opendocument([cd,'/Trans_single_conv_IR.fem']);
% catch
   opendocument('Trans_single_conv_IR_10.fem');
%end
mi_saveas('temp.fem');
mi_analyze;
mi_loadsolution;

[Fx3,Fy3,Bx3,By3,Br3,x3,y3] = force_ex(I);
[Fx7,Fy7,Bx7,By7,Br7,x7,y7] = force_tc(I);
closefemm;

openfemm;
% try
%     vv=ver;
%     opendocument([cd,'/Trans_single_conv_SC.fem']);
% catch
   opendocument('Trans_single_conv_SC_10.fem');
%end
mi_saveas('temp.fem');
mi_analyze;
```

```
mi_loadsolution;

[Fx4,Fy4,Bx4,By4,Br4,x4,y4] = force_ex(I);
[Fx8,Fy8,Bx8,By8,Br8,x8,y8] = force_tc(I);
closefemm;

y = y1-min(y1);
y2 = y;
x1 = x1-min(x1);
x2 = x2-min(x2);

figure(1),hold on
p1 = plot(mean(Fy1'),y,'blue');
p2 = plot(mean(Fy2'),y,'red');
p3 = plot(mean(Fy3'),y2,'black');
p4 = plot(mean(Fy4'),y2,'green');
ylabel('Distance (mm)'),xlabel('Axial Force (N)'), grid('on'),legend([p1(1) p2(1) p3(1)
p4(1)],'Amorphous IR','Amorphous SC','M-5 IR','M-5 SC')
hold off
print('-dpng','-r300','axial1.png');

figure(2),hold on
p1 = plot(Fx1,y,'blue');
p2 = plot(Fx2,y,'red');
p3 = plot(Fx3,y2,'black');
p4 = plot(Fx4,y2,'green');
ylabel('Distance (mm)'),xlabel('Radial Force (N)'), grid('on'),legend([p1(1) p2(1) p3(1)
p4(1)],'Amorphous IR','Amorphous SC','M-5 IR','M-5 SC')
hold off
print('-dpng','-r300','radial1.png');

figure(3),hold on
p1 = plot(mean(Fy1'),y,'blue');
p2 = plot(mean(Fy2'),y,'red');
p3 = plot(Fy5(:,1),y2,'black');
```

```
p4 = plot(Fy6(:,1),y2,'green');
ylabel('Distance (mm)'),xlabel('Axial Force (N)'), grid('on'),legend([p1(1) p2(1) p3(1) p4(1)],'Winding IR','Winding SC','Tap Changer IR','Tap Changer SC')
hold off
print('-dpng','-r300','axial1.png');

figure(4),hold on
p1 = plot(Fx1,y,'blue');
p2 = plot(Fx2,y,'red');
p3 = plot(Fx5,y2,'black');
p4 = plot(Fx6,y2,'green');
ylabel('Distance (mm)'),xlabel('Radial Force (N)'), grid('on'),legend([p1(1) p2(1) p3(1) p4(1)],'Winding IR','Winding SC','Tap Changer IR','Tap Changer SC')
hold off
print('-dpng','-r300','radial1.png');


% figure(3),pcolor(abs(Fy1)),h = colorbar,h.Label.String='Axial Force [N]',caxis([0 100]),ylabel('Length (mm)'),xlabel('Width (mm)'),colormap('jet')
% figure(4),pcolor(abs(Fy2)),h = colorbar,h.Label.String='Axial Force [N]',caxis([0 100]),ylabel('Length (mm)'),xlabel('Width (mm)'),colormap('jet')

% figure(5),hold on
% p1 = plot(Bx1(1,:),y,'blue');
% p2 = plot(Bx2(1,:),y,'red');
% p3 = plot(Bx3(1,:),y2,'black');
% p4 = plot(Bx4(1,:),y2,'green');
% ylabel('Distance (mm)'),xlabel('Radial Magnetic Flux Density (T)'), grid('on'),legend([p1(1) p2(1) p3(1) p4(1)],'Amorphous IR','Amorphous SC','M-5 IR','M-5 SC')
% hold off
% print('-dpng','-r300','radial2.png');
%
% figure(6),hold on
% p1 = plot(x1,Br1,'blue');
```

```
% p2 = plot(x1,Br2,'red');
% p3 = plot(x1,Br3,'black');
% p4 = plot(x1,Br4,'green');
% xlabel('Distance (mm)'),ylabel('Axial Magnetic Flux Density (T)'), grid('on'),legend([p1(1) p2(1) p3(1) p4(1)],'Amorphous IR','Amorphous SC','M-5 IR','M-5 SC')
% hold off
% print('-dpng','-r300','axial2.png');

% figure(7),pcolor(abs(By1)),h = colorbar,h.Label.String='Axial Force [N]',caxis([0 1]),ylabel('Length (mm)'),xlabel('Width (mm)'),colormap('jet')
% figure(8),pcolor(abs(By2)),h = colorbar,h.Label.String='Axial Force [N]',caxis([0 1]),ylabel('Length (mm)'),xlabel('Width (mm)'),colormap('jet')
```

APPENDIX A2: MATLAB CODE 2

This code was written for the radial pressure and axial forces analysis and is used (i.e. called up) in the code in Appendix A1.

```
function [Fx,Fy,Bx,By,Br,x5,y] = force_tc(I_1)
%
%I_1 = 20;
CA_1 = 0.7/1000^2;
J = I_1/CA_1; %A/m2
%J = 12.7e6

x = [52:(74-52)/25:74];
x5 = [52:1:255];
y = 96:(278-96)/228:278; %103...267
l = (278-96)/1000;      %[m]
dl = y(2)-y(1);
V = dl*(x(2)-x(1))*170; %[mm3]
V = V/1000^3;           %[m3]

for k = 1:length(x)
for kk = 1:length(y)
      M = mo_getpointvalues(x(k),y(kk));
      Bx(k,kk)=M(2);
      By(k,kk)=M(3);
end

end

for h = 1:length(x5)
M = mo_getpointvalues(x5(h),187);
Br(h,1) = abs(M(2)+j*M(3));
end

% Axial forces
```

```
%for k = 1:length(y)
%    sum(Bx(1,:))
%Fy1 = J*l*t/3/l*2*pi*r*dl*/1000;

%Fy2 = J*Bx(2,:)/1000;
%Fy3 = J*Bx(3,:)/1000;
%end

Fy = J*Bx*V;
%for k = 1:100
 for k = (228/2-50):1:(228/2+50)
   Fy(1,k) = 0;
end
Fyt = sum(sum(Fy))
Fy = cumsum(Fy');
%Fy = sum(Fy');

%Fyt2 = cumsum(Fy2);
%Fyt3 = cumsum(Fy3);

%Fy = Fy1+Fy2+Fy3;
%Fy = abs(sum(Fy))

% Radial pressure
Fx = J*By*V;
%for k = 1:100
for k = (228/2-50):1:(228/2+50)
   Fx(1,k) = 0;
end
Fx = sum(Fx);
%Px2 = J*By(2,:)/1000;
%Px3 = J*By(3,:)/1000;

%Px = Px1+Px2+Px3;
Fxt = sum(Fx)
```

APPENDIX B: PERMISSION FOR PICTURES

Figure B 1 displays the e-mail for permission granted to display pictures courtesy of Eskom.

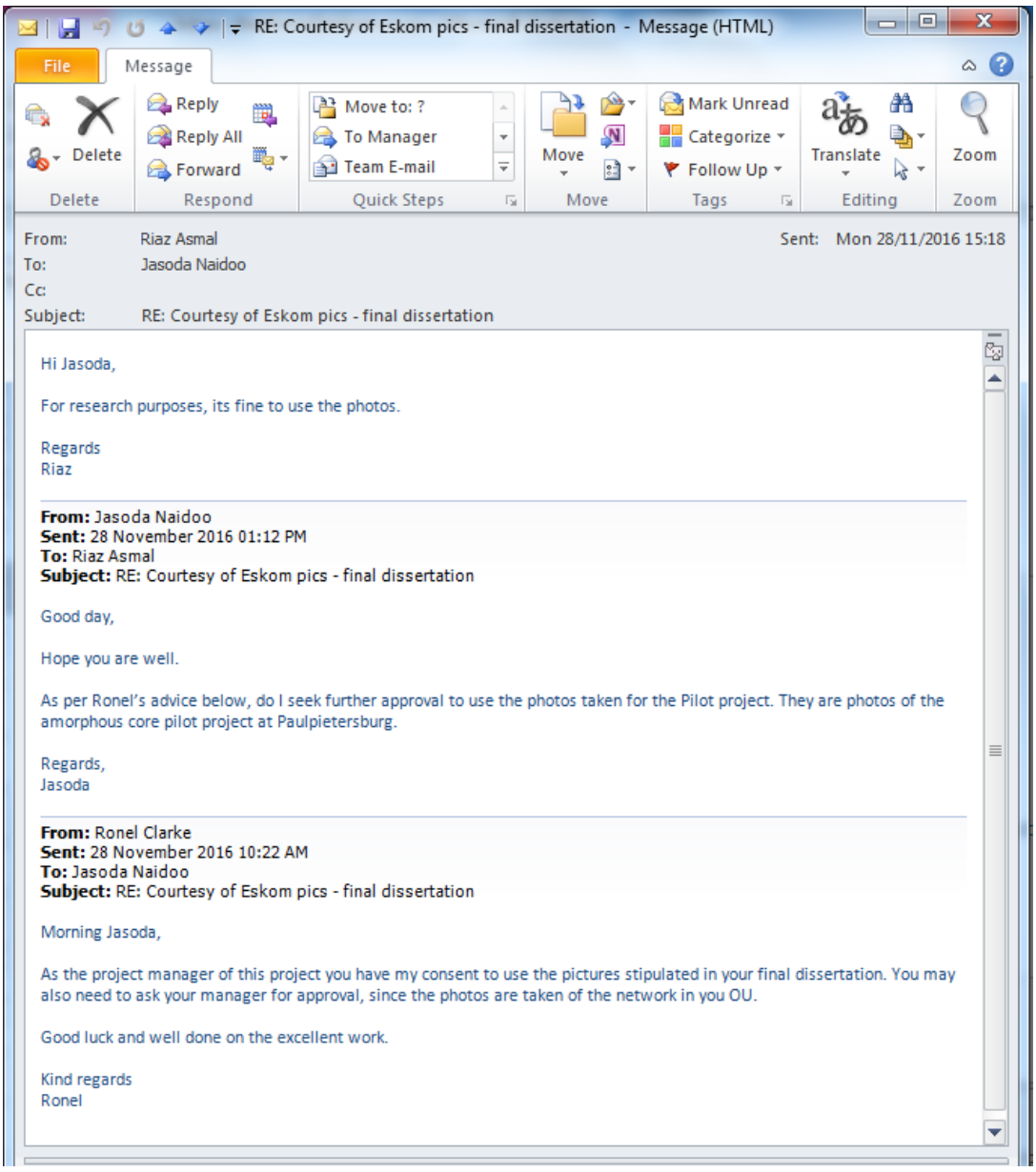

Figure B 1: Permission for courtesy of Eskom pictures